HAL
open science

Selected issues for the LHC luminosity upgrade

Emanuele Laface

To cite this version:

Emanuele Laface. Selected issues for the LHC luminosity upgrade. High Energy Physics - Experiment [hep-ex]. Université Blaise Pascal - Clermont-Ferrand II, 2008. English. NNT : . tel-00377619

HAL Id: tel-00377619

https://theses.hal.science/tel-00377619v1

Submitted on 22 Apr 2009

HAL is a multi-disciplinary open access archive for the deposit and dissemination of scientific research documents, whether they are published or not. The documents may come from teaching and research institutions in France or abroad, or from public or private research centers.

L'archive ouverte pluridisciplinaire **HAL**, est destinée au dépôt et à la diffusion de documents scientifiques de niveau recherche, publiés ou non, émanant des établissements d'enseignement et de recherche français ou étrangers, des laboratoires publics ou privés.

Numéro d'ordre: DU 1905 PCCF T 0806
EDSF: 599

UNIVERSITÉ CLERMONT-FERRAND II - BLAISE PASCAL
(U.F.R. de Recherche Scientifique et Technique)

Ecole Doctorale des Sciences Fondamentales

THÈSE

préparée au CERN/AT/MCS
pour obtenir le grade de

Docteur d'Université
dans la specialité de Physique des Particules

par

Emanuele Laface

Selected issues for the LHC luminosity upgrade

Thèse soutenue le 19 décembre 2008 devant le jury:

Président:	M. Pierre Henrard	UBP Clermont-Ferrand, France
Examinateurs:	M. François Méot	LPSC, Grenoble, France
	M. Leonid Rivkin	EPFL, Lausanne, Switzerland
Directeur the thèse:	M. Claudio Santoni	UBP Clermont-Ferrand, France
	M. Walter Scandale	CERN, Genève, Switzerland

The theory is when you know everything and nothing works.
The practice is when everything works and nobody knows why.
We have put together the theory and practice: there is nothing that works and nobody knows why.

Albert Einstein

Abstract

The Large Hadron Collider started its operations on September 10th 2008. In a realistic forecast it is supposed to demonstrate (or confute) the existence of the Higgs boson for the year 2014. After this date the physics of rare events will be explored more in details and an upgrade of the luminosity can make an important difference in the program of experiments at CERN.

This thesis proposes several ideas to increase the luminosity of ATLAS and CMS experiments and the acceptance of TOTEM experiment. The main object of study is the Interaction Region, that consists in the set of magnets in charge to provide the final beam focalization for the collisions.

The Interaction Region is studied with the methods of beam optics and beam dynamics to design new layouts for the upgrade. These layouts are also explored from the point of view of integrability in the existing experiments developing the analysis of energy deposition and misalignment tolerances.

This study was performed with the use of analytical methods for the general considerations and numerical methods for the parameters optimization, the results are published in original papers presented in several international conferences and workshops of luminosity upgrades.

Résumé

Le grand collisionneur de hadrons (LHC) a commencé les opérations de faisceau de protons le jour 10 septembre 2008. Respectant le programme d'expériences prévues pour les prochaines années, le LHC devrait démontrer ou réfuter l'existence du boson de Higgs de façon réaliste d'ici 2014. Après cette date il est raisonnable de faire l'hypothèse du début d'amélioration de luminosité de la machine pour explorer en détail les événements rares.

Le présent travail de thèse propose diverses idées pour augmenter la luminosité des expériences ATLAS et CMS, les deux principales expériences du programme scientifique du LHC. De plus, l'idée de l'amélioration de l'acceptation de l'expérience TOTEM est présentée. Le principal sujet d'étude pris en considération dans la thèse est la région d'interaction : l'ensemble des aimants qui réalisent la focalisation finale du faisceau par la collision. La région d'interaction est étudiée d'un point de vue de l'optique des accélérateurs et de la dynamique des faisceaux, à travers l'utilisation des méthodes soit analytiques soit numériques par la réalisation de la région des interactions optimisées pour augmenter la luminosité des expériences.

La thèse est subdivisée en 4 chapitres et une annexe : le premier chapitre démontre la structure de la thèse, résume les contributions personnelles et originales apportées par l'auteur et illustre les instruments utilisés durant le développement de la thèse.

Le deuxième chapitre décrit l'état actuel du LHC, les paramètres de fonctionnements nominaux de la machine, les propriétés des deux faisceaux de protons, la structure des régions d'interaction et les fonctions optiques. Cette illustration générale a pour but de fournir au lecteur toutes les définitions des concepts utilisés dans la partie suivante de la discussion sur l'amélioration. Le chapitre se conclut avec la définition de la luminosité pour les expériences ATLAS et CMS et l'acceptation de l'expérience TOTEM. Ces concepts seront après développés dans les chapitres successifs démontrant comment les améliorer.

Le troisième chapitre est focalisé sur l'amélioration de la luminosité des expériences ATLAS et CMS. La première proposition d'amélioration consiste à déplacer l'actuel télescope composé des trois quadrupôles, alias triplet, des actuels 23 m à la distance de 13 m du point d'interaction (IP). De cette façon, on peut plus comprimer le faisceau en réduisant la fonction β de 0.55 m à 0.25 m, en produisant un nombre majeure de collisions à chaque collision de faisceaux en faveur de la luminosité. La solution avec le triplet à 13 m du IP requiert un champ magnétique élevé des aimants du triplet et l'actuelle technologie du NbTi n'est pas suffisante pour réaliser un tel champ, c'est pourquoi on doit considérer l'utilisation du Nb_3Sn pour cette solution. Toutefois, il n'est pas tout à fait clair combien la technologie

basée sur le Nb_3Sn soit prête pour l'utilisation dans les conditions de stress d'un accélérateur comme le LHC, c'est pourquoi une solution basée sur NbTi est un moment souhaitable ; la partie centrale de ce chapitre présente précisément cette solution. Un couple de quadrupôle (Q0) est mise à 13 m du IP, devant le triplet actuel, permettant de réaliser une réduction de la fonction β jusqu'à 0.25 m, avec des champs magnétiques compatibles avec le NbTi. Pour les deux solutions, c'est-à-dire le triplet à 13 m et le Q0 à 13 m, sont illustrées en détail l'optique et les problématiques liées à l'intégrabilité des aimants dans les expériences : puisqu'à 13 m du IP se trouve encore les expériences (une structure d'absorption des radiations pour ATLAS et le calorimètre externe pour le CMS), insérer des aimants dans cette région laisse de nombreuses questions ouvertes. La problématique principale concerne la douche de radiations auxquels sont sujets les aimants et donc le réchauffement est dû aux radiations. Ce problème est traité en proposant des solutions dans la dernière partie du chapitre.

Le quatrième chapitre affronte l'amélioration de l'acceptation du TOTEM. Le chapitre commence avec la description des paramètres d'un cristal de silice et comment celui-ci se comporte quand il interagit avec les protons. En particuliers la discussion est faite à partir des résultats de l'expérience (H8RD22) exécuté en SPS en 2007. Sont mis en particuliers en avant les propriétés de canalisation et de réflexion qui permettent au cristal de dévier les faisceaux des particules chargées. Ces propriétés sont donc introduites dans le contexte de l'expérience TOTEM démontrant comment un cristal mis dans le halo du faisceau peut dévier les protons produits d'interactions élastiques ou diffractive à l'intérieur des détecteurs de l'expérience (Roman Pots) accroissant la tolérance d'eux-mêmes. Le modèle de simulation employé pour évaluer les prestations du cristal dans TOTEM est en outre utilisé pour faire des prévisions sur l'expérience CRYSTAL qui aura lieu dans SPS en 2009. Cette expérience mettra en évidence les propriétés et les limites des cristaux utilisés comme collimateurs d'une machine à hadrons. Simuler cette expérience et successivement la comparer avec les résultats expérimentaux que l'expérience produira, sert à évaluer combien le système de simulation est fiable pour les prévisions de la tolérance dans TOTEM.

L'annexe décrit le fonctionnement d'une base de données de superconductivité. La base de données a été développée dans la période de recherche des informations pour les solutions optiques du triplet à 13 m et du Q0. Les données récoltées ont été rassemblées dans une structure basée sur MediaWiki (le moteur de Wikipédia) et rendues publiques pour le bien de la communauté de la superconductivité.

Les contributions personnelles de cette thèse sont les nouvelles solutions optiques basées sur le triplet à 13 m et sur le Q0, avec toutes les études collatérales des problèmes d'intégrabilité ; en outre l'idée est originale d'utiliser les cristaux de silice pour améliorer la tolérance de TOTEM, et les résultats de simulation pour l'expérience CRYSTAL. Ces contributions ont été présentées et publiées dans diverses conférences internationales et atelier de secteurs.

Contents

1 Introduction **1**
1.1 Synopsis . . . 1
1.2 Personal contribution associated with this thesis . . . 2
1.3 Methods and tools . . . 2

2 LHC: insight of the nominal parameters **5**
2.1 Basic layout and performances . . . 5
2.2 Interaction Regions . . . 7
2.3 Beam parameters . . . 10
2.4 Optical functions and apertures . . . 11
2.5 Luminosity of ATLAS and CMS . . . 17
2.6 Acceptance of TOTEM . . . 22

3 Low β: how to reduce the beam size at the Interaction Point **27**
3.1 Preliminary considerations . . . 27
3.2 Triplet at 13m . . . 31
3.3 Q0 . . . 33
3.4 Alignment . . . 40
3.5 Energy Deposition . . . 43

4 Crystals **49**
4.1 Crystal-particle interaction . . . 49
4.2 Acceptance of TOTEM experiment with crystal . . . 52
4.3 Crystal characterization in the SPS: experiment layout . . . 58
4.4 Crystal characterization in the SPS: simulation results . . . 66

5 Conclusions **71**

6 Appendix: Superconductors Database **75**

Bibliography **92**

Chapter 1

Introduction

1.1 Synopsis

The topic of this thesis concerns the luminosity upgrade of the Large Hadron Collider interaction regions ATLAS and CMS and the acceptance upgrade of the TOTEM experiment.

Chapter 1 illustrate the thesis skeleton, the personal contributions and the tools used during the development of the thesis itself.

Chapter 2 presents an introduction of the LHC nominal parameters for beam, interaction regions layout and optical functions. The aim of this chapter is to explain the present situation of LHC and which possibilities are considered for the upgrade. The chapter concludes with the definition of luminosity for ATLAS and CMS and the definition of acceptance for TOTEM.

Chapter 3 focuses on the luminosity upgrade of ATLAS and CMS experiments with different quadrupole-first layouts: a final focusing telescope (the so-called triplet) at 13 m from the interaction point, and a doublet (called Q0) in front of the present triplet. For each solution advantages and issues are illustrated and considered in comparison with respect to the nominal layout.

Chapter 4 introduces the property of silicon crystals in the interaction with protons and how the acceptance of the TOTEM experiment can benefit of such properties. A new optical layout is presented and the new acceptance is compared with the nominal one. In order to validate the crystal behavior an experiment is under preparation and will be performed in 2009: the chapter ends with a simulation that should predict the experimental results.

The appendix presents the Superconductors Database, a tool developed during the PhD work to collect informations about superconductivity.

1.2 Personal contribution associated with this thesis

The original work incorporated in and arising from this thesis can be organized in the following categories:

Original design of quadrupole-first options for the LHC luminosity upgrade: Triplet at 13m from the Interaction Point and doublet at 13m from the Interaction Point, in front of the nominal triplet. For each option are evaluated: optics; performances in term of luminosity; hardware requirements; possible misalignments with field errors; energy deposition of back scattered particles from experiments [1], [2], [3],[4].

Original design of a layout for the TOTEM experiment with crystal in the framework of an acceptance upgrade: analysis of optics and acceptance performance through a full tracking simulation [5]. The tracking tools used for TOTEM are also used to design an original simulation to predict the behavior of crystal in the Crystal SPS Experiment due in 2009; the comparison between this experiment and the simulation will be used to validate the crystal and the tracking code.

Development and optimization of software tools for optic design. Development of tools for data storage [6].

1.3 Methods and tools

The research of this thesis is mainly based upon tracking particles in electromagnetic fields and into materials. Many standard tools exist to track particles but in general they need customization for specific problems.

For the design of the optics, the general procedure used here is to design the optical object (quadrupoles or sextupoles) in a MATLAB-Simulink design kit developed ad-hoc for this purpose in order to have a preliminary idea around the main problem of optics, matching etc.

The second step consist in implementation of new designed optics with the Methodical Accelerator Design tool (MadX) [7] and connection of new optics with the standard one, for example with the optics of LHC or the optics of SPS.

The tracking is performed with the MadX PTC [8] tracking code when the device used in the simulations are already available in MadX (dipoles, quadrupoles, etc.) otherwise the sector maps matrices are exported from MadX and used in a custom C/C++/Fortran code with the implementation of unusual objects (for example crystals).

To evaluate the misalignment issues of magnets, standard analytical tools based on multipolar expansion of the magnetic field are used.

For the energy deposition, and more generally for the evaluation of interaction of particles with matter, the fully integrated particle physics MonteCarlo simulation package (FLUKA) [9] is used.

The software releases used are: MATLAB 7.5.0.338 (R2007b), Simulink 7.0 (R2007b), MadX 3.04.29, FLUKA 2008 v1.0. The C, C++ and Fortran compiler are gcc, g++ and gfortran in the release 4.2.1.

Chapter 2

LHC: insight of the nominal parameters

The main reference for this chapter is the LHC Design Report [10].

2.1 Basic layout and performances

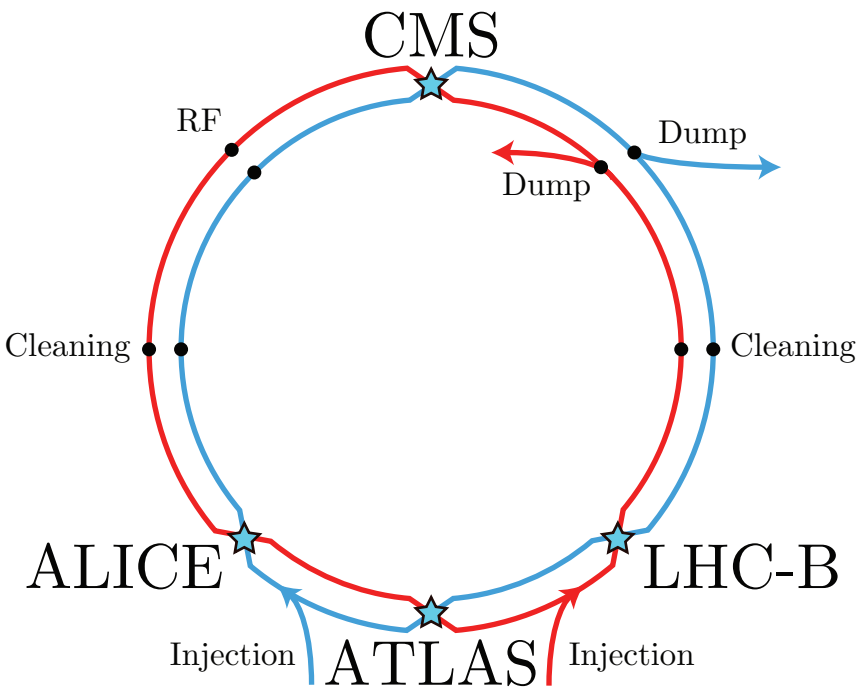

Figure 2.1: LHC Layout.

The Large Hadron Collider is a collider of protons and lead ions with several scopes: to find experimental evidence of the Higgs mechanism for the particle mass generation; to show gluon plasma properties in order to complete the QCD model; to find supersymmetric particles and, more in general, to explore the frontiers of the standard model of particles. [11]

To fullfill these goals LHC is designed to collide hadrons at unprecedented energy: 14 TeV in the center of mass for the proton-proton reaction and 5.52 TeV for nucleons in lead ions. Another important parameter of LHC is the very high luminosity, i.e. the number of collisions per unit of area and time that is 10^{34} cm^{-2} s^{-1}.

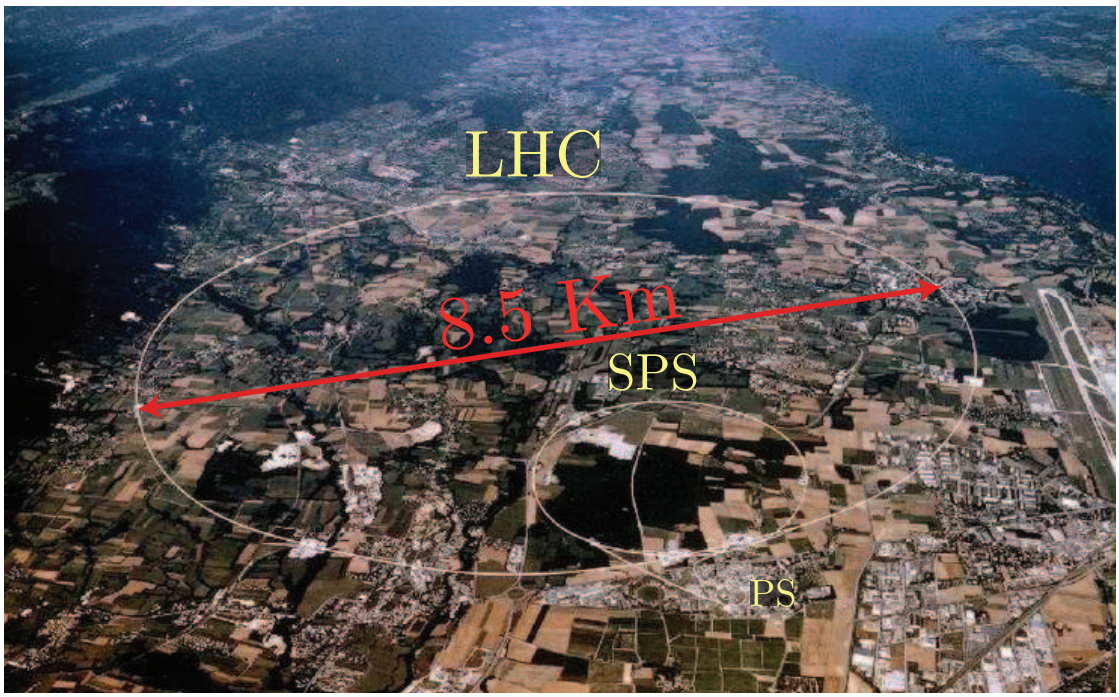

Figure 2.2: CERN Accelerators

LHC can reach this value of energy because it is a 26.7 Km synchrotron ring (Fig. 2.2) made up 1232 superconducting dipoles (Fig. 2.3): each dipole is 15 m long and provides a magnetic field of 8.4 T giving a kick of 5.1 mrad to protons with 7 TeV of energy.

The high luminosity of the interaction regions is obtained using a telescope of three quadrupole magnets (the so-called triplet) in the straight section before the experiments: here the beam is squeezed through the action of the quadrupoles reaching a transversal rms size on the interaction point of 16.63 μm; this size is enough to generate $\sim$ 40 collisions per bunch crossing every 25 ns.

The energy and luminosity of LHC are the present ultimate frontier for an

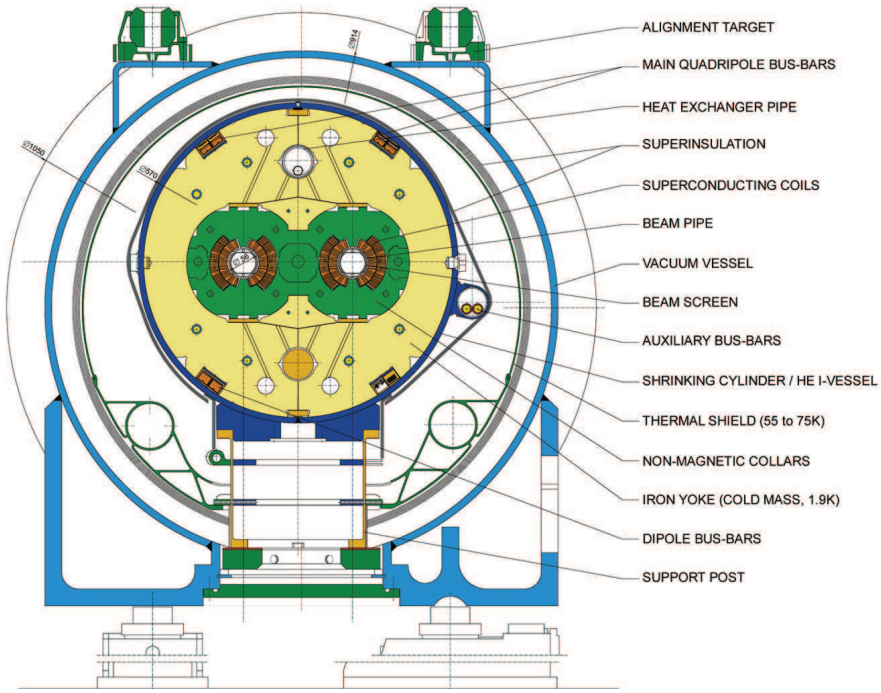

Figure 2.3: LHC Dipole Cross Section.

hadron collider but the new physics produced by this machine could require to increase the energy or the luminosity in order to extend the measurements program of LHC to unexpected phenomena and rare events. This is the reason why in 2001 CERN launched an R&D program [12] to study the feasibility of an upgrade of the two key parameters, energy and luminosity.

2.2 Interaction Regions

LHC is a collider with four interaction regions: ATLAS, CMS, ALICE and LHCb. For the purpose of this thesis only ATLAS and CMS are considered.

The layout of the interaction regions of ATLAS and CMS is the same and is obtained with the follow magnets (for half IR, see Fig. 2.4):

- 8 main dipoles;
- 4 quadrupoles, from Q11 to Q8, used to avoid the dispersion at the interaction point;
- 4 quadrupoles, from Q7 to Q4, to give the degree of freedom for the matching of optical functions;
- 2 dipoles: D2 and D1, to change the orbit of the two beams changing the trajectory from the two separate beam pipe to a shared pipe. D1 is built

with 6 dipoles.

- 3 quadrupoles with shared beam pipe, from Q3 to Q1, to focalize the beam in order to create a low-β interaction point. Q2 is not a single magnet but it is built with 2 quadrupoles.

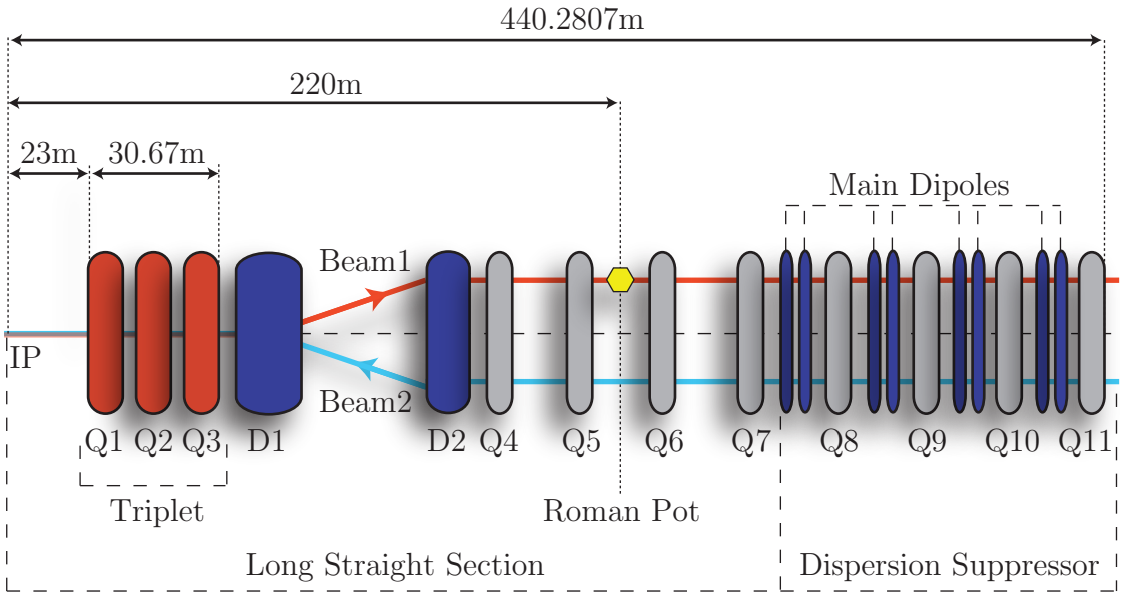

Figure 2.4: Half LHC (ATLAS and CMS) Interaction Region Layout.

The space of 23 m from IP to Q1 is surrounded with the detector (ATLAS or CMS): this is an important point to consider for the purpose of this thesis because, in order to increase the luminosity of ATLAS and CMS experiments, it will be considered the option to put quadrupoles at 13 m from IP, that is inside the experiments, with all the issues that the integration of magnets into experiments can create. The luminosity upgrade and the issues of integrability will be discussed in details in Chapter 3. A schematic view of the two main detectors is shown in Fig. 2.5 and Fig. 2.6.

The Roman Pot at 220 m from IP is part of the Total Cross Section Elastic Scattering and Diffraction Dissociation (TOTEM) device used for the measurement of the protons' cross section at 7 TeV/c. This device will be considered in Chapter 4.

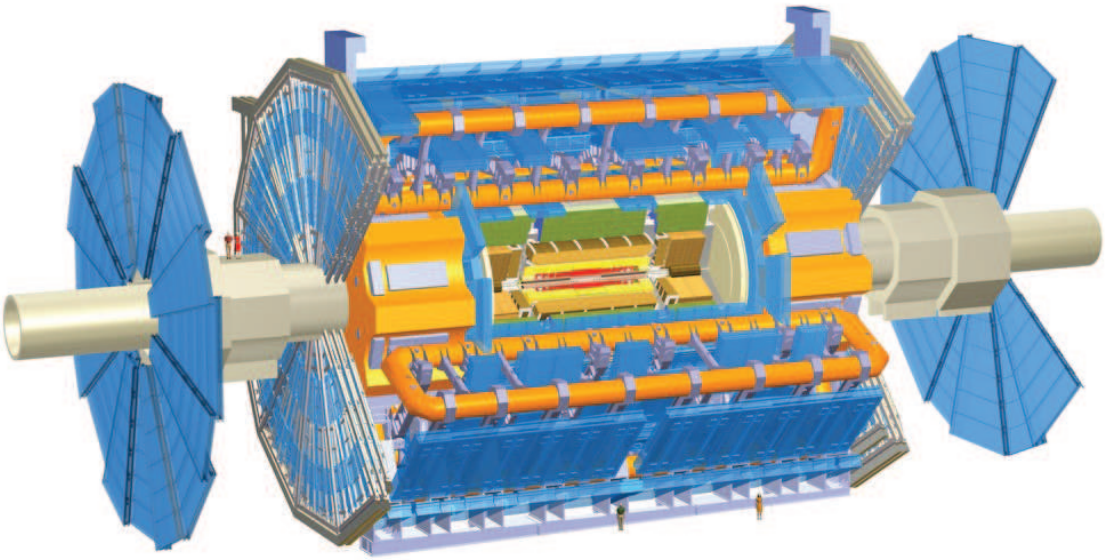

Figure 2.5: A Toroidal LHC ApparatuS (ATLAS).

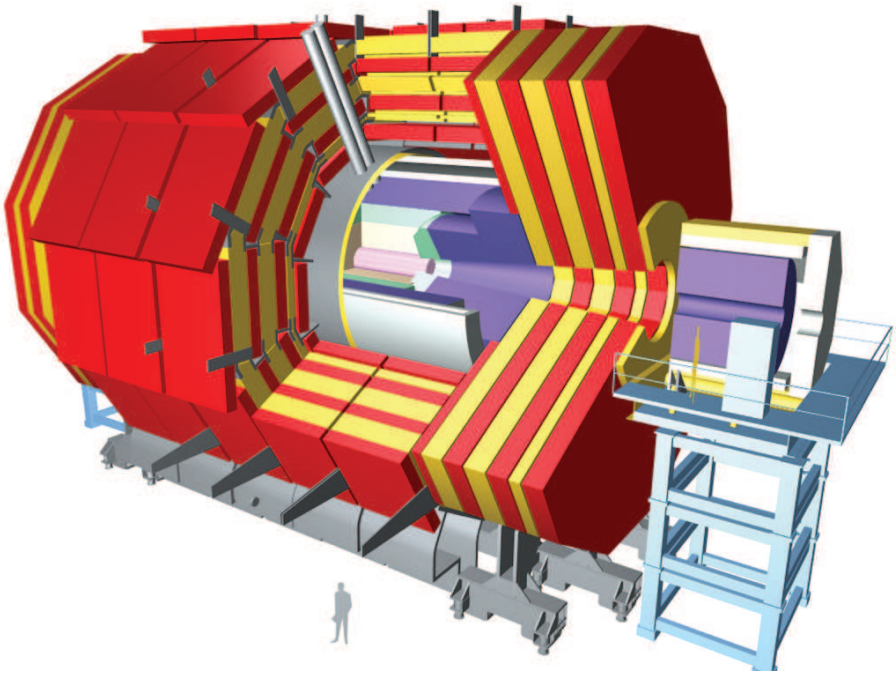

Figure 2.6: Compact Muon Solenoid (CMS).

2.3 Beam parameters

LHC is a machine capable to accelerate and to collide protons or lead ions. For the purpose of this thesis only protons will be considered.

The nominal proton beam, during the phase of collision, is composed of 2808 bunches separated by 25 ns; each bunch has 1.15×10^{11} protons, each with 7 TeV of energy, for a total stored energy of 362 MJ and a total circulating current of 0.582 A.

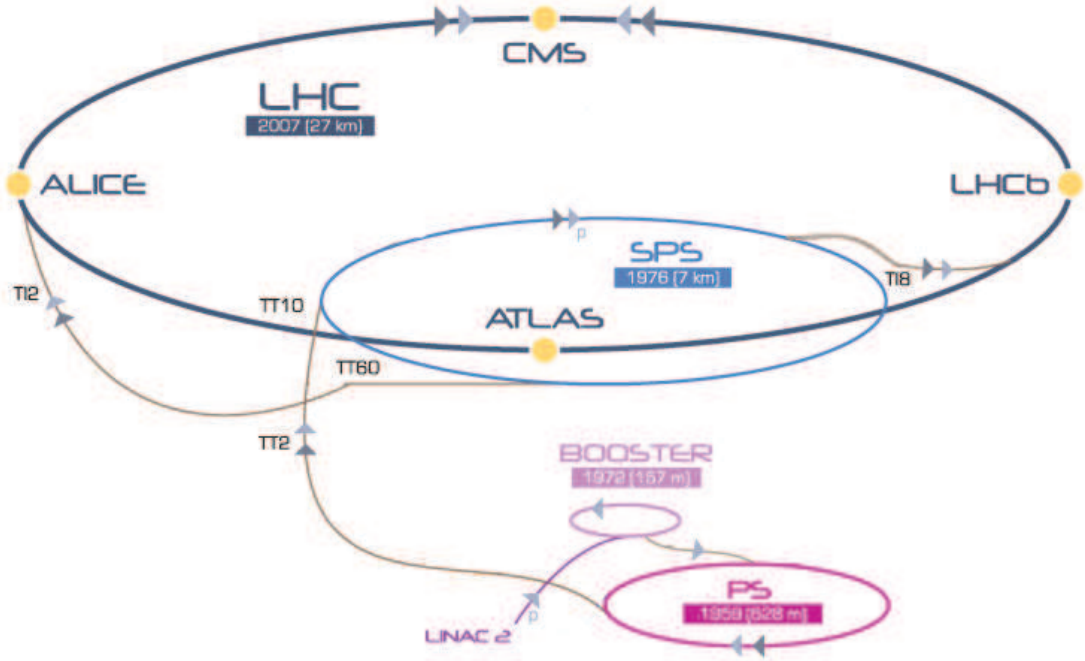

Figure 2.7: LHC Injection chain.

This beam is generated by a source of ionized hydrogen and accelerates in the chain shown in Fig. 2.7. Each accelerator contributes in the increase of energy: LINAC2 accelerates the beam to 50 MeV; Booster from 50 MeV to 1.4 GeV; PS from 1.4 GeV to 26 GeV and SPS up to 450 GeV. The result of the injection is a beam with an energy of 450 GeV with a normalized emittance, the two dimensional spread of the gaussian distribution for the conjugate variables position and momentum, normalized to the relativistic $\beta\gamma$ coefficients, defined as

$$\epsilon_x = \frac{\sqrt{\langle x^2 \rangle \langle x'^2 \rangle - \langle xx' \rangle^2}}{\beta\gamma} \tag{2.1}$$

$$\epsilon_y = \frac{\sqrt{\langle y^2 \rangle \langle y'^2 \rangle - \langle yy' \rangle^2}}{\beta\gamma} \tag{2.2}$$

of 3.5 μm rad that can increase up to 3.75 μm rad, due to the crossing of several resonances during the ramp of energy, when the beam is accelerated to 7 TeV and the machine is in collision.

The value of emittance is due to several factors (see Fig. 2.8): the source of protons, the coulombian repulsion in a bunch when the beam is not yet relativistic (in LINAC2 and Booster) and the small mismatch of the optics when the beam goes from an accelerator to the other.

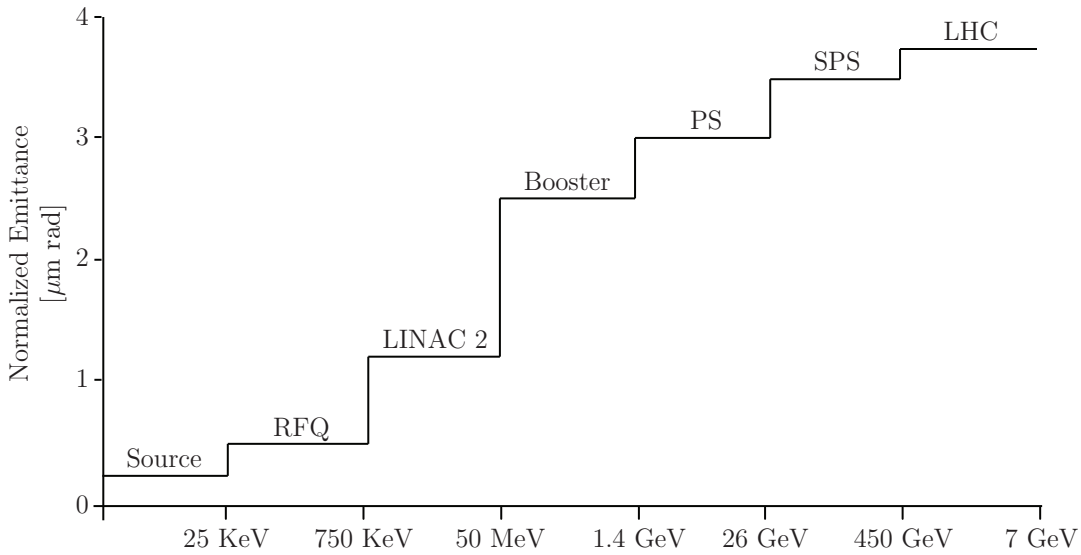

Figure 2.8: Emittance grow up in the injection chain.

2.4 Optical functions and apertures

The optics of LHC is a 15 years old work that starts with the "Design study of the Large Hadron Collider (LHC) : a multiparticle collider in the LEP" tunnel [13] and ends with the "LHC Design Report" [10]. During this time several optics are developed with many variants; the optics considered in this thesis is the version 6.5 generated with the software MadX [14] that is the final optics for the first years of experiments of LHC. There exists another release of the optics that is more recent than v6.5 and it is the release v6.500, but the only difference between the two optics is that in v6.500 the aperture of LHC elements is taken into account in the

model of simulations. From any other point of view the v6.5 and v6.500 are the same optics.

The LHC optics design follows a modular approach where the functionality of each insertion is extended by one arc-cell on each side of the insertion [15]. This approach allows an optics matching with fixed and equal phase advances over the insertions for both beams that does not perturb the optics in the rest of the machine. The total tune of the machine is adjusted via the arc cell optics.

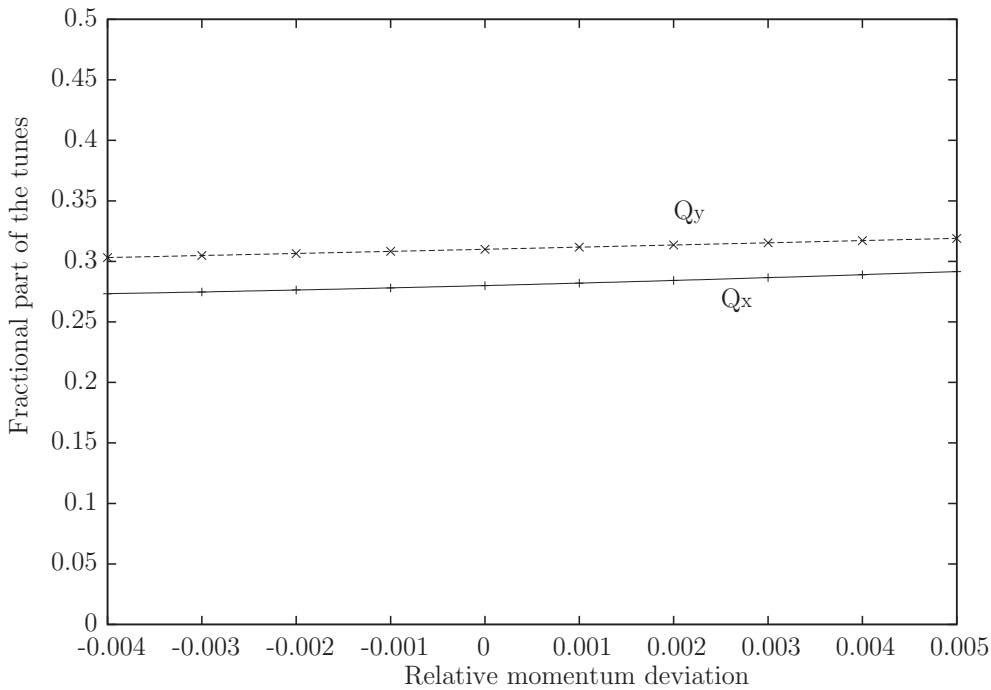

Figure 2.9: Unperturbed linear lattice with sextupole magnets and corrected chromaticity for the injection optics without multipole errors.

In conjunction with the series powering of the Ring 1 and Ring 2 quadrupole magnets, this approach automatically generates the same tunes for both beams. The flexibility of the phase advance over the insertions provides a measure for the exibility of the total LHC optics and the range over which the phase advance between the main experimental insertions can be changed.

The common low-β triplets in the experimental insertions provide opposite focusing for the two counter-rotating beams. A strictly antisymmetric powering was adopted for the feasibility study as a natural symmetry for a proton-proton machine with common magnetic elements [16]. However, in the present optics design the antisymmetric powering is only approximately kept, except in the low-β triplets where it is exact.

Table 2.1: Phase Advance in LHC for the injections optics.

	1 arc (21 cells)	**IRs contribution**	**LHC total**
$\frac{\Delta\mu_x}{2\pi}$	5.49725	20.302	64.28
$\frac{\Delta\mu_y}{2\pi}$	5.099375	18.515	59.31

The LHC arc cells feature a FODO lattice with approximately 90° phase advance per cell in both planes. A perfect 90° lattice generates equal tunes in the horizontal and vertical planes (apart from phase advance differences generated in the insertion regions) and minimizes the optics perturbations by tuning the trim quadrupole circuits at the end of each arc [17].

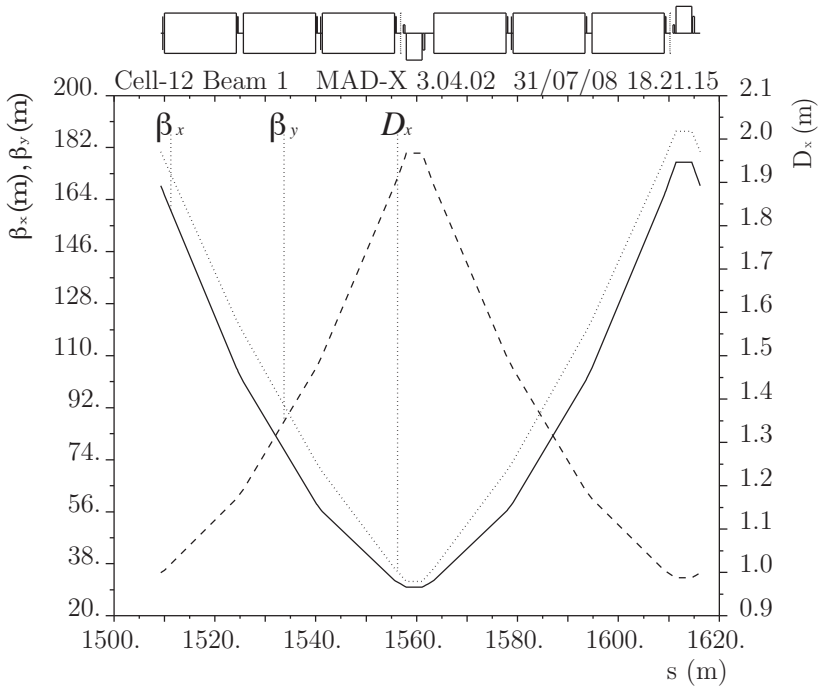

Figure 2.10: LHC Arc cell.

The LHC lattice is based on a total integer tune split of 5 units which is the combined result of the differences in the horizontal and vertical phase advances in the arcs and the insertion regions. This solution presents a good compromise between operational margins for the magnet strengths, aperture and a compensation efficiency of systematic resonances.

The optics of the interaction regions IR1 and IR5 (the two regions of interest for this thesis) are characterized by the request of a small value for β^* during the collisions. This β^*, in both horizontal and vertical plan, is 0.55 m; considering a transversal size of the beam, defined as:

$$\sigma_x = \sqrt{\beta_x \frac{\epsilon_n}{\gamma\beta}} \tag{2.3}$$

where ϵ_n is the normalized emittance, that for LHC in collision is 3.75 μm rad; γ and β are the relativistic parameters of the beam and at 7 TeV/c of momentum are $\gamma = 7461$ and $\beta \approx 1$; the resulting σ_x and σ_y at the Interaction Point (IP) are: $\sigma_x = \sigma_y = 16.7$ μm.

The closest quadrupole to the IP is Q1 and it is located at 22.965 m from the IP, so the space between IP and Q1 is, from an optical point of view, a drift and the beta function increases with the quadratical law [18]:

$$\beta_x = \beta_x^* - 2l_d\alpha_x^* + l_d^2(\frac{1+\alpha_x^{*2}}{\beta_x^*}) \tag{2.4}$$

where l_d is the length of the drift, α is $-\frac{1}{2}\frac{\partial\beta(s)}{\partial s}$ (0 at the interaction point because

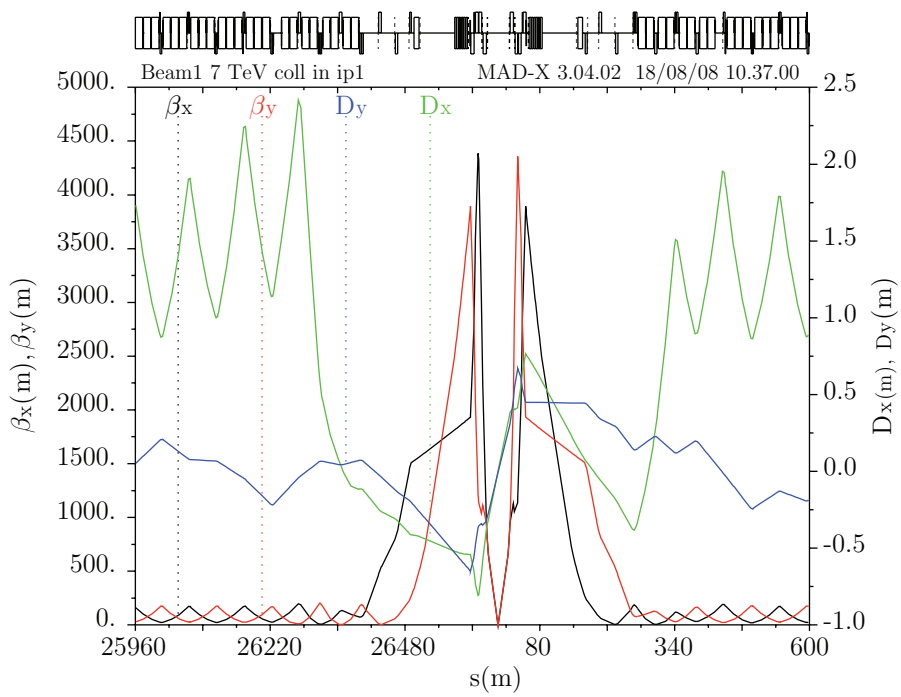

Figure 2.11: IR1 Collision Optics.

the β-function is in a minimum). Thus the equation for the drift for IR1 and IR5 yelds:

$$\beta_x = 0.55 \text{ m} + \frac{(22.965 \text{ m})^2}{0.55 \text{ m}} = 959.44 \text{ m}. \tag{2.5}$$

This value of the β function increases in the plane defocused by Q1 and reaching a maximum in Q2 of 4500 m, the resulting shapes are in Fig. 2.11 and 2.12.

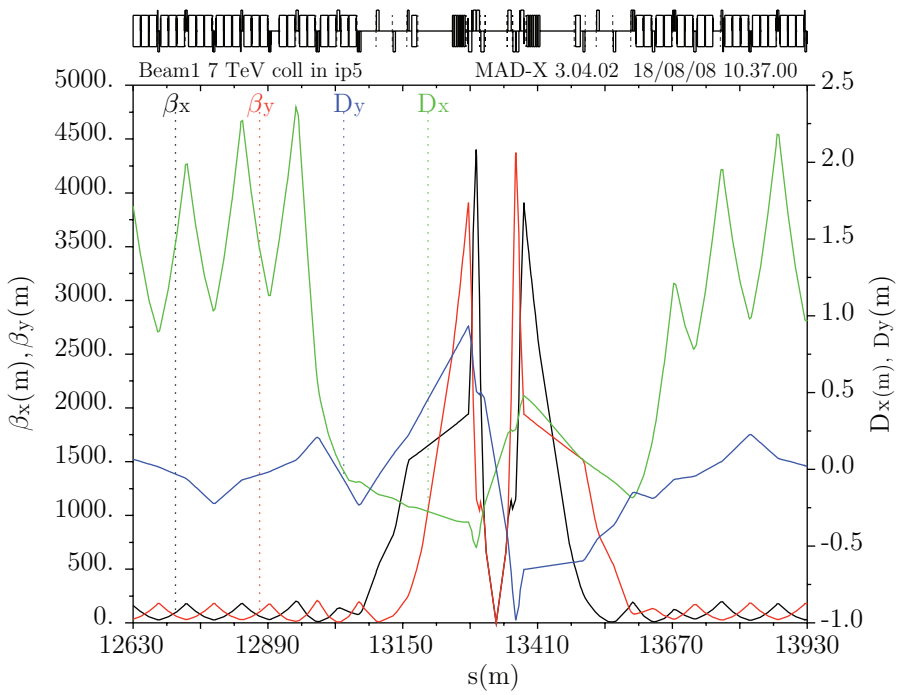

Figure 2.12: IR5 Collision Optics.

The region between D2 and IP (Fig. 2.4) have a shared beam pipe and the two beams reduce the transversal distance in order to collide at the IP. The ideal collision is when the two beams are aligned in a frontal collision, in this way the probability of collision at maximum energy is maximized. The problem of the frontal collision is that for each bunch that collide at IP there are other 15 bunches that collide in the half of a shared region, for a total number of 31 $(15 + 15 + 1)$ parasitic encounters per interaction region. In LHC there are 4 interaction regions so the total number of encounters will be 124, with 120 parasitic encounters and 4 useful encounters for the experiments.

The 120 parasitic encounters would destroy the beam in few turns due to the electrostatic repulsion of the bunches (the so-called beam-beam effect [19]), this is the reason why the two beams do not collide frontally but with a crossing angle that is established in 285 μrad and introduces an orbit separation between the

two beam trajectories. With the crossing angle the beam-beam effect is reduced, the only head-on collision is in the IPs of the experiments, the other parasitic encounters produce a long-range beam-beam effect that depends on the separation of the two beams. With a crossing angle of 285 μrad the separation scheme for IP1 and IP5, in term of σ is shown in Fig. 2.13.

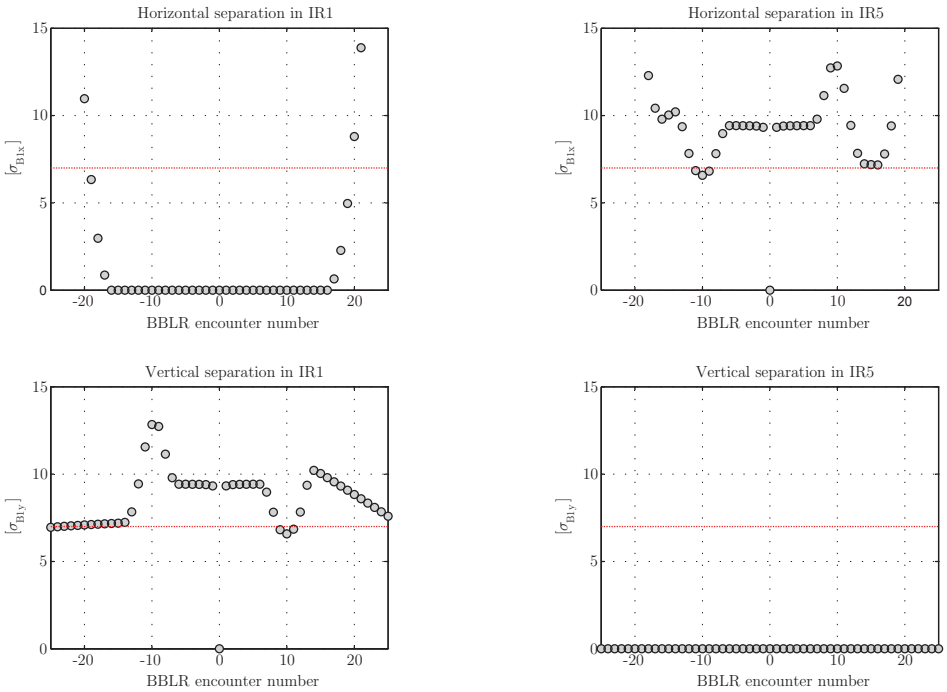

Figure 2.13: Beam-beam long range encounters in IP1 and IP5. Notice that the crossing angle is vertical for IP1 and horizontal for IP5.

The aperture of the triplet (Q1-Q2-Q3) is the largest in the machine because of the value of the β function and the beam-separation; the diameter of this aperture can be computed using equation 2.6 [20]:

$$D_{\min} = \sqrt{\beta_{beat}}(B_s + 2B_e)\sigma + 2(d + O_e + M_t) \tag{2.6}$$

where B_e is the beam envelope, in general the envelopes for the two beams are different, for a first estimation the envelope is considered 8.5 σ because the collimation system can provide a clean beam beyond 8.5 σ. B_s is the beam separation and can be evaluated in 9.5 σ considering the crossing angle of 285 μrad and the quadratic increase of the beta function in the drift space. β_{beat} is the β-beating that is a function of several phenomena in the machine and gives an estimation of the possible error in the value of the β function. For LHC the β-beating is 20%. d is the spurious dispersion orbit; this quantity represents the variation of the orbit for

the off-momentum particles and for LHC it is estimated as 2.6 mm. O_e is the orbit excursion peak with respect to the center of the magnets: this value is 3 mm and it is due to the displacement of the orbit that is not centered. M_t is the mechanical tolerance in the production of the magnet and the beam pipe and it is estimated to be 1.6 mm. The maximum value of σ is 1.5 mm (Eq. 2.3) and it is reached when β function is 4500 m. The result is:

$$D_{\min} = \sqrt{1.2}(9.5+2\times 8.5)1.5 \text{ mm}+2(2.6 \text{ mm}+3 \text{ mm}+1.6 \text{ mm}) \approx 58 \text{ mm}. \quad (2.7)$$

The coils of the quadrupole are with a diameter bigger than 58 mm because of the thickness of the beam pipe, the beam screen and the helium pipe: the resulting aperture for the coils is 70 mm. The gradient produced by quadrupoles of the triplet is of 215 T/m, with a peak field in the coil of 8.6 T. These magnets are considered the state of the art for superconducting quadrupoles: it is not possible today to build a quadrupole with an higher gradient with the same aperture or a quadrupole with the same gradient but with a bigger aperture. This statement plays a fundamental role in the decision to explore other possibility than the replacement of the triplet for the luminosity upgrade of LHC as explained in the next chapter.

2.5 Luminosity of ATLAS and CMS

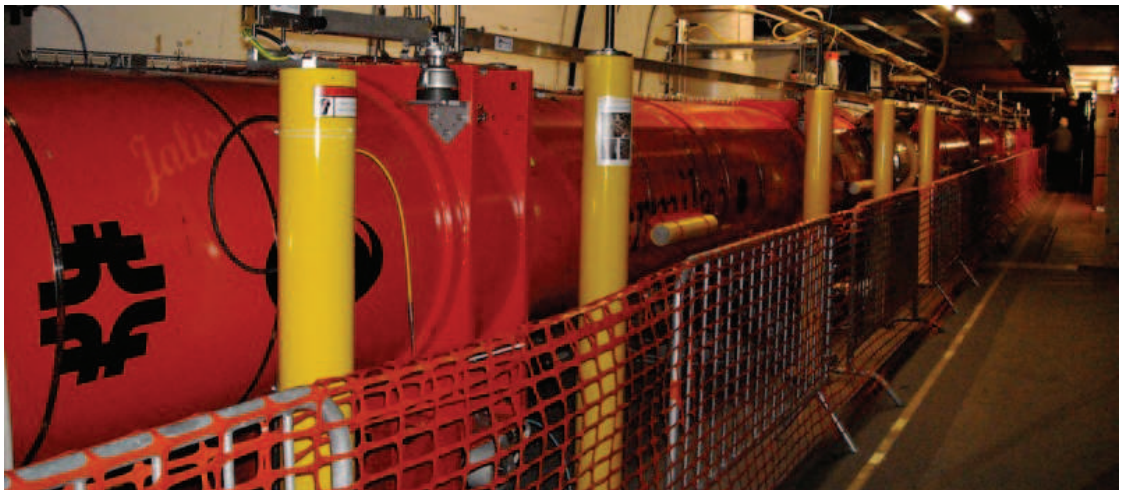

Figure 2.14: LHC Triplet.

LHC is a machine with a high luminosity, i.e. number of collisions per time unit and per area unit, in the two experiments ATLAS and CMS: 10^{34} cm^{-2}s^{-1}. A high

luminosity is required in order to explore rare events and to produce statistics to increase the precision of experiments. The peak luminosity is given by:

$$L = F\frac{\mathrm{n_b N_b^2 f_{rev}}}{4\pi\sigma^{*2}} \tag{2.8}$$

where $\mathrm{n_b}$ is the number of bunches circulating in the machine, $\mathrm{N_b}$ is the number of protons per bunch, $\mathrm{f_{rev}}$ is the revolution frequency of the machine and σ^* is the transverse RMS beam size at the collision point. The factor F is the geometrical factor, for a frontal collision (without crossing angle) this factor is 1, for small angles (like 285 μrad of LHC) the expression of geometrical factor is:

$$F \approx \frac{1}{\sqrt{1 + (\frac{\theta_c \sigma_z}{2\sigma^*})^2}} \tag{2.9}$$

and expresses how much is the luminosity loss due to the crossing angle. θ_c is the crossing angle and σ_z is the RMS bunch length. The evaluation of luminosity for LHC is resumed on Tab. 2.2.

Table 2.2: Beam parameters for LHC luminosity.

$\mathrm{n_b}$	2808
$\mathrm{N_b}$	1.15×10^{11}
$\mathrm{f_{rev}}$	11.245 khz
σ^*	16.7 μm
θ_c	285 μrad
σ_z	7.55 cm
F	0.84
L	10^{34} cm^{-2}s^{-1}

Starting from the peak luminosity it is possible to calculate the total luminosity that the experiments can see in a standard year of operations. This luminosity is function of many parameters, a simplified model is expressed by the following equations:

$$L_{\mathrm{int}} = L_{\mathrm{peak}}\tau_{\mathrm{L}}(1 - e^{-T_{\mathrm{run}}/\tau_{\mathrm{L}}}) \tag{2.10}$$

$$L_{\mathrm{tot}} = \frac{W_{\mathrm{days}} \times 24[\mathrm{h}]}{T_{\mathrm{run}}[\mathrm{h}] + \mathrm{T_{turnaround}}[\mathrm{h}]} L_{\mathrm{int}} \tag{2.11}$$

L_{int} is the integral of the peak luminosity in a run (T_{run}); the run is defined as the time between an injection and a dumping of the beam. During the run the

luminosity decreases exponentially due to the scattering of protons with protons (at the IPs), the scattering of protons with residual particles in the beam pipe (the vacuum is not absolute) and several other phenomena, for this reason the peak luminosity is scaled during the run time according to a parameter that is the luminosity lifetime (τ_{L}). The total luminosity (L_{tot}) experienced by detectors in one year is the luminosity of a run multiplied for the total number of runs in a year that is function of the number of working days (W_{days}) and the turnaround time ($T_{\mathrm{turnaround}}$), the time from the dumping of the beam and to the injection of a new beam.

All this parameters are functions of several events that are not always very well predictable before the first test of an accelerator (for example the instabilities of the machine can decrease significantly the beam lifetime, or the injection chain reacts well to the injection cycles so that the turnaround time is smaller than previsions). For LHC the parameters used to calculate the integrated luminosity and the total luminosity in one year are estimated extrapolating the experience of HERA [21], the the DESY electron-proton collider located in Hamburg, and the resulting data are resumed in Tab. 2.3.

Table 2.3: Beam parameters for LHC luminosity.

L_{peak}	10^{34} s^{-1}cm^{-2}
τ_{L}	14.9 h
T_{run}	$5.5 - 12$ h
W_{days}	200
$T_{\mathrm{turnaround}}$	$1.2 - 7$ h
L_{int}	~ 0.27 fb^{-1}
L_{tot}	~ 100 fb^{-1}

The evidence of the Higgs boson should be guaranteed by a total luminosity of 30 fb^{-1} [22], that is in four months of LHC operations at the nominal luminosity. In a reasonable scenario of beam commissioning and preliminary tests, LHC should reach its main goal before 2014, and for the further physics an upgrade of luminosity could be interesting to explore the unusual events discovered by LHC.

Many scenarios are possible to increase the luminosity: each term of equations 2.8 and 2.11 can be changed to increase the total luminosity of the machine. The main discussion about the luminosity upgrade took place during three workshops of the CARE-HHH (Coordinated Accelerator Research in Europe - High Energy High Intensity Hadron Beams) network: LHC-LUMI-05 (in Arcidosso, Italy), LHC-LUMI-06 (in Valencia, Spain) and IT '07 (in Frascati, Italy). During these workshops several ways of upgrade were considered:

- reduction of the turnaround time ($T_{\text{turnaround}}$ in Eq. 2.11): the turnaround time can be reduced with a faster injection chain, this requires major changes in the present accelerators (LINAC, PS and SPS) and it is a long term upgrade because of the cost and the time required [23];
- increase of the number of bunches circulating in the machine (n_b in Eq. 2.8) reducing the bunch space from 25 ns to 12.5 ns. This option was rejected during LHC-LUMI-06 due to the huge heat load of the cryogeny [24];
- increase of the number of protons per bunch (N_b in Eq. 2.8): this option, as the previous one, increases the current of the protons and the overall of energy absorbed by each component of the system such as collimation (for the collimation there is also a problem of impedance: the beam induces a parasitic current on the surface of the collimator that is made of resistive material and this generates an impedance on the beam), magnets, cryogeny etc. To obtain a reasonable ratio between heat load and increase of current the proposal is a 50 ns bunch space (double with respect to the nominal 25 ns) and 3 times the number of protons per bunch;
- increase of the geometrical factor (F in Eq. 2.8): the geometrical factor is mandatory to avoid the beam-beam effect in the shared regions of LHC. Each technique proposed to increase this factor is based on the possibility to workaround the beam-beam effect in some way, a proposal is to put a dipole inside the experiments very close to the IP (D0 option [25]), another is to tilt the bunch in order to provide a frontal collision (Crab Cavities option [26]), or simply to compensate the beam-beam effect with the field produced by a wire [27] or electron lenses [28].
- reduction of transversal beam size (σ^* in Eq. 2.8): the beam size at the IP is a consequence of the final focusing magnets in the interaction region (Q1-Q3 on Fig. 2.4) and these magnets should be replaced after a period of 7 years of nominal luminosity because of the damage produced by the back scattered radiations coming from the IP [29]. The proposal is to re-design the interaction region in order to reduce the size of the beam for the luminosity upgrade. The next chapter will be focused on this option and several studies will be presented about a new interaction region.

As general remark it is important to observe that the parameters involved in the luminosity are strictly correlated, for example the peak luminosity should increases quadratically with the decrease of the σ^* but a reduction of σ^* produces a larger beam inside the triplet and a large beam-beam effect. Thus, in order to keep constant the distance between the two beams, the crossing angle will be increased by means of a reduction of the geometrical factor. The final peak luminosity will not be quadratic in σ^* but will be linear at first approximation (Eq. 2.8 and 2.9). Moreover the increase in peak luminosity will consume the beam faster than in the

nominal condition and the luminosity lifetime τ_L will be smaller than the nominal one; in this situation LHC would be dumped and refilled more frequently and the integrated luminosity will not increase even linearly with σ^*.

Table 2.4: LHC Luminosity upgrade scenarios.

Parameter	**Unit**	**Early Separation**	**Large Piwinski Angle**
transverse emittance	ϵ [μm]	3.75	3.75
protons per bunch	N_b [10^{11}]	1.7	4.9
bunch spacing	Δt [ns]	25	50
beam current	I [A]	0.86	1.22
longitudinal profile		Gauss	Flat
rms bunch length	σ_z [cm]	7.55	11.8
β^* at IP 1 and 5	β^* [m]	0.08	0.25
full crossing angle	θ_c [μrad]	0	381
Piwinski parameter	$\phi = \theta_c \sigma_z / 2\sigma_x^*$	0	2.0
hourglass reduction		0.86	0.99
peak luminosity	L [10^{34}cm^{-2}s^{-1}]	15.5	10.7
peak events per crossing		294	403
initial luminosity lifetime	τ_L [h]	2.2	4.5
effective luminosity	L_{eff} [10^{34}cm^{-2}s^{-1}]	2.4	2.5
($T_{turnaround}$ = 10 h)	T_{run} [h]	6.6	9.5
effective luminosity	L_{eff} [10^{34}cm^{-2}s^{-1}]	3.6	3.5
($T_{turnaround}$ = 5 h)	T_{run} [h]	4.6	6.7
e-c heat SEY=1.4(1.3)	P [W/m]	1.04(0.59)	0.36(0.1)
SR heat load 4.6-20 K	P_{sr} [W/m]	0.25	0.36
image current heat	P_{ic} [W/m]	0.33	0.78
gas-s. 100 h (10 h) T_b	P_{gas} [W/m]	0.06(0.56)	0.09(0.9)
extent luminous region	σ_l	3.7	5.3
comment		D0 crab(+Q0)	Wire Compensation

Courtesy of Frank Zimmermann (LUMI '06).

The upgrade scenarios considered during the CARE-HHH workshops are in the number of two and all the relevant parameters are summarized in Tab. 2.4. The Early Separation is an upgrade based on the possibility to reduce the crossing angle up to 0 (and increase the geometrical factor to up to 1), the idea is to integrate a dipole (D0) into the experiments or to use an RF device (Crab Cavities) to tilt

the bunch and to cancel the crossing angle. The other option is the Large Piwinski Angle (defined as $\frac{\theta_c \sigma_z}{2\sigma^*}$, see Eq. 2.9) and it is based on an increase of beam current up to 1.22 A (more than two times the nominal one) with a bunch space of 50 ns. In this option the beam-beam effect is bigger than the nominal situation and requires a compensation with some devices such as a wire or electron lenses.

Both scenarios are good for luminosity upgrade only after a reduction of the β^*; the solutions presented in the next chapter are therefore valid for both scenarios.

2.6 Acceptance of TOTEM

LHC will provide beams for several different experiments, ATLAS and CMS are the biggest and will show the physics at 7 TeV of energy, but there are other experiments to see different behavior of high energy protons. One of these is the Total Cross Section Elastic Scattering and Diffraction Dissociation (TOTEM) that is designed to measure the total elastic scattering over a large range of four-momentum transfer and single diffractive scattering cross section in proton-proton collisions from 10 to 14 TeV center of mass energies [30].

The angle of collision of such particles with elastic or diffractive scattering is small and the particles, after the scattering, propagate inside the beam pipe following a trajectory that is close to the unperturbed beam. The differences between the beam particles and the scattered particles are in the angle and in the variation of momentum with respect to the nominal one ($\frac{\Delta P}{P}$): these two parameters are small and the scattered particles start to separate from the main beam at a distance of some hundred meters from IP. The TOTEM experiment is composed by several detectors called Roman Pots, placed at various distances from IP, the most important are at 220 and 420 m from IP. The optics is in Fig. 2.15

In this region the horizontal dispersion is not zero due to the bump used to create the crossing angle of 285 μrad. Because of the dispersion, the particles with a momentum lower than 6930 GeV/c can be deviated into the Roman Pot placed at 220 m from the IP. The horizontal distance between the Roman Pot and the closed orbit is 10 $\sigma + 0.5$ mm (1.21 mm).

This implies that the particles with an amplitude greater than 10 $\sigma + 0.5$ mm, calculated as the betatron oscillation plus the angular kick due to the elastic scattering plus the contribution of dispersion due to the energy loss in the diffractive scattering, are detected by the Roman Pot. The trajectory of a single particle is reconstructed and, in this way, it is possible to evaluate the elastic and diffractive cross section of the protons at 7 TeV. To understand which kind of particles the detector can see, two kinds of acceptances are defined:

- the first one is the number of particles detected by the Roman Pots versus the energy loss (Log($-\xi$) where ξ is the $\frac{\Delta P}{P}$ ratio of energy loss)

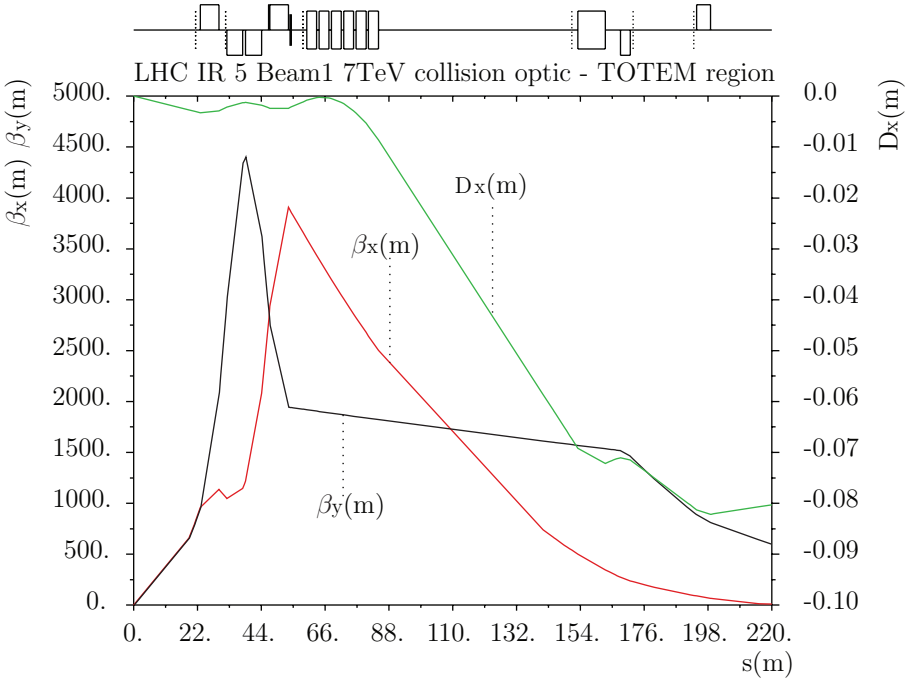

Figure 2.15: TOTEM optics, from IP5 to 220 m with $\beta^* = 0.55$ m and a full crossing angle of 285 μrad.

this acceptance is an estimation of the sensitivity of the Roman Pot in function of the energy loss in a diffractive scattering, for example: a particle with a $\mathrm{Log}(-\xi) = -1 \Longrightarrow \xi = \frac{\Delta \mathrm{P}}{\mathrm{P}} = 10^{-1} \Longrightarrow (P{=}7\ \mathrm{TeV})\ P_{\mathrm{diff}} = 6.3$ TeV has a probability of $\sim 94\%$ to be detected in the Roman Pot at 220 m from IP.

- the second acceptance is the number of particles detected by the Roman Pot versus the Lorentz-invariant Mandelstam variable t defined as the Minkowski norm of the four-momentum vector obtained with the difference between the four-momentum before the scattering and the four-momentum after the scattering [32]:

$$t = -\eta^{\mu\nu}(P_{\mathrm{orig}} - P_{\mathrm{scatt}})_\mu (P_{\mathrm{orig}} - P_{\mathrm{scatt}})_\nu \tag{2.12}$$

$$P = \begin{pmatrix} p_0 \\ p_1 \\ p_2 \\ p_3 \end{pmatrix} = \begin{pmatrix} -E \\ p_x \\ p_y \\ p_z \end{pmatrix} \tag{2.13}$$

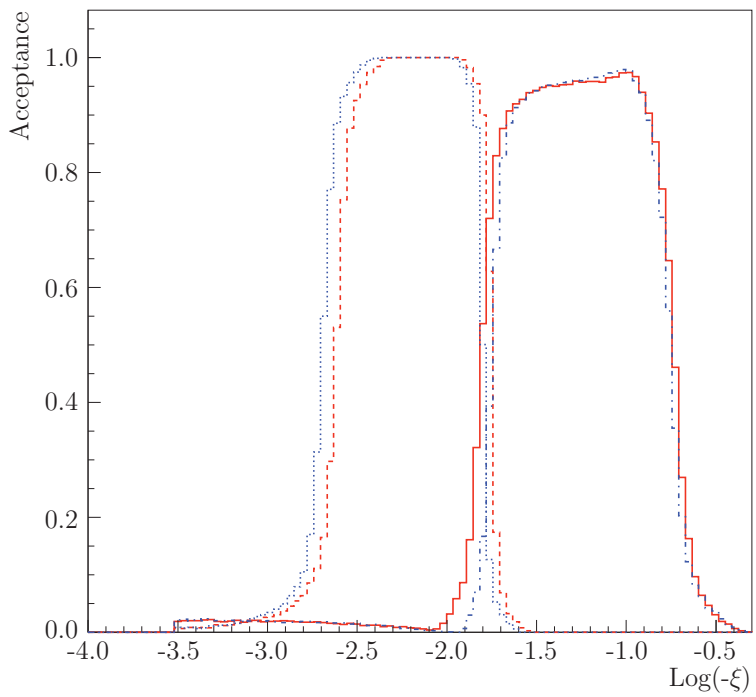

Figure 2.16: TOTEM acceptance vs $\log_{10}(-\xi)$: beam 1 station at 220 m (solid red) and 420 m (dashed-red) and beam2 station at 220 m (dashed-dotted blue) and 420 m (dotted-blue) (Fig. from [31]).

$$\eta^{\alpha\beta} = \begin{pmatrix} \frac{-1}{c^2} & 0 & 0 & 0 \\ 0 & 1 & 0 & 0 \\ 0 & 0 & 1 & 0 \\ 0 & 0 & 0 & 1 \end{pmatrix} \tag{2.14}$$

This acceptance is a general estimation of the sensitivity of the Roman Pot in function of many parameters of scattering: a particle can have a $\mathrm{Log}(-\mathrm{t}) = -1$ after an elastic scattering with a change in the direction of the four-momentum or after an energy loss due to a diffractive collision.

In Chapter 4 it will be illustrated how to increase the TOTEM's acceptance exploiting the properties of a crystal interacting with the beam. The attention will be focused especially on the acceptance vs. $\mathrm{Log}(-\xi)$ because it is easier to understand the crystal effect considering a single parameter of collision.

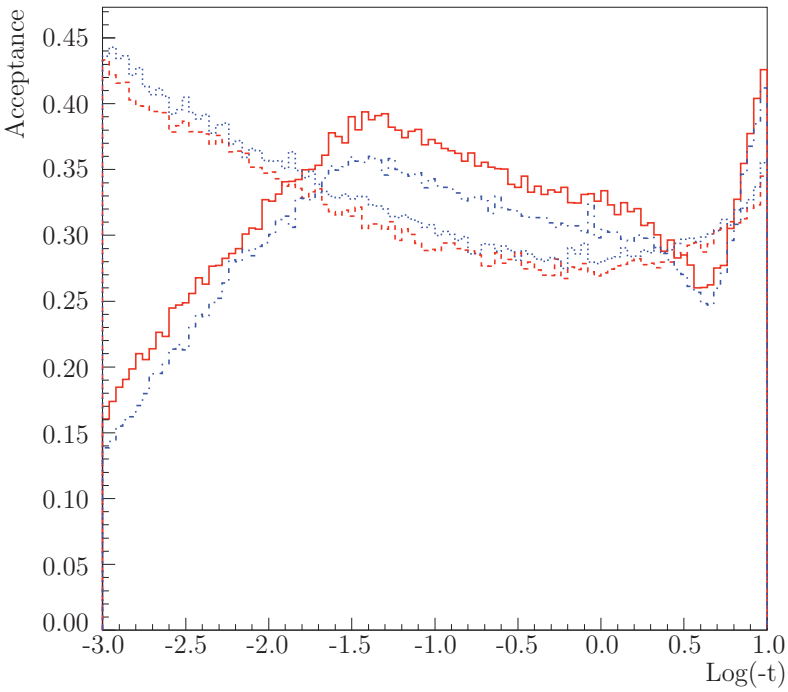

Figure 2.17: TOTEM acceptance vs $\log_{10}(-t)$: beam 1 station at 220 m (solid red) and 420 m (dashed-red) and beam2 station at 220 m (dashed-dotted blue) and 420 m (dotted-blue) (Fig. from [31]).

Chapter 3

Low β: how to reduce the beam size at the Interaction Point

3.1 Preliminary considerations

In the previous chapter it is defined the luminosity for a collider (Eq. 2.8), the parameters used in LHC (Tab. 2.2) and the reasons for a luminosity upgrade. The reduction of β^* is a requirement for every scenario of upgrade (Tab. 2.4) and this chapter shows different ideas for the reduction of the beam size at the IP.

The nominal optics v6.5 for LHC in collision, produce a $\beta^* = 0.55$ m and, for ATLAS and CMS, it is shown respectively in Fig. 2.11 and in Fig. 2.12. This optics is produced by the contribution of quadrupoles from Q1 to Q11 and is a solution for the differential equation [33]:

$$\frac{1}{2}\beta\beta'' - \frac{1}{4}\beta'^2 + K\beta^2 = 1 \tag{3.1}$$

$$\beta \equiv \beta(s), K \equiv K(s) \tag{3.2}$$

where β is the betatron function and K is the gradient of the quadrupoles normalized to the magnetic rigidity of the particles that, for LHC, is 23349.2 Tm. In general, for each quadrupole there are four differential equation like 3.1: one for each plane (horizontal and vertical) and one for each beam (in both directions), but the problem is symmetric for an exchange of direction and plane, so if a solution exists for beam1 this is also valid for beam2, the only difference is that the horizontal plane is exchanged with the vertical plane. Another effect of this symmetry is that the interaction region is symmetric with respect to the IP exchanging of the horizontal plane with the vertical plane from one side to the other of the IP. This means that it is possible to consider only one side of the IP and only one beam, and solve the Eq. 3.1 for this case preserving the generality of the problem.

Looking in detail the Interaction Region from IP to 70 m it is possible to see that the β function is as in Fig. 3.1 this function is generated from the nominal

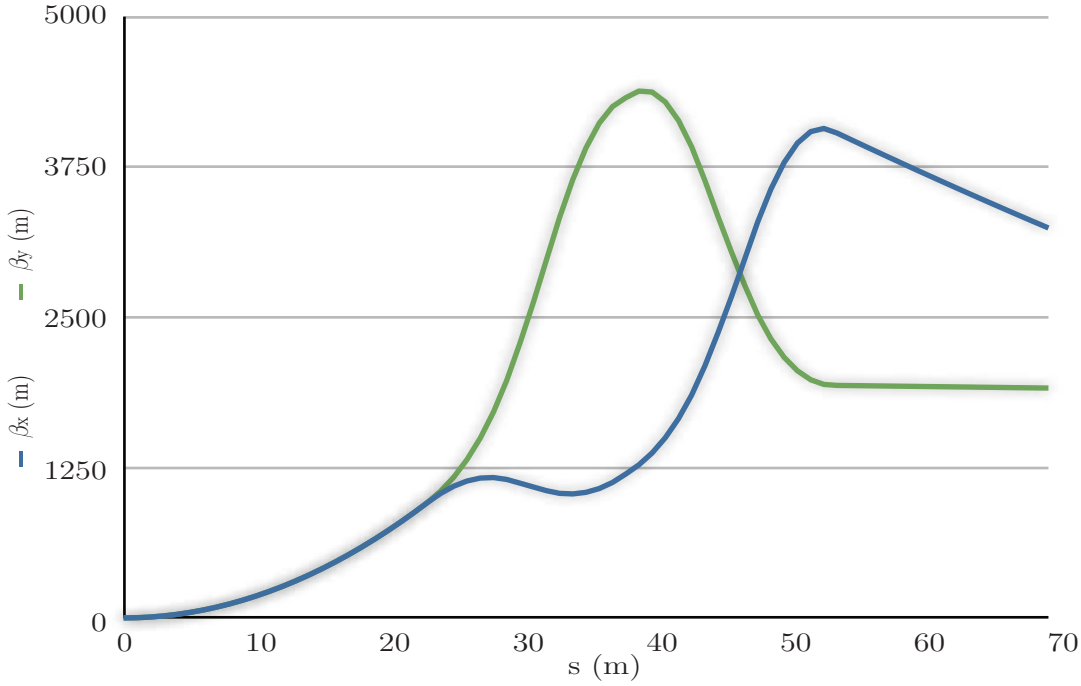

Figure 3.1: Nominal triplet with $\beta^* = 0.55$ m.

triplet (Q1-Q3) and is "matched" into the nominal LHC optics, this means that the quadrupoles from Q4 to Q11 are capable to take the horizontal and vertical β functions from the end of the triplet and connect they to the β functions at the entrance of the FODO cell.

The problem to design a new interaction region is, in general, to solve the equation 3.1 with the boundary conditions imposed at IP and before the matching section [34]. A first observation for equation 3.1 is that K is not a generic function of s but is, in general, a piecewise constant function: zero in a drift space, a positive or negative gradient for a focusing or defocusing quadrupole.

The boundary conditions for both β_x and β_y can be summarized as:

- the value of β^* (at IP) : the nominal is 0.55 m, the options for upgrade are for 0.25 and 0.15 m, a smaller β^* can be affected by the hourglass effect (whereby the transverse beam size depends on the longitudinal coordinate [35]) and a detailed study is necessary to explore β^* smaller than 0.15 m;
- the value of the beta slope at IP: the request is for a minimum, so the slope should be 0;
- the β function must be matched in the machine: the slope of the β functions

after the triplet must be negative (or at most zero) in order to enter in the matching section with a small value of the β function.

These requirements are general but are not enough to construct the interaction region because there is yet an uncertain in the choice of $K(s)$: how many quadrupoles can be used to build the best interaction region? The answer to this question depends on many factors: which technology is available for magnets, that is what is the maximum available gradient for a quadrupole; how much is the space available for magnets, how much is the radiation produced by collisions and how much of radiation can be tolerated by magnets with an appropriate shielding system, etc.

The best starting point is the present triplet of LHC that is the ultimate frontier for quadrupoles technology in a working accelerator. The geometric layout of triplet is shown in Fig. 3.2:

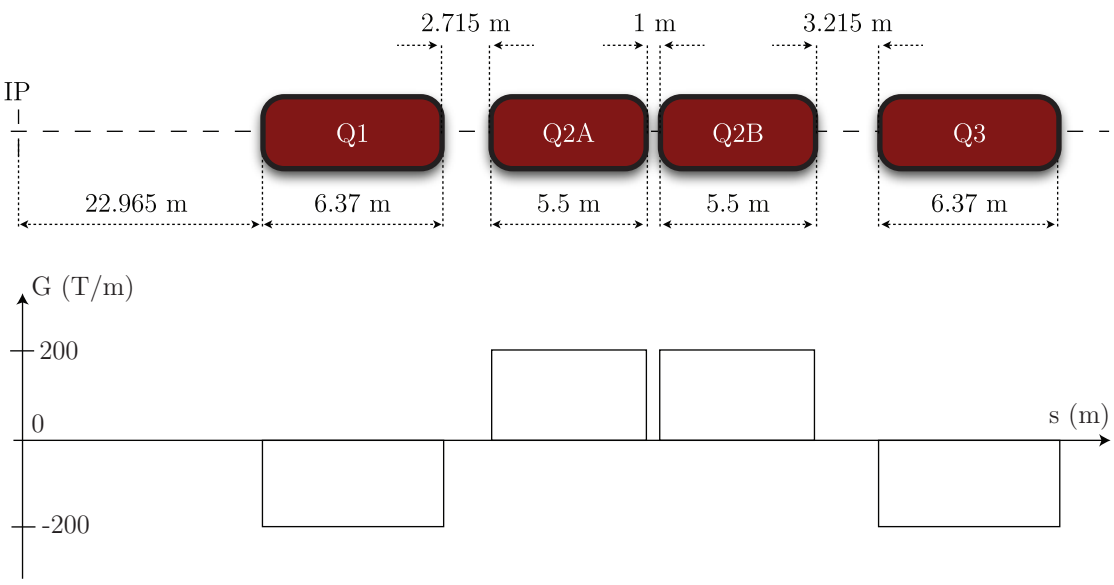

Figure 3.2: Nominal Triplet.

This triplet is capable of 200 T/m for the gradient and it is with an aperture of 70 mm. An increasing in aperture with the same gradient, or an increasing of gradient with the same aperture is considered impossible with Nb-Ti, the superconducting material used to build the nominal triplet. Other materials can be considered to build new magnets with larger aperture or greater field, as Nb_3Sn and this options will be considered in details later. This technological limit, together with the boundary conditions of the β function, is the base for the study of a luminosity upgrade for LHC.

As first example it is interesting to consider the nominal LHC triplet and a β^* of 0.25 m as initial condition. The resulting β function, without any change in $K(s)$, is in Fig. 3.3 The maximum value of the beta function ($\sim$ 9600 m) is double

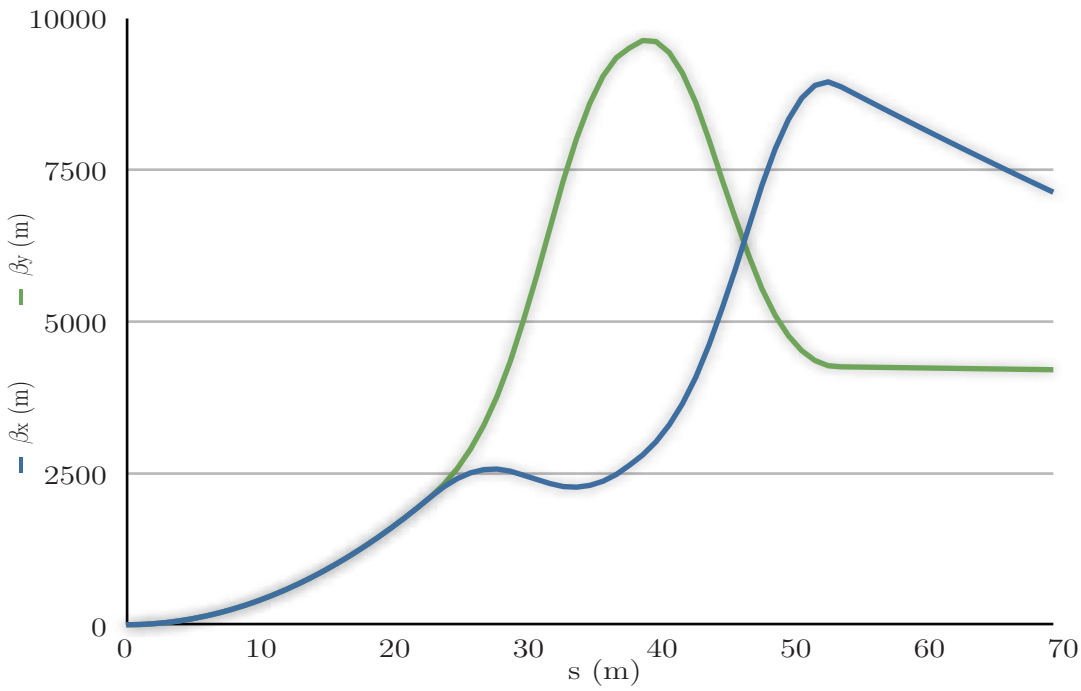

Figure 3.3: Nominal triplet with $\beta^* = 0.25$m.

with respect to the situation with $\beta^* = 0.55$ m, this behavior can be explained in a quite simple way using some approximation for the equation 3.1. First of all in a drift space the equation becomes:

$$\frac{1}{2}\beta\beta'' - \frac{1}{4}\beta'^2 = 1 \tag{3.3}$$

with the solution

$$\beta(s) = \frac{1}{16}\frac{(16+\alpha_0^2)s^2 - 8\alpha_0\beta_0 s + 16\beta_0^2}{\beta_0} \tag{3.4}$$

where $\alpha(s) = -\frac{1}{2}\beta'$ and α_0, β_0 are the initial conditions of the drift. In the case of LHC $\alpha_0 = 0$ and $\beta_0 = \beta^*$, and the solution becomes:

$$\beta(s) = \frac{s^2 + \beta^{*2}}{\beta^*} \tag{3.5}$$

when s is larger with respect to β^* (for LHC the drift in front of the triplet it is 23 m and $\beta^* = 0.55$ m) the value of $\beta(s)$ at the end of the drift is doubled when β^* is halved.

The second step is to show that the maximum of β inside the triplet is doubled when the value of the beta function is doubled at the beginning of the triplet. In this case the Eq. 3.1 can be rewritten as:

$$\omega(s) = \sqrt{\beta(s)} \tag{3.6}$$

$$\omega'' + K(s)\omega = \frac{1}{\omega^3} \tag{3.7}$$

for large values of β, i.e. when $\frac{1}{\omega^3}$ is negligible, the equation 3.7 becomes linear and homogeneous in ω and if the initial condition becomes double all the values assumed by $\beta(s)$ are double.

3.2 Triplet at 13m

Considering again the values for LHC the situation obtained with a $\beta^* = 0.25$ m is illustrated in Fig. 3.3. The equation 2.6 tells that the aperture of the magnets have to increase, roughly, with the square root of the maximum of β that, in this case, is $\sqrt{2}$.

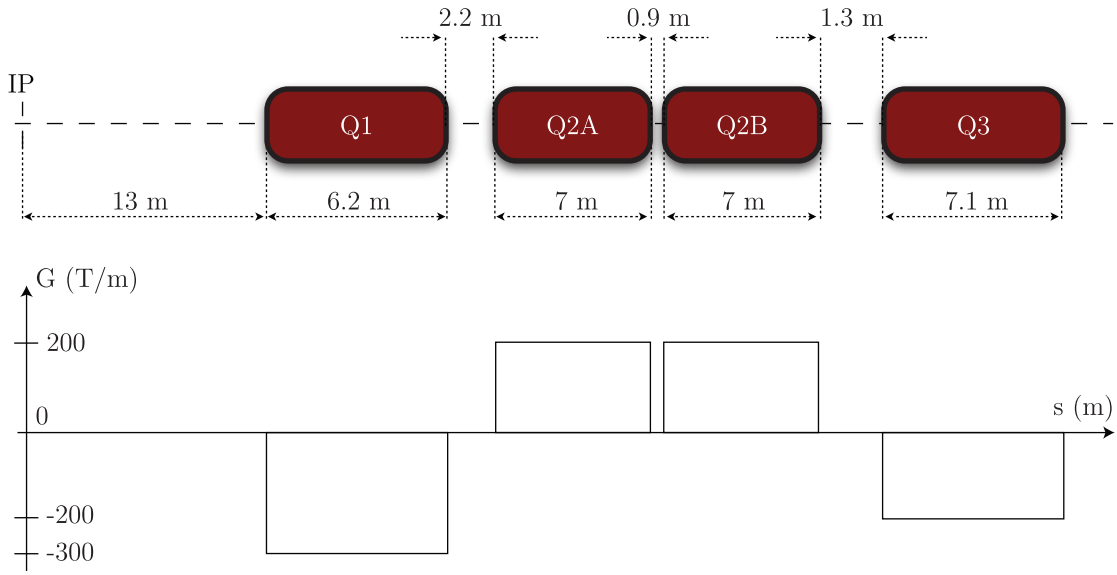

Figure 3.4: Triplet at 13 m.

Thus, leaving unchanged the gradients of the triplet (K(s)) the condition of $\beta^* = 0.25$ m requires a triplet with an aperture of ~ 84 mm instead of 70 mm (see Eq. 2.6, Eq. 2.7 and [3]). As already told this aperture is too large for a gradient of 200 T/m and this is the reason why the nominal triplet cannot provide a β^* smaller than 0.55 m.

To avoid this problem a first step can be to reduce the l^* (the distance from IP to Q1) down to 13 meters as shown in Fig. 3.4. In order to satisfy the conditions of matchability as the negative slope of the β function after the triplet, the triplet is changed in lengths, gradients and apertures with a maximum gradient (Q1) of 300 T/m, and a maximum aperture (Q2) of 72 mm because the maximum β is 5630 m.

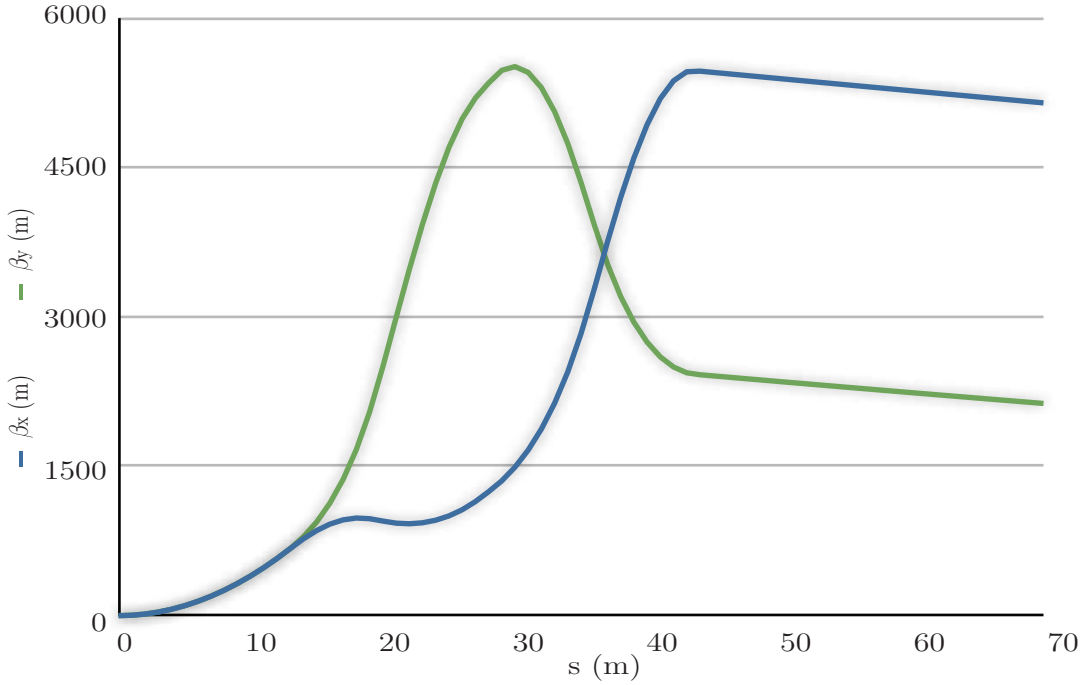

Figure 3.5: A triplet at 13 m from IP with $\beta^* = 0.25$ m.

The β function is shown in Fig. 3.5 The advantage of this solution is that the quadrupole with the largest gradient (Q1) is placed at 13 m where the β function is relatively low and, in fact, the maximum value of the β function inside Q1 is 1475 m that requires an aperture of 52 mm. A quadrupole with a gradient of 300 T/m and an aperture of 52 mm is theoretically possible with Nb-Ti but it is challenging because of the gradient of 300 T/m; moreover the other quadrupoles of the triplet (Q2 and Q3) have to be replaced to fit the requirements of the interaction region.

The solution with l^* at 13 m is interesting but can be improved using another

idea as shown in the next pages: the so-called Q0. For this solution it will be investigated also the gain in chromaticity with respect to the triplet presented in this section, will also be shown the issues and the solutions related to the integrability of magnets at 13 m from IP, that is inside the experiments.

3.3 Q0

In the previous section some considerations were presented about what happens to the β function when the β^* is reduced, and the central point is that with the same K, that is with the same configuration of quadrupoles, it is not possible to decrease the β^*.

The first alternative proposed is to reduce l^* in order to intercept the β function when it is not big and exploit this condition to have a smaller maximum β inside the triplet with a consequent small increase in the triplet aperture. The next step is to continue on the way of $l^* = 13$ m but with an optimized layout.

Before continue in the exploration of Q0 solution it is important to point out two questions that have to be clarified before the next discussion: the first question is why the present l^* is 23 m and not already 13 m if at 13 m it is possible to have a better squeezed beam? The answare can be preliminary shown with two pictures, Fig. 3.6 and Fig. 3.7.

Here it is possible to see that 13 m is not a free region but it is already inside the experiments, this means that to put a magnet at 13 m is not for free but there is an impact on experiments and several issues to overcome from the point of view of the quadrupoles like energy deposition and misalignments. These issues will be explored in detail in the next sections.

The second question is: what does it mean to optimize an interaction region? The answer can be analyzed from several point of view, for example an optimization can be to build a triplet with magnets of the same length, same aperture and same field. This layout optimizes the cost of the triplet because to build several times the same magnet is cheaper than produce different magnets, and also to have the same field permits to use only one power supply for the triplet with a reduced impact of the support structure for the quadrupoles like cables and pipes.

The optimization considered for Q0 is in term of aperture, the request is to preserve the nominal structure of the triplet (Fig. 3.2) and to add two quadrupoles (Q0A and Q0B) in front of this triplet in order to gain a factor 2 or more in β^*.

The idea of Q0 [1] is to break the quadratic behavior of the β function in the drift in front of the triplet in order to join the behavior of the β function with $\beta^* = 0.25$ m and the nominal β function, with $\beta^* = 0.55$ m, that enters in the triplet as shown in Fig. 3.8

To obtain this effect a doublet is placed before the triplet, and the optical

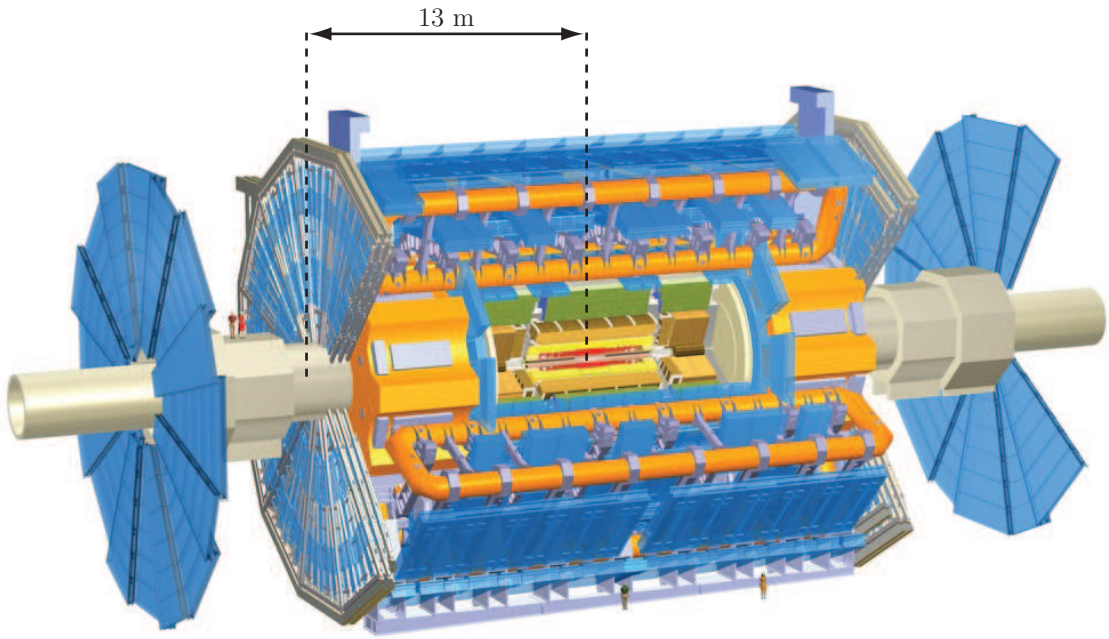

Figure 3.6: 13 m from IP in ATLAS.

layout is shown in Fig. 3.9. The triplet behind the Q0 is mostly unchanged (Fig. 3.2) and the corresponding β function is in Fig. 3.10.

The maximum value for the β function is 5700 m that corresponds to an aperture of $\sim$ 75 mm, the resulting parameters for the new interaction region are in Tab. 3.1. The result is an interaction region with $\beta^* = 0.25$ m, that is a gain of a factor 2 in luminosity if a beam-beam compensation scheme is applied, with magnet parameters compatible with NbTi technology and, in particular, with a triplet close to the nominal one.

Table 3.1: Q0 layout at $\beta^* = 0.25$ m.

Magnet	β Max [m]	D_{min} [mm]	G (T/m)	Peak Field (T)
Q0A	2300	60	240	7.1
Q0B	4300	70	196	6.8
Q1	5700	75	200	7.5
Q2	5700	75	200	7.5
Q3	5700	75	160	6.0

The behavior of the β function at the end of the triplet is close to the nominal

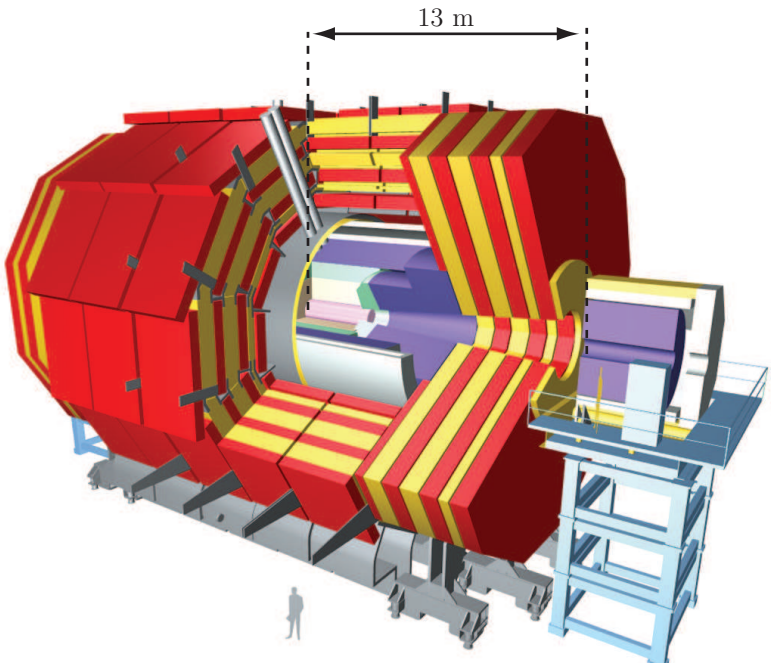

Figure 3.7: 13 m from IP in CMS.

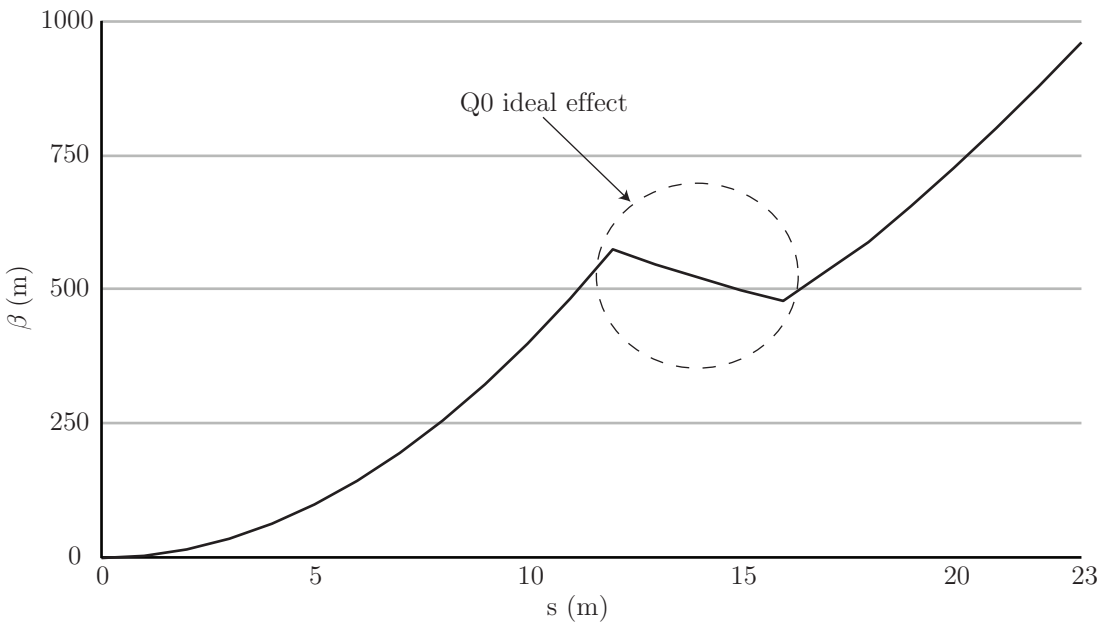

Figure 3.8: Q0 ideal behavior.

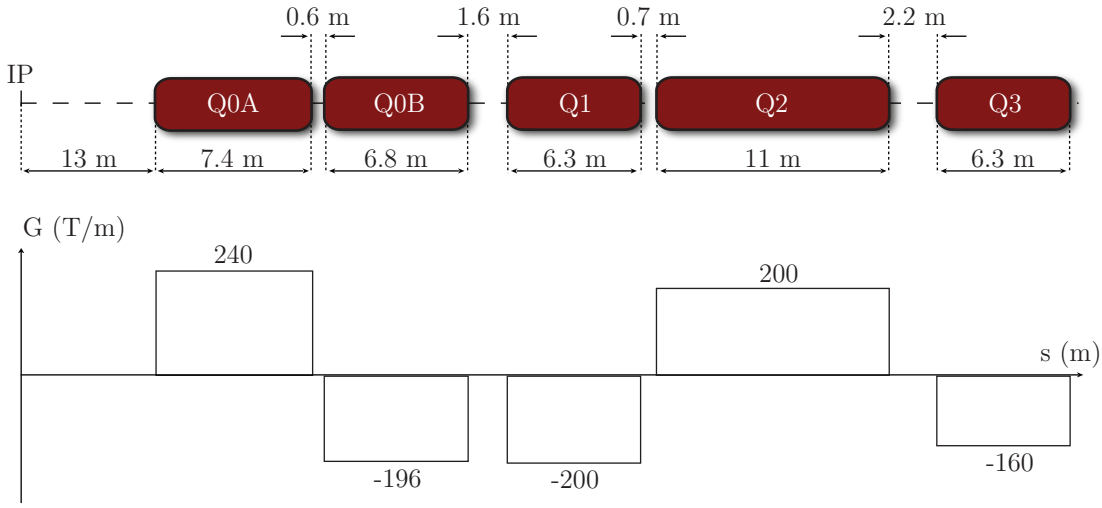

Figure 3.9: Q0 layout.

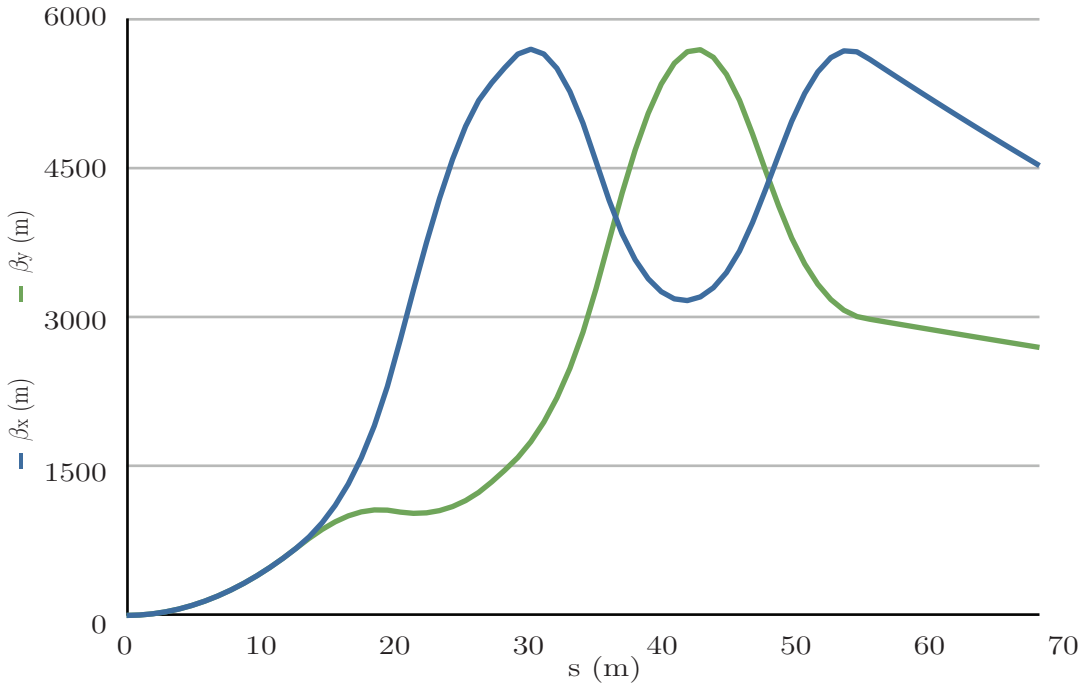

Figure 3.10: Q0 at 13 m from IP with $\beta^* = 0.25$ m.

one, so this solution can be matched in the nominal LHC optics without major problems for the matching section, the resulting optics for the interaction region

produced by MadX is shown in Fig. 3.11.

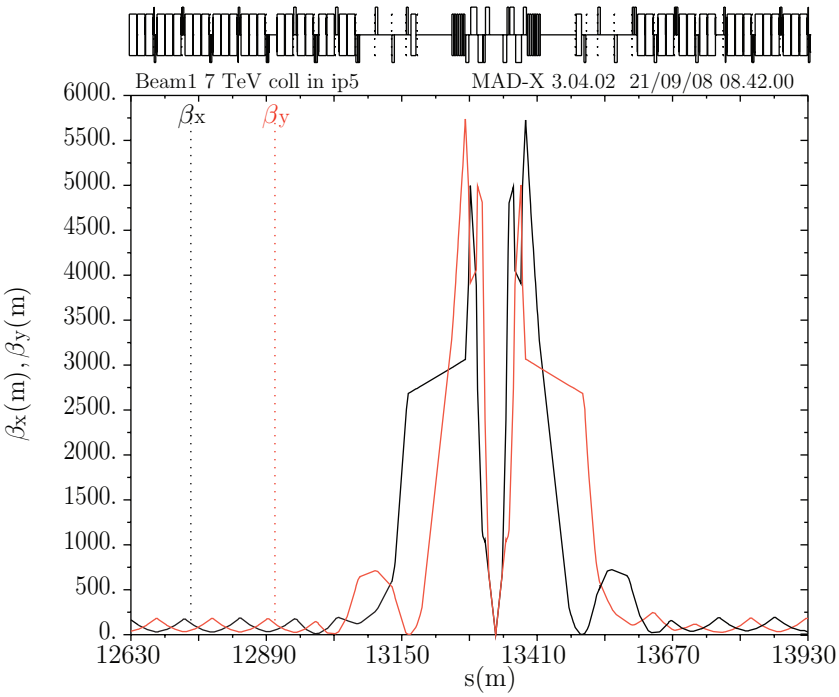

Figure 3.11: MadX optics for Q0 at $\beta^* = 0.25$ m (IP5).

The Q0 solution produces an optics that can keep under control the maximum value of β and the advantage is not only in terms of aperture but also from the point of view of chromaticity. The first-order chromaticity contribution of the interaction region is dominated by the effect of a large β function (see Eqs. 3.8 3.9 [18]) and the advantages of Q0 are resumed in Tab. 3.2.

$$\xi_x = -\frac{1}{4\pi}\int K(s)\beta_x(s)ds \tag{3.8}$$

$$\xi_y = \frac{1}{4\pi}\int K(s)\beta_y(s)ds \tag{3.9}$$

The squeezing ramp up from injection to collision of Q0 is not far from the nominal squeeze solution because when Q0A and Q0B are switched off the interaction region is the same as the nominal one, and the matching section is unchanged. The only difference, during the squeeze, is the tune of the machine because, with four more quadrupoles (two Q0s per each side) the phase advance changes. The detuned optics is in Fig. 3.12.

The quadrupoles from Q4 to Q11 are used to match the squeezing of the beam from injection to collision: the beam accelerate from 450 GeV to 7 TeV and the

Table 3.2: Q0 summary for β^*=0.25 m.

	Q0	**Triplet 13 m**	**Nominal**
Max β [m]	5700	5630	9673
Max Aperture [mm]	75	72	84
IR Chromaticity	−22.92	-19.45	−28.12
Peak Field [T/m]	7.5	7.8	8.3

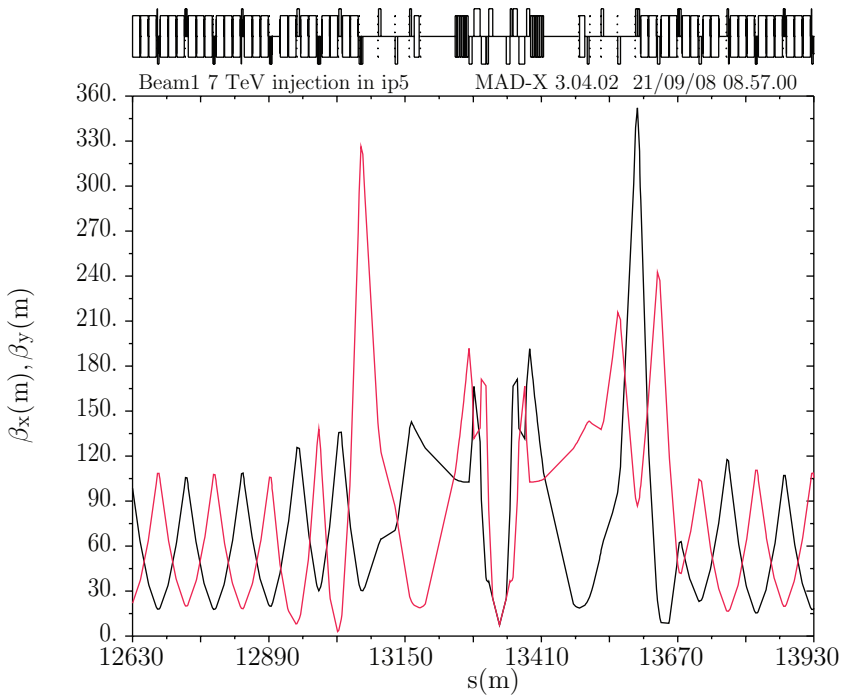

Figure 3.12: Q0 optics at injection.

β^* goes from 10 m to 0.25 m. The requests in term of aperture are the same as the nominal interaction region because the matching section is already designed to match an optics with β^* of 0.25 m.

A constraint for superconducting magnets is to work with a minimum operating current, that means the current, during the ramp, it cannot cross the zero line and consequently cannot changes the value of the gradient from positive to negative or from negative to positive.

The reasons for this limit are because a technological design and the intrinsic behavior of the superconducting magnets: a magnet presents an hysteresis cycle and when the current is fully discharged the field is not zero and this means that the parasitic current into the coils is not zero. From the other point of view the

power supply have to establish the circulating current into the coils in order to know how to correctly power the magnet to reach the desired magnetic field. If the power supply is not powering it should be read a zero difference of potential between the coils and the ground, but the parasitic current will generate a different value of voltage and the power supply should have to compensate in some way to reach the zero voltage. This compensation depends on the previous magnetization and is not always the same. Of course a power supply that can take into account this behavior can be designed but it is more complex and for LHC the choice was for a power system with a lower limit of current.

The changes in the gradients for Q4-Q11 from injection to collision is in Fig. 3.13.

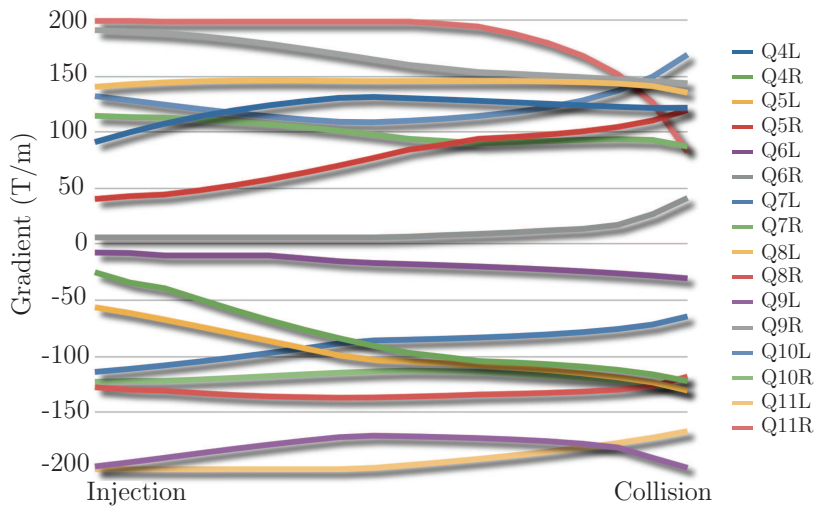

Figure 3.13: Gradients of IR magnets during the squeezing.

In the preliminary considerations of this chapter was expressed the idea that a reduction in β^* is almost linearly related to an increases in the maximum β function. Following this idea can be interesting to push more the Q0 scheme and to see what happens when β^* goes to 0.15 m, that is a potential gain of a factor 4 (or more, it depends on the beam-beam compensation method), the resulting β function is in Fig. 3.14 and the corresponding parameters are in Tab. 3.3

Here it is possible to note that the Q0 solution with $\beta^* = 0.15$ m is very close to the situation of a triplet at 23 m with a $\beta^* = 0.25$ m. This consideration assumes

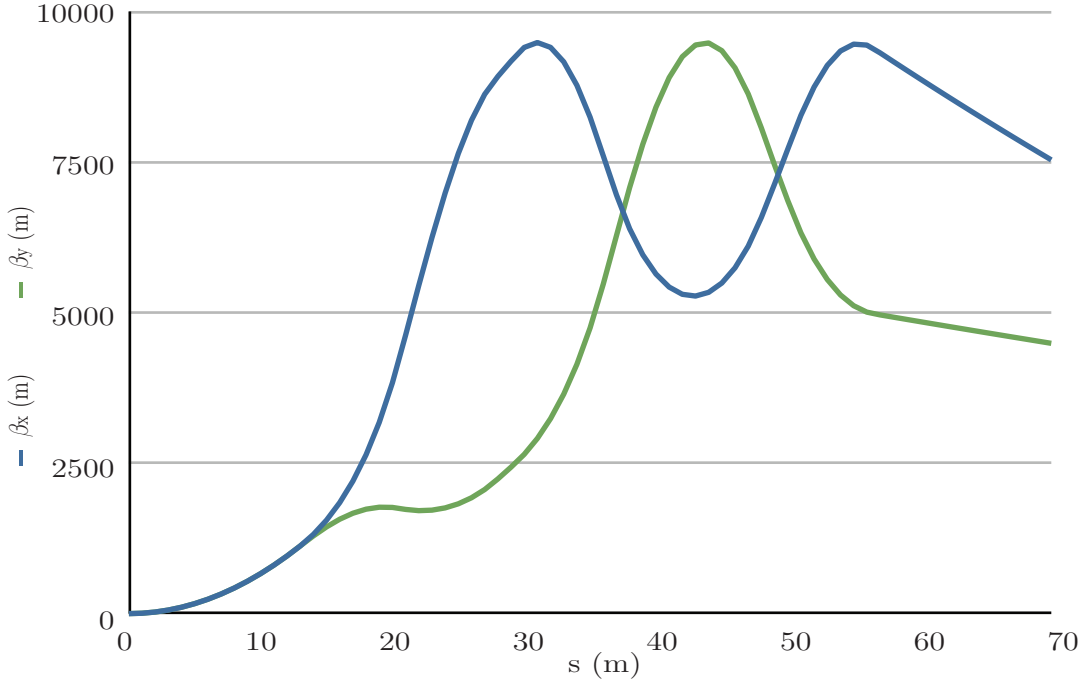

Figure 3.14: Q0 at 13 m from IP with $\beta^* = 0.15$ m.

Table 3.3: Q0 summary for β^*=0.15 m.

	Q0	**Triplet 13 m**	**Nominal**
Max β [m]	9511	9383	16120
Max Aperture [mm]	84	82	95.61
IR Chromaticity	−38.2	-32.41	−46.87
Peak Field [T/m]	8.3	8.7	9.6

particular relevance in the framework of the LHC Phase-I upgrade [36] where a new triplet at 23 m, with large aperture, and increased length, will replace the present triplet to push the β^* up to 0.25 m. In this scenario the Q0 solution can be used to reduce the β^* up to 0.15 m without further increases in the triplet aperture.

3.4 Alignment

The Q0 optics is with a distance of 13 m from IP. As already told this distance is inside the detectors and not on the tunnel, some issues due to the installation problems should be considered in order to understand the feasibility of an optical

solution at 13 m.

A known problem for an interaction region is the stability of the alignment for quadrupoles that have to manage large β functions [37]. This issue is of particular relevance in an environment that can be unstable; in the ordinary tunnel the basement of quadrupoles is made by concrete and can sustain huge masses without relevant movements, but at 13 m from IP there is no concrete ground and the magnet should be fixed in a different way.

A quadrupole misaligned creates a dipolar component that provokes a kick and, consequently, a change in the closed orbit. For the evaluation of the shift $\delta_x(s)$ (for example in the horizontal plane, but the description for the vertical plane is the same) that the particles will have with respect to the reference orbit, it is possible to consider the Eq. 3.10 valid in the approximation that a quadrupole is a thin object (thin lens approximation):

$$\delta_x(s) = \frac{\sqrt{\beta_x(s)}}{2\sin(\pi Q_x)} \left[\sum_i \left(\theta \sqrt{\beta_x} \right)_i \cos\left(\pi Q_x - |\Delta\mu_i|\right) \right] \tag{3.10}$$

The index i is used to take into account the contributions of several misaligned quadrupoles. The angle θ_i is defined as $K_i l_i \Delta x_i$ with K_i the gradient for the quadrupole, l_i the length of the quadrupole and Δx_i the displacement in the horizontal plane. The β_{x_i} is the value of the β function in the horizontal plane assumed inside the magnet; of course this value is not constant and this is the reason of thin lens approximation, in this approximation the value of β is well defined. Q_x is the tune of the machine and $\Delta\mu_i = \mu_x(s) - \mu_x(s_i)$ is the phase advance due to the quadrupole.

The parameters for Q0 layout are resumed in Tab. 3.4 the sign of the displacement is related to the sign of the gradient (for convention is positive in the horizontal plane for the beam1) and the direction of the beam.

Table 3.4: Q0 layout at $\beta^* = 0.25$ m.

Magnet	K [m^{-2}]	l [m]	β_x [m]	Q_x	$\Delta\mu$	$\delta_x(s)$ [m]
Q0A	0.0102	7.4	2300	64.31	$\frac{\pi}{2}$	$1.81\sqrt{\beta(s)}\Delta x$
Q0B	−0.0084	6.8	4300	64.31	$\frac{\pi}{2}$	$-1.87\sqrt{\beta(s)}\Delta x$
Q1	−0.0085	6.3	5700	64.31	$\frac{\pi}{2}$	$-2.02\sqrt{\beta(s)}\Delta x$
Q2	0.0085	11	5700	64.31	$\frac{\pi}{2}$	$3.53\sqrt{\beta(s)}\Delta x$
Q3	−0.0068	6.3	5700	64.31	$\frac{\pi}{2}$	$-1.62\sqrt{\beta(s)}\Delta x$

For example a displacement $\Delta x = 50$ μm for Q0A generate a shift in the triplet (when $\beta(s) = 5700$ m) of 6.8 mm. This is unacceptable from the point of view of

the aperture because with 6.8 mm of displacement the beam collides on the beam pipe and the coils.

However that's not the only problem due to misalignment: consider a displacement of 17 μm that corresponds, in the triplet, to a shift of 2.4 mm that is close to the mechanical tolerance and, maybe, can be tolerated; if the misalignment is estimated at the IP ($\beta = 0.25$ m) the value for $\delta_x(s)$ is 16 μm. The beam size at IP (as beam size it is considered the amplitude of σ) is about 11.2 μm, that means that the core of the beam is completely displaced with respect to the point of collision and the luminosity is almost zero.

To solve this problem it is important to consider the sign of the displacement, for example the sign of Q0A is opposite the sign of Q0B and the magnitude is almost the same. If Q0A and Q0B are mounted in a rigid structure a displacement of Δx will be positive for Q0A and negative for Q0B and, at the end, it will be compensated. To obtain a shift of 16 μm at the IP the displacement of Q0A and Q0B must be of 500 μm, that is 30 times bigger than with a relative misalignment. The tolerances are resumed in Fig. 3.15

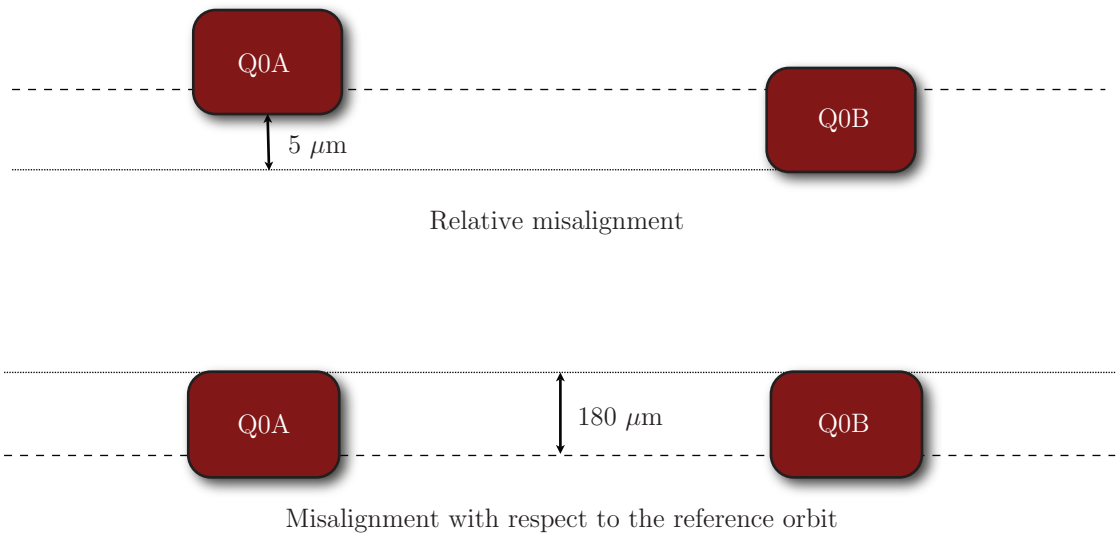

Figure 3.15: Misalignment tolerances for Q0.

The issue of misalignment can be solved with a rigid structure that prevents vibrations greater than few μm and with a scheme of correctors that correct the systematic errors of alignments due to the precision limit of the instrumentation used to align the magnet in the tunnel.

3.5 Energy Deposition

An important issue to consider for Q0 is the energy deposition: the interaction point is an hot spot that generates particles in any direction; a large amount of this particles are with small angle with respect to the beam trajectory and the result is a shower of particles that collide with the magnet (Q0A and B), in particular with the superconducting coils, increasing the temperature of the cable over the limit of the quench.

The way to estimate the energy deposition on the magnet is to create a geometrical model of the magnet, a model for the collision at IP and to implement these models in a Montecarlo simulator that can generates the events and simulate the interaction of particles with matter. The tool used for the Q0 simulation is the fully integrated particle physics Montecarlo simulation package FLUKA [9].

In this simulator it is possible to define the geometry of the object as intersection of simple 3D geometrical figure; to simulate a magnet the best choice is to use concentrical cylinders in order to respect the symmetry of a magnet.

The model used for Q0A and Q0B is as presented in Fig. 3.16 and the geometrical parameters are resumed in Tab. 3.5 and Tab. 3.6. The superconducting cable is schematized with a cylinder made of copper (the cable is in fact in a matrix of copper and as a first approximation can be considered made of copper) with a thickness of 60 mm. The cylinder is divided into four layers of 15 mm, each layer is a superconducting cable that create a coil. This four-layers design is the same used for MQXA magnets (Q1 and Q3 quadrupoles in the triplet) [10].

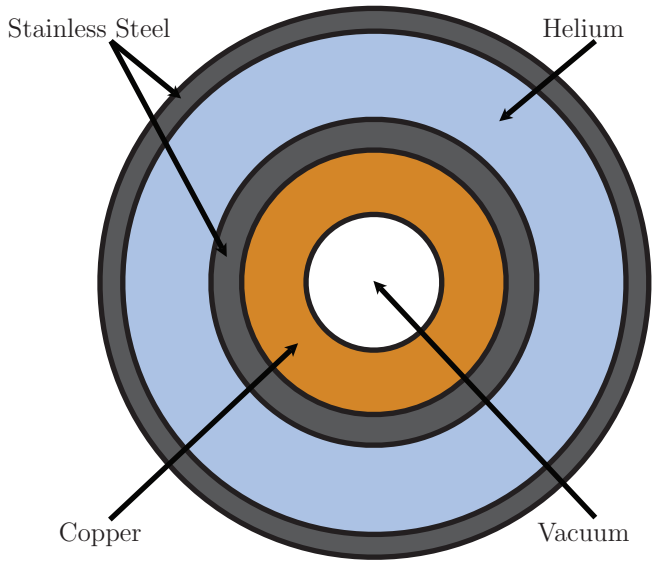

Figure 3.16: Q0 schematization for FLUKA simulation.

Table 3.5: Geometry of Q0A considered in the FLUKA model.

Vacuum	0 - 30 mm
Copper	30 - 90 mm
Iron Yoke (Stainless Steel)	90 - 150 mm
Helium	150 - 260 mm
External structure (Stainless Steel)	260 - 280 mm

Table 3.6: Geometry of Q0B considered in the FLUKA model.

Vacuum	0 - 35 mm
Copper	35 - 95 mm
Iron Yoke (Stainless Steel)	95 - 155 mm
Helium	155 - 260 mm
External structure (Stainless Steel)	260 - 280 mm

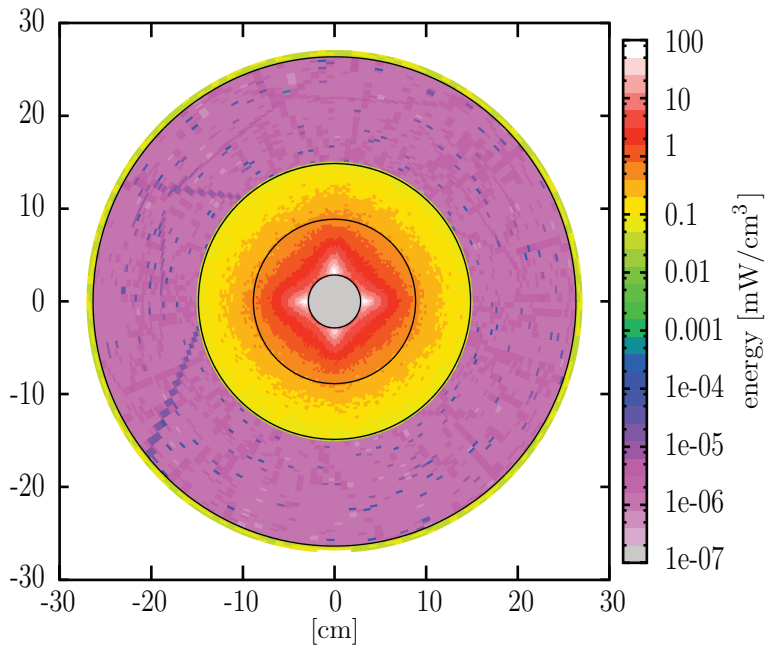

Figure 3.17: Q0A cross section energy deposition.

As event generator FLUKA use the DPMJET code [38] that is a MonteCarlo event generator. The primaries passed to DPMJET are protons with the nom-

inal parameters: 7 TeV/c of total momentum and 285 μrad of full crossing angle. The energy deposition per crossing is scaled considering a peak luminosity of 10^{35} cm^{-1}s^{-1} that is the luminosity with an upgrade of a factor 10 with respect to the nominal condition. The resulting energy deposition plot is shown in Fig. 3.17.

This picture is the power per unit of volume averaged along the length of Q0A quadrupole considered in IP1. The first observation is that the peak energy is on the coils and it is around 100 mW/cm^3 (the four white spots; the small vertical asymmetry on the peaks is due to the crossing angle that in IP1 is vertical). This power is considered far from the maximum energy tolerated by a cryogenic system for superconducting magnets: the maximum energy tolerated by Nb-Ti is 4.3 mW/cm^3 and for Nb_3Sn is 12 mW/cm^3 [29]. An energy deposition that overcomes these values, and for Q0 the energy deposition is ten times greater than the highest limit, produce a quench in superconductor and the magnet will not be anymore superconductive.

A shielding structure is mandatory to preserve the coils from the energy deposited by particles: a solution proposed in [4] and [39] is to insert a tungsten liner between the vacuum pipe and the coils. The resulting layout is in Fig. 3.18.

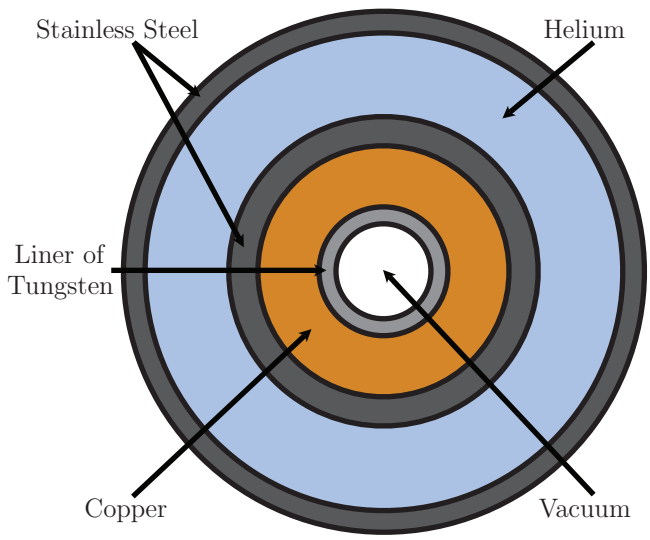

Figure 3.18: Q0 schematization with liner for FLUKA simulation.

The liner is 10 mm thick and the new geometry for Q0A and Q0B is presented in Tab. 3.7 and Tab. 3.8. From the point of view of the primaries the configuration is the same as in the case without liner; the resulting energy deposition is in shown in Fig. 3.19.

This picture is like the 3.17 but the binning is emphasized to show the difference between liner and cables: the energy peak of 100 mW/cm^3 is inside the tungsten

Table 3.7: Geometry of Q0A with Liner considered in the FLUKA model.

Vacuum	0 - 30 mm
Liner	30 - 40 mm
Copper	40 - 100 mm
Iron Yoke (Stainless Steel)	100 - 160 mm
Helium	160 - 260 mm
External structure (Stainless Steel)	260 - 280 mm

Table 3.8: Geometry of Q0B with Liner considered in the FLUKA model.

Vacuum	0 - 35 mm
Liner	35 - 45 mm
Copper	45 - 105 mm
Iron Yoke (Stainless Steel)	105 - 165 mm
Helium	165 - 260 mm
External structure (Stainless Steel)	260 - 280 mm

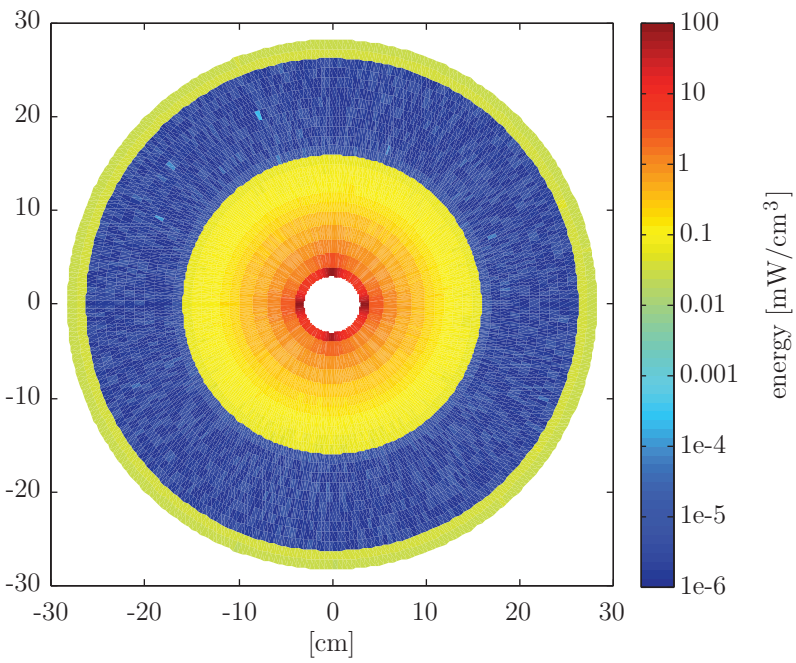

Figure 3.19: Q0 cross section energy deposition with liner.

and the power absorbed by the coils decreases rapidly with the distance from the liner.

The most irradiated cable is the inner one with a peak of power around 10 mW/cm^3, that is compatible with a layout based on Nb_3Sn material. The peak of power along the cable is represented in Fig. 3.20

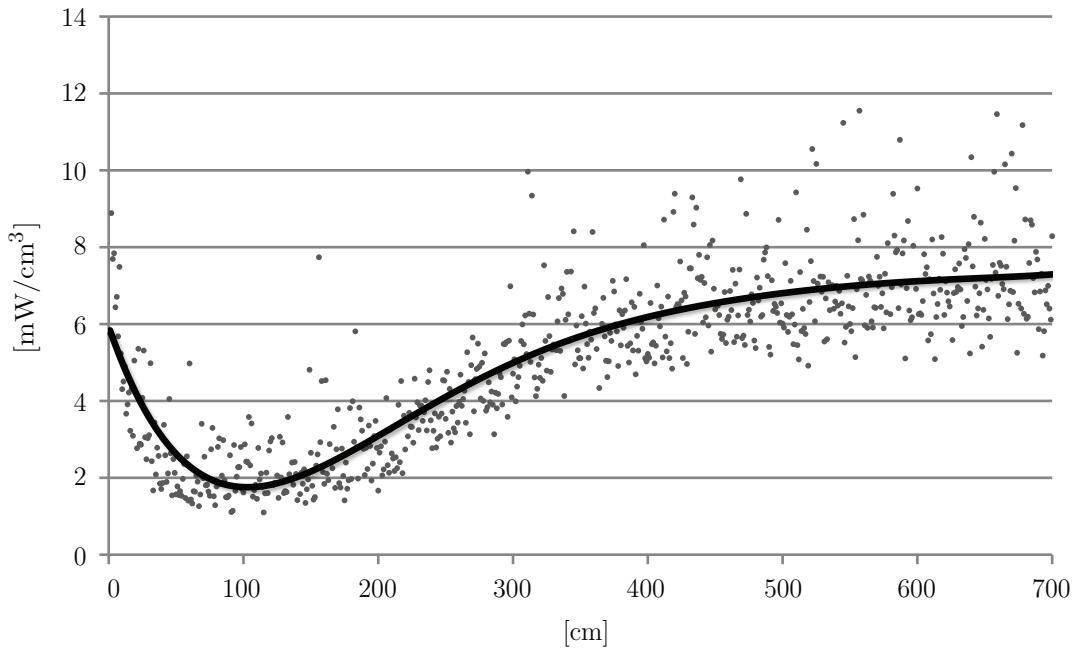

Figure 3.20: Peak of energy deposition in the first cable of Q0A with liner.

The trendline of the power is below 8 mW/cm^3 and this confirm that the shielding with liner seems to protect the cable from the large part of the particles. The decreasing of the power in the first 100 cm of cable is due to the high energy component of the shower: there are many particles with an energy that permit a penetration in the coil without significant increasing in the energy. The mean free path for this particles is around 400 cm, that is compatible with the plot.

For Q0B the situation is better than for Q0A because a large part of particles are already absorbed by Q0A (by the tungsten shield) and the peak of the power is not greater than 6.5 mW/cm^3. The resulting plot of power in the first cable of Q0B is in Fig. 3.21

The Q0 optics can be useful for the luminosity upgrade of LHC (Phase-II upgrade) to keep under control the beta function inside the triplet. This optics is also a good candidate as extremely pushed optics ($\beta^* = 0.15$ m) because it does not suffer of the known problems of aperture and chromaticity. The issues related

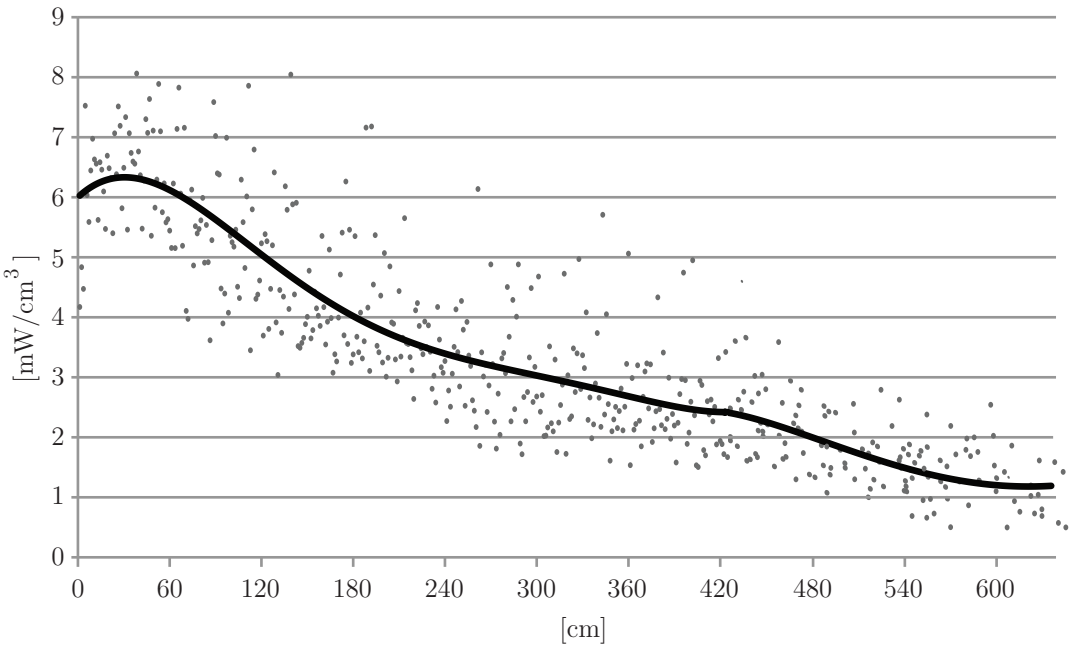

Figure 3.21: Peak of energy deposition in the first cable of Q0B with liner.

to this solution are mainly because the integrability into experiments: 13 m from IP seems to be a possible slot for some modifications of experiments, of course to perform major changes into experiments is challenging and can conditioning the Q0 layout. From the point of view of the technology of the superconductor to use for Q0 seems that Nb-Ti can be used for the goal of the optics (at $\beta^* = 0.25$ m); the real limit for the technology seems to be the energy deposition that impose the Nb_3Sn in order to have more margin for temperature.

The feasibility of Q0 will be clear after some years of LHC run because the experiments have to give a clear statement about what they want as upgrade and what it is possible to change in experiment itself in order to increase the luminosity. In principle this optical solution does not present evident show-stoppers and the technological issues are comparable with the other solutions presented for a luminosity upgrade (crab-cavities, electron lens, etc...).

Chapter 4

Crystals

4.1 Crystal-particle interaction

The previous chapter describes a way to improve the luminosity of two main experiments ATLAS and CMS, the present chapter is devoted to another experiment, TOTEM, and to a possible way to improve its acceptance. The increasing of acceptance can be obtained exploiting the features of the ordered atomic structure of a silicon crystal when it interacts with a high energy beam of charged particles.

Let consider a crystal made of parallel planes: each plane can be considered as a continuous charge distribution that produces a potential inside each space between two planes (the interplanar region). A particle with the trajectory parallel to the crystalline planes can cross the crystal without changes in the trajectory. If the particle trajectory is with a small angle with respect to the direction of the crystalline planes, the particle scatters elastically with the potentials produced by the planes and it is trapped in an interplanar space or channel.

If the angle (and the energy) is big enough, the particle can cross a plane and jump from one channel to another, the condition on the transverse energy is:

$$|\theta| < \sqrt{\frac{2E_c}{pv}} \tag{4.1}$$

with θ the angle between particle trajectory and crystal planes, E_c the maximum value of inter-planar potential and p and v are respectively the momentum and velocity of the particle. The quantity $\sqrt{\frac{2E_c}{pv}}$ is the maximum allowed angle (in general: critical angle and indicated as θ_L) to stay in a channel. Just to show the magnitude of these parameters it is possible to consider the case of a (*110*) silicon crystal with $E_c = 16$ eV and a beam of protons with momentum $p = 400$ GeV/c. In this case $\theta_L = 8.94$ μrad.

If the crystal is bent through a mechanical device, a channeled particle is forced to follow the crystal curvature emerging from the crystal with a different angle. The scheme of a bent crystal is shown in Fig. 4.1. In this picture it is possible

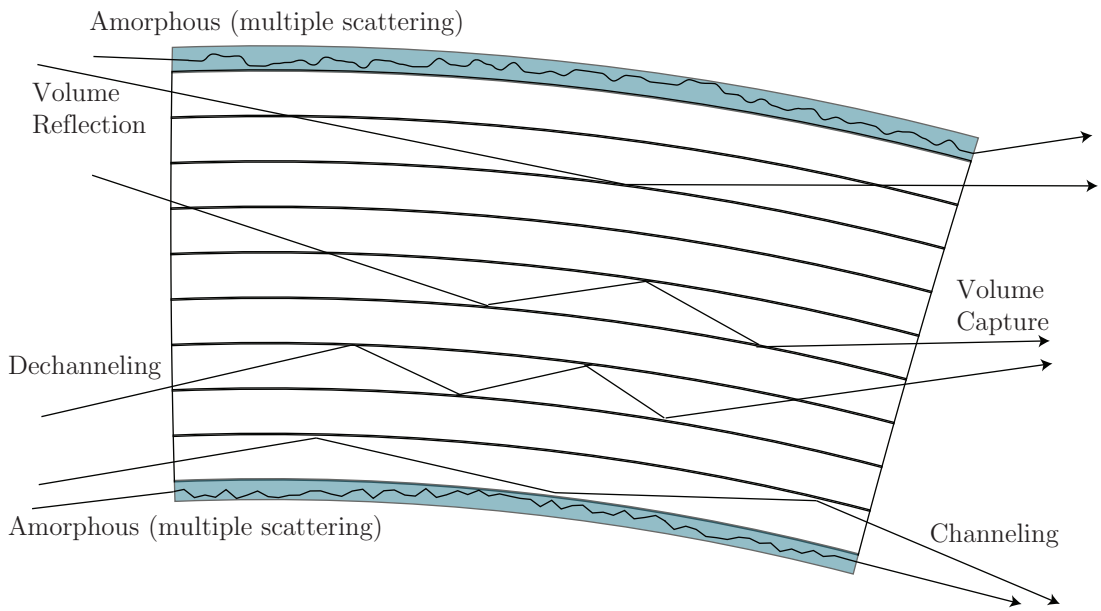

Figure 4.1: Scheme of a bent crystal.

to see the five behaviors that a charged particle can experience in function of the initial conditions:

- Amorphous: can happen in a region of the crystal that is amorphous and there are no ordered planes. The amorphous behavior can also be observed for a particle with $\theta < -\theta_L$, that is when the particle enters the crystal with an angle that is bigger than the critical angle and goes in the direction opposite to the curvature; in this case the angle between the particle and the planes increases for each collision of the particle with the planes and the particle can cross the plane. The final trajectory is almost the same as the initial because the only contribution is the small scattering that the particle experiences when cross the planes.
- Channeling: when $-\theta_L < \theta < \theta_L$ the particle is captured and the final trajectory is with an angle given by $\theta_C = l/R$ with l crystal length and R curvature radius. The final angle is subjected to an uncertainty due to the last collision of the particle with the crystal: if the particle collides with the plane on the top it will receive a kick that is the opposite if the same particle

collides for the last time with the plane on the bottom of the channel. The uncertainty is (at most) $\pm\theta_L$.

- Volume Capture: this happens when the initial angle of the trajectory is $\theta > \theta_L$ but after some amorphous scattering the energy of the particle is reduced, moreover the angle between the trajectory and the plane decreases due to the curvature of the crystal. In some place inside the crystal the angle θ becomes smaller that θ_L and the particle is captured in the channel.
- Volume Reflection: when $\theta > \theta_L$ a single reflection on a crystal plane can happen, after the reflection the angle is bigger enough to amorphously cross the remaining planes exiting the cristal. The final angle for a volume reflection is $\theta_{VR} = 1.5\theta_L$.
- Dechanneling: the angle is $\theta < \theta_L$ and a channelling starts, but after some scattering the the particle escapes from the channel crossing the remaining planes. The reason for the escape is that the reflection process is statistic and the particle has a non-zero probability to cross the potential.

The behavior of the crystal was predicted in several theoretical works [40] and experiments, one of these experiments was performed in the Super Proton Synchrotron (SPS) at CERN in the extraction line H8 [41] and the main result is shown in Fig. 4.2.

This experiment was performed with protons of $p = 450$ Gev/c and a bent crystal with a resulting $\theta_L = 10$ μrad. The crystal is mounted on a goniometer in order to perform a scan of the angle between the crystal and the beam. At the beginning there is an offset of -50 μrad with respect to the reference orbit of the particles. The particle angular distribution after the crystal is plotted as a function of the crystal rotation angle θ: for $\theta < 30$ μrad the crystal is misaligned and produces only multiple scattering. For 30 μrad $< \theta <$ 90 μrad, the crystal is aligned and the channeling peak appears with the channeling angle $\theta_C \sim 160$ μrad. It's interesting to note that, for a crystal of $\theta_L = 10$ μrad, and an alignment offset of -50 μrad, the channeling region should be between 40 μrad and 60 μrad, but in the Fig. 4.2 it is between 30 μrad and 90 μrad. This smearing effect is produced by the beam divergence: the protons are not perfectly aligned with the reference orbit but their trajectories are with a gaussian spread of angles distributed around the reference orbit. Moreover there is a small contribution due to the imperfections of the crystal. The dust of particles below the channeling signal are produced by dechanneling. For 90 μrad $< \theta <$ 250 μrad the tangency point between the particle trajectory and the crystal planes is in the crystal volume. The diagonal line is filled with volume captured particles when the beam core is shifted of $\theta_{VR} \sim 14$ μrad.

Volume reflection is an interesting phenomenon as it has a high efficiency and a large angular acceptance; the crystal presented in Fig. 4.2 shows an angular acceptance greater than 150 μrad and an efficiency of about 98%. The amplitude

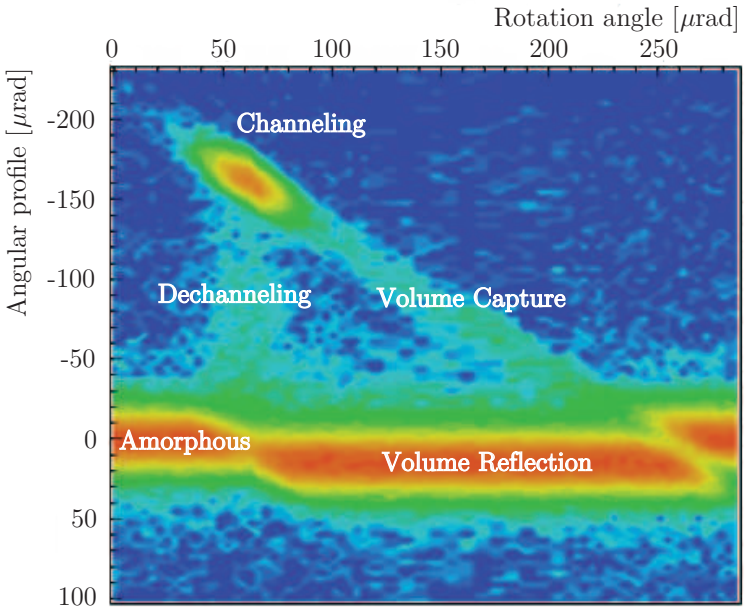

Figure 4.2: The crystal behaviour in H8RD22 [41].

of the final angle after the volume reflection is limited by the total momentum according to the Eq. 4.1: a large momentum, as for example the momentum of LHC protons, produces small angles. A deflection angle greater than θ_{VR} can be obtained by means of subsequent reflections in a series of aligned crystals since the total angle is given by the single reflection sum [42]. In this way is possible to use the high efficiency of volume reflection with big enough angle useful to extract particles from the beam as illustrated in the next section.

4.2 Acceptance of TOTEM experiment with crystal

In the previous section it is explained how the crystal can interact with a particle, and so with a beam, in order to modify the trajectory in two different ways: channeling and volume reflection. The idea is to use these crystal capabilities in the TOTEM experiment to increase the acceptance of the Roman Pots; a schematization is in Fig. 4.3.

To provide a kick to the protons, that is a change in the angle of the momentum direction, the crystal can be used in channeling or volume reflection: the angle of

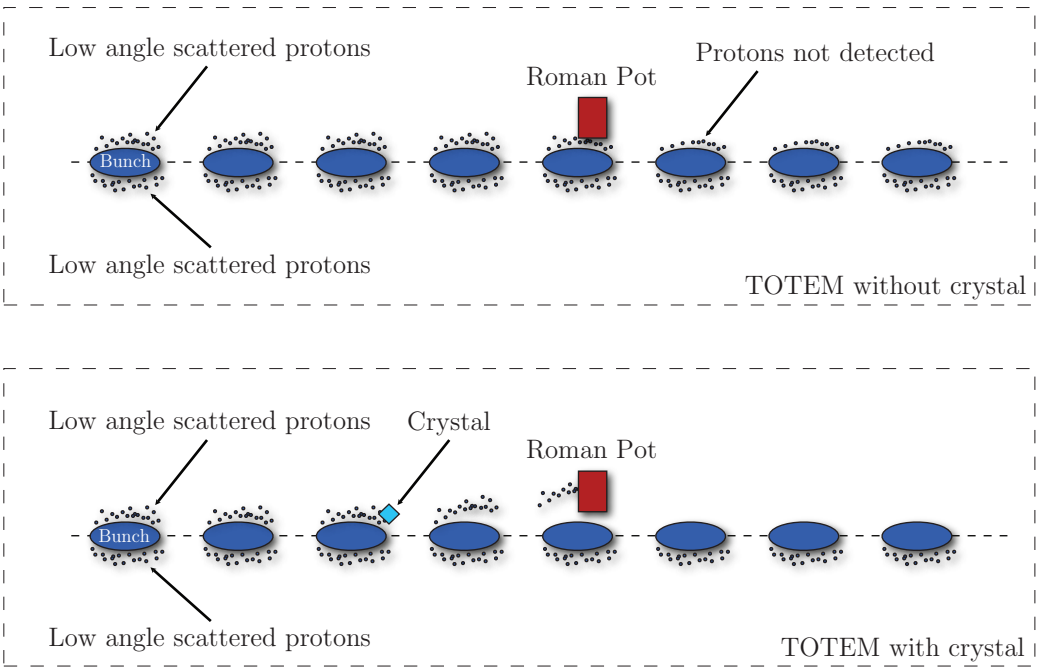

Figure 4.3: TOTEM schematization without and with crystal.

channeling, that is typically of some hundreds of μrad is fixed by the mechanical bending angle but it is with an uncertainty that depends on the critical angle. Moreover the range of valid angles for channeling is ~ 50 μrad.

On the other hand the volume reflection is with a larger tolerance for the angle (~ 170 μrad) with a greater efficiency and an angle of reflection that is well defined. This phenomenon, volume reflection, is better for the application of a crystal in the TOTEM experiment because the Roman Pots must reconstruct the orbit of the particles and a precise reflection angle is mandatory to trace back the particle from the Roman Pot to the collision vertex.

The main issue in the use of volume reflection is that the angle of reflection(θ_{VR}) should scale with the inverse of the momentum's square root according to the equation 4.1. The measured θ_{VR} in SPS H8 experiment at 400 GeV is 13.41 μrad but LHC will work at 7 TeV and the corresponding rescaled θ_{VR} is 3.2 μrad. This angle is too small to provide a kick big enough to increase significantly the acceptance of the Roman Pots, a solution to this problem is to use multiple volume reflections provided by multiple strips of crystal as proposed in [42].

The proposed layout for the interaction region is shown in Fig. 4.4.

The crystal is placed at 100 m from IP, between D1 and D2, with a distance from the beam, in the horizontal plane, of 6 σ, that, at 100 m from IP, corresponds

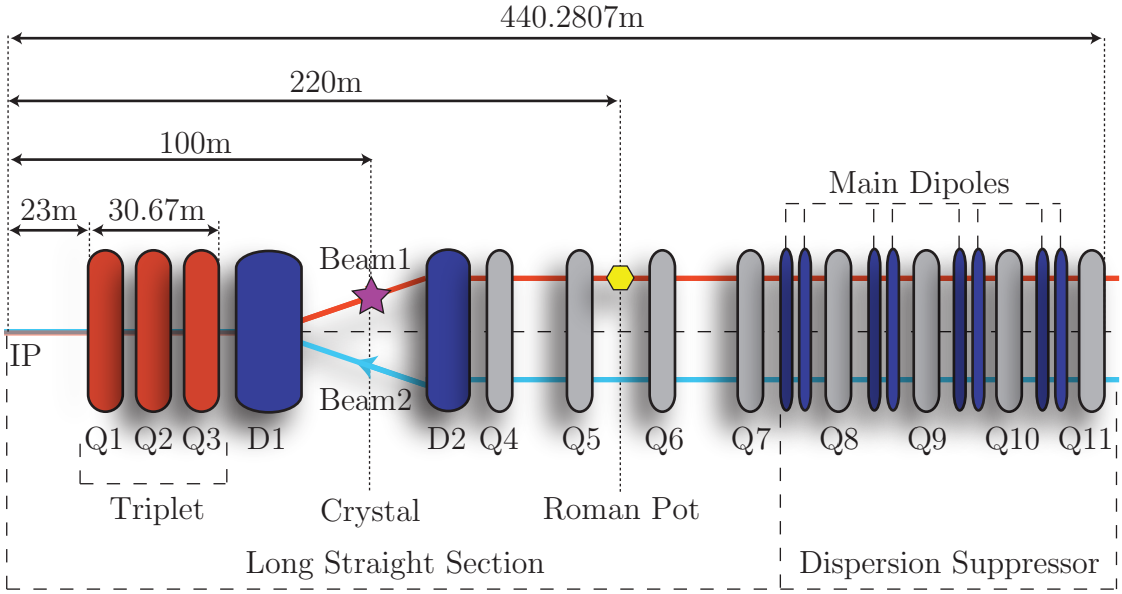

Figure 4.4: TOTEM layout with crystal.

to a distance of 5.8 mm because $\beta = 1913$ m and the normalized emittance is 3.75×10^{-6} m $\cdot$ rad; the Roman Pot considered in this layout is the one at 220 m from IP and it is placed at 10 σ + 0.5 mm of distance in the horizontal plane. In this layout it is possible to intercept the scattered protons with an amplitude of 6 σ and modify the p_x component of the momentum of about 16 μrad of angle with the action of a multi-layer crystal composed by 5 layers.

A particle with an energy close to 7 TeV (elastic scattering), that receives the kick from the crystal, can benefit of a lever arm of 120 m and a phase advance of 12°. For particles with a non negligible energy loss (diffractive scattering), the scenario is more complex because the phase advance changes in function of the energy loss and the dispersion starts to play a role in the trajectory of such particles. With a tracking code can be possible to take into account the linear and non-linear behavior and try to predict the difference in acceptance of a Roman Pot with and without a crystal.

A first step in the tracking is the particle events generator: the requirement is a collision between two beams with a normalized emittance of 3.75×10^{-6} m $\cdot$ rad; the β function at the collision point must be the nominal one, that is 0.55 m; the two beams collide with a full crossing angle of 285 μrad; finally the total momentum of the protons is 7 TeV/c. With this parameters it is possible to use a Monte Carlo generator like the software DPMJET [38] providing a pair of protons with the parameters just described and taking back the elastic and diffractive events.

The generated protons are tracked with matrices produced by the optics implemented in MadX. The first check is to reproduce the acceptance of TOTEM without crystal in the nominal conditions. The result of the simulation is in Fig. 4.5.

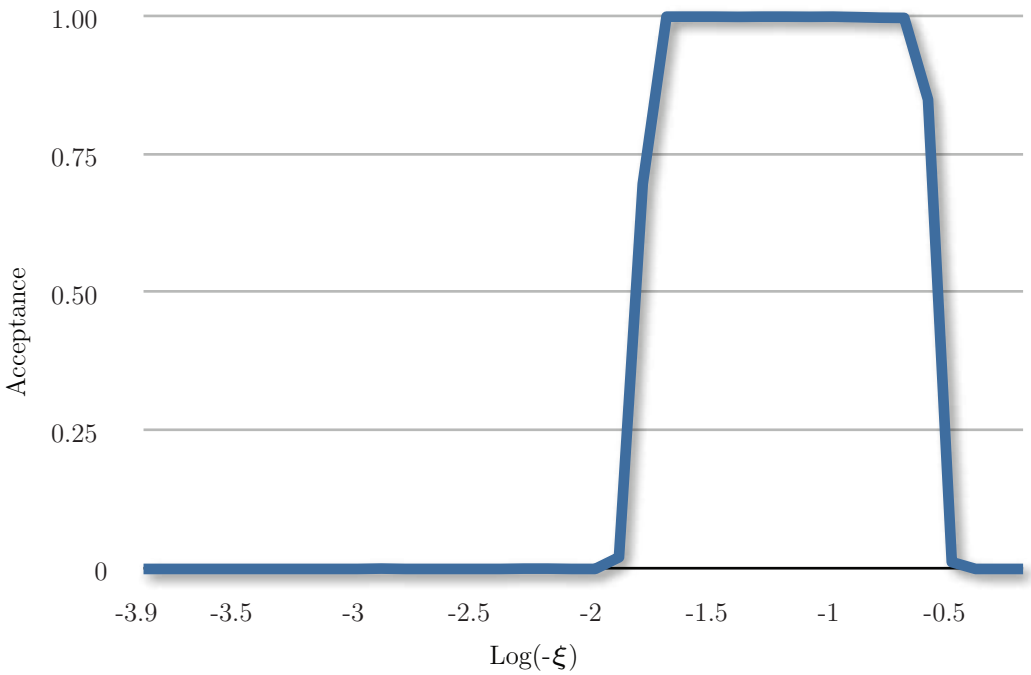

Figure 4.5: Nominal acceptance of Roman Pot. Acceptance vs. $\log_{10}$ of energy spread.

This result is compatible with the plot in Chapter 2 Fig. 2.16: the considered Roman Pot in the simulation is the one at 220 m from IP and the beam represented in the plot is the beam 1. In this plot are evident three regions:

- $\text{Log}(-\xi) < -2$, that is $-\xi = -\frac{\Delta P}{P} < 10^{-2}$, that is 6.93 TeV/c <P< 7 TeV/c. The energy loss in this region, coupled with the dispersion, is not enough to create a significant deflection in the trajectory of protons, and the Roman Pot does not see any signal.
- $-2 < \text{Log}(-\xi) < -0.5$, that is $10^{-2} < -\frac{\Delta P}{P} < 10^{-0.5}$, that is 4.78 TeV/c <P< 6.93 TeV/c. In this region the energy loss creates a dispersive kick that is capable to move protons, at 220 m from IP, to an amplitude greater than 10 σ + 0.5 mm, inside the Roman Pot. It is interesting to note that the apparent rapid increase in acceptance around $\text{Log}(-\xi) = -2$ is due to the logarithmic scale in $\text{Log}(-\xi)$; for each momentum the angular spread of the protons due to the elastic scattering should be considered, but it is small

with respect to the effect of the energy loss.

- $\text{Log}(-\xi) > -0.5$ that is $\frac{\Delta P}{P} > 10^{-0.5}$, that is $P < 4.78$ TeV/c. The momentum loss in this situation is very large and the protons collide with the beam pipe and the collimation system. For this situation the tracking code is not anymore reliable because it is based on the matrices produced by the Hill equation that is a linearization of the equations of the motion in the magnets. When the energy of the particles is far from the designed energy, the linear approximation is not anymore valid, moreover the quasi-axial approximation, the approximation that the transversal component of the momentum is small with respect to the longitudinal component, is not valid. For these reasons this part of the plot should be considered over-approximated, but the interest of the TOTEM experiment is in the first and second region, when all the approximations are valid.

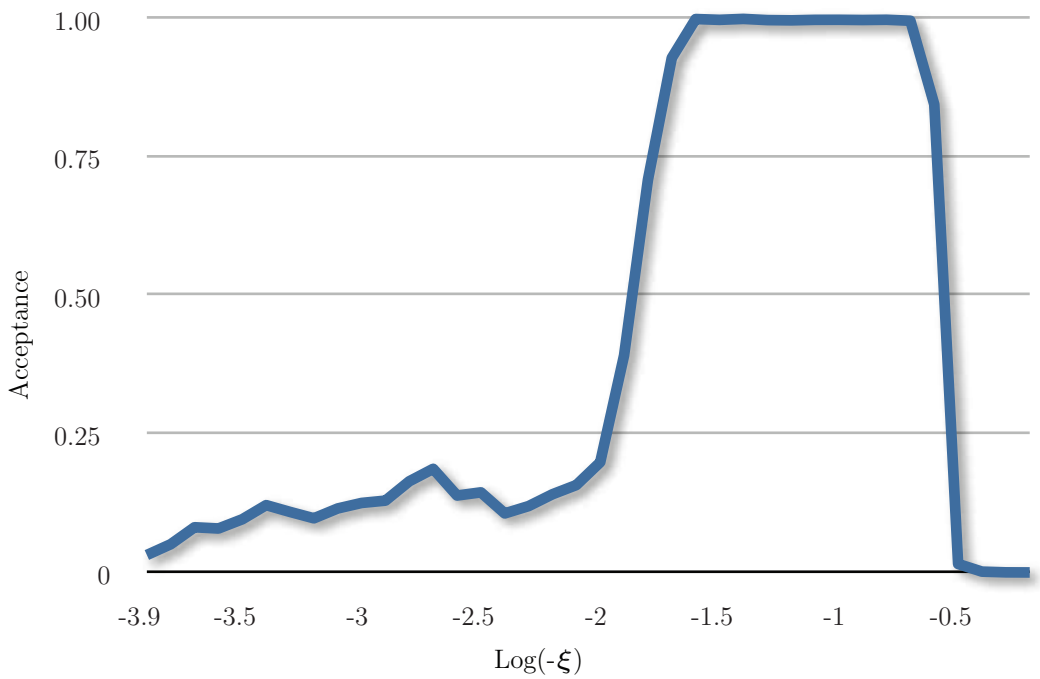

Figure 4.6: Acceptance with crystal.

A crystal at 100 m from IP and at 6 σ changes the trajectory of particles with an amplitude of 6 σ changing the acceptance of the Roman Pot. The result is shown in Fig. 4.6.

In the first region of the plot, the one with $\text{Log}(-\xi) < -2$ and 6.93 TeV/c <P< 7 TeV/c there are elastic scattered protons with a momentum loss not big enough to feel the dispersion, but the 10 μrad kick that the crystal provides to such protons

is, in the $10-20\%$ of the cases, capable to deflect the particle into the Roman Pot.

This result can also be improved with an optimization of the crystal's position, for example if the crystal is moved to 5 σ the acceptance for elastic protons can increase up to 40%. The problem to go below 6 σ is that some proton is not produced by an elastic collision but it comes from the natural tail beam diffusion, that for LHC is of 5.3 nm per turn [43]. After 6 σ the diffusion is cut by the collimation system of LHC: the primaries collimators are designed to intercept particles with an amplitude greater than 6 σ [44] and they clean the beam after that amplitude.

The application of the crystal to TOTEM can be a good direction to increase the acceptance of the experiment, in particular this technique can be a candidate to explore the region of the small momentum loss and to characterize the elastic cross section of protons at 7 TeV with a greater accuracy with respect to the nominal TOTEM layout.

It is possible to dig out in this research in several directions, for example: which one is the best position for a crystal? Is it possible to build and ad-hoc optics for TOTEM that is optimized for a layout with a crystal? Is there any impact for the magnets and cryogeny if the crystal start to deflect protons with a big momentum loss to the coils of the magnets?

All these problems, and the issue of acceptance itself, are strictly connected to the affordability of the simulator model: if the code that simulates the crystal and the tracking of the particles in LHC is good, then it is possible to predict many physical events, if the code is not accurate, any speculation is not reliable enough for a prediction. The accuracy of the simulation is not so easy to evaluate: first of all it is impossible to make experiments with a crystal and a beam at 7 TeV of momentum because LHC is the only machine capable to manage beam at that energy; moreover the systematic study of the interactions of high energy beams with crystals is a quite young science and there are several open question about how to build a model of crystal.

To verify the trustability of the model used to simulate the TOTEM acceptance it is possible to apply the same model to a real experiment and see if the model can predict the experimental measurements. An experiment with crystal in SPS was proposed [45] and accepted by scientific committee at CERN and it will check the reliability of a crystal in a multi turns layout at different energy.

This experiment will take place in 2009 and the tracking model used for TOTEM can be adapted to predict the behavior of the crystal in the SPS machine in order to obtain a prediction comparable with measurements. As preliminary check the simulation is compared with the one presented in [45]. This experiment and the results of the simulation are explained in the next two sections.

4.3 Crystal characterization in the SPS: experiment layout

CRYSTAL will be an experiment in SPS with the aim of testing if bent crystals, used as primary collimators in a two-stage collimation system, are more effective than amorphous collimators. This experiment will take place late in 2009 [46]. The full description of the layout used for the simulation is presented through these elements:

- Lattice and Beam: the lattice of SPS and the beam used for the simulation.
- Geometrical layout: the physical positions of the crystal and instrumentation in the machine.
- Crystal: the parameters of the crystal used in the experiment.
- Halo exciting system (dumper): the device used to dump protons from the core of the beam to the halo in order to emphasize the behavior of the crystal.
- Roman Pot: the device used to see the track of protons.

Lattice and Beam

The lattice used for the SPS is the release 2008 implemented with MadX and available on the Internet site [47]. The experiment will be performed with three different layouts, one at high energy (270 GeV) and two at lower energy (120 GeV) with (bunched) or without (unbunched) the radio-frequency enabled. The beam intensity will be of a few 10^{11} up to 10^{12} protons with an RMS size of 1 mm measured in the middle of a focusing quadrupole.

The beam lifetime is estimated in 80 h in the nominal conditions: an external noise generator that dumps the protons from the core to the halo of the beam should reduce the beam lifetime from a few tens of minutes to a tens of hour. The main parameters of the beam are resumed in Tab. 4.1.

The halo flux will hit the crystal and subsequently the Roman Pots detectors producing one of the two conditions: a halo flux in the range of $10^2 \div 10^4$ particles per turn distributed along the revolution period in the unbunched case or synchronized with the bunch in the bunched beam; this flux of particles does not saturates the Roman Pots that can be used as primary detector for the experiment. The second possible scenario is a flux of 10^5 particles per turn that can saturate the roman pots and should be studied with the beam loss monitor in the SPS.

Layout

The crystal will be placed at 5128 m from the beginning of the machine (BA1), just before the focusing quadrupole QF.518. The first Roman Pot will be 43.45

Table 4.1: SPS beam parameters.

	High Energy	**Unbunched**	**Bunched**
Momentum P [Gev/c]	270	120	120
Tune Q_x	26.13	26.13	26.13
Tune Q_y	26.18	26.18	26.18
Tune Q_s	0.0021	0	0.004
Norm. emittance at 1 σ [m rad]	1.5×10^{-6}	1.5×10^{-6}	1.5×10^{-6}
Transverse radius (RMS) [mm]	0.67	1	1
Momentum spread (RMS) $\frac{\Delta P}{P}$	$2 \div 3 \times 10^{-4}$	$2 \div 3 \times 10^{-4}$	4×10^{-4}
Longitudinal emittance [eV s]	0.4	≤ 0.4	0.4
Beam intensity [Protons]	$10^{11} \div 10^{12}$	$10^{11} \div 10^{12}$	$10^{11} \div 10^{12}$
RF Voltage [MV]	1.5	0	1.5
Beam lifetime [h]	80	80	80

m after the crystal and 6.739 m after the defocusing quadrupole QD.519. The second Roman Pot is 15.602 m after the first one and 3.03 m before the absorber in tungsten (TAL). These positions are selected on the basis of several simple arguments: the layout is as compact as possible to save cost of infrastructures like cables; the first Roman Pot is the prototype used for TOTEM and the aperture is already fixed in 80 mm so this device must be placed after a defocusing quadrupole where the horizontal beam size is small enough.

The second Roman Pot is new and with an aperture of 160 mm so without restriction in SPS. The position of the crystal is chosen to satisfy the requirements of clearance size of the deflected particles from the circulating beam (some millimeters). The idea is to prove the efficiency of the crystal as collimator and to see if the crystal is working well, it is important to see a clear signal on the Roman Pots avoiding eventual tight mechanical tolerance, but it is also important to measure the residual particle density in a large fraction of the clearance area and check to which extent it is really empty.

To estimate the beam clearance it is possible to proceed considering normalized coordinates as defined in [48]: a kick of θ in a point of the machine with a value of β function of β_d produces a perturbation in the orbit in the point of the detector with a β_o given by:

$$\Delta x = \theta \sqrt{(\beta_d \beta_o)} \sin(\Delta\psi) \tag{4.2}$$

$\Delta\psi$ is the phase advance between the deflection and observation point.

β_o is fixed due to the issue of aperture previously described and the angle is fixed by the characteristics of the crystal, so the free parameters which maximize

the effect of the deflection are β_d and $\Delta\psi$: β_d should be as larger as possible and $\Delta\psi$ should be as closer as possible to $\frac{\pi}{2}$. For the SPS these requirements are satisfied when the deflection point is close to a focusing quadrupole and the observation point is one cell apart. These considerations must be refined considering that the crystal will intercept protons of the halo, with a distance from the closed orbit of x_{bc}; this produces a new phase advance given by:

$$\Delta\psi = \arccos\left(\frac{1}{\sqrt{1+(\frac{\beta_{bc}\theta}{x_{bc}})^2}}\right) \tag{4.3}$$

This phase advance is reduced with respect to the $\frac{\pi}{2}$ from deflection to observation and the simultaneous condition of β and $\Delta\psi$ cannot be practically verified. A set of parameters used in the simulation is:

$$\begin{aligned} x_{bc} &= 6\ \sigma = 6.345 \text{ mm} \\ \theta &= \alpha_{\text{channeling}} = 150\ \mu\text{rad} \\ \Delta\psi &= 1.156 \text{ rad} \end{aligned}$$

Table 4.2: Crystal experiment final layout.

Device	**S [m]**	β_x **[m]**	$\Delta\psi$ **[rad]**
Crystal	5182.0000	96.048	0.0000
QF.518	5186.7129	103.429	0.0452
QD.519	5218.7106	20.696	0.8664
RP1	5225.4500	31.004	1.1334
RP2	5243.4500	85.180	1.4916
TAL	5245.1250	92.247	1.5104
QF.520	5250.7083	103.424	1.5651

The summary of these considerations produces the layout in Fig. 4.7 and is summarized on Tab. 4.2.

From the point of view of the transversal position in the horizontal plane the request for the crystal is to act as a primary collimator: it should be positioned in the halo to intercept particles for channeling, and the particles not channeled but amorphously scattered will have the possibility to intercept the crystal again in the next turns. The Roman Pots and the TAL will be placed at a distance greater than the crystal in order to intercept only protons deflected by the crystal and not directly protons of the halo. If the crystal is placed at 6 σ from the beam core, the

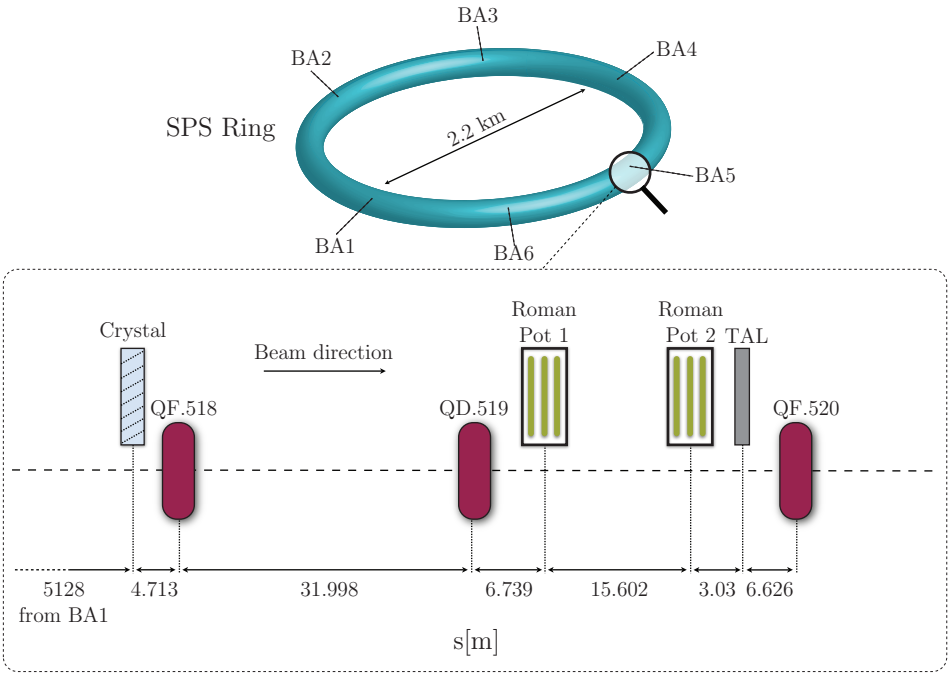

Figure 4.7: SPS layout with crystal.

Roman Pots and the TAL will be placed at 6 $\sigma + x_{of}$ where x_{of} is a fixed offset chosen to optimize the multi-turn effect of the crystal. If a particle hits the crystal and it is not channeled, it is subjected to a random scattering with an angle that is around 10 μrad for an energy of 120 GeV.

Table 4.3: Transversal positions of Crystal, Roman Pots and TAL.

	Crystal	**Roman Pot 1**	**Roman Pot 2**	**TAL**
6 σ [mm]	6.35	3.61	5.98	6.23
x_{of} [mm]	0	0.5	0.83	0.86
6 $\sigma + x_{of}$ [mm]	6.35	4.11	6.81	7.09

The requirement is that the particle randomly scattered will not hit the Roman Pot or the TAL at the first turn of amorphous scattering, and to ensure this behavior the tolerance is fixed in 42.5 μrad that is with a probability to intercept the proton at the first turn lower than 10^{-5}. Horizontal positions are summarized in Tab. 4.3

Dumper

At 6 σ the number of particles is $\sim 10^{-9}$ of the initial distribution, that is, for the SPS beam charged with 10^{11} protons, 100 particles are in the halo. If the crystal can channel 1 proton per turn the measurement lifetime will be ~ 2 second because the revolution frequency of SPS is 43375 Hz and the number of bunches is 800. After this time the beam should be dumped and re-injected into the machine. This procedure is not necessary (or not so often) if a forced diffusion system is implemented in the machine: a system that can extract constantly 10 protons per turn from the core to the 6 σ amplitude can provide a stable flux of particles for more than 60 hours of run.

This device was proposed in [49] and schematized in Fig. 4.8

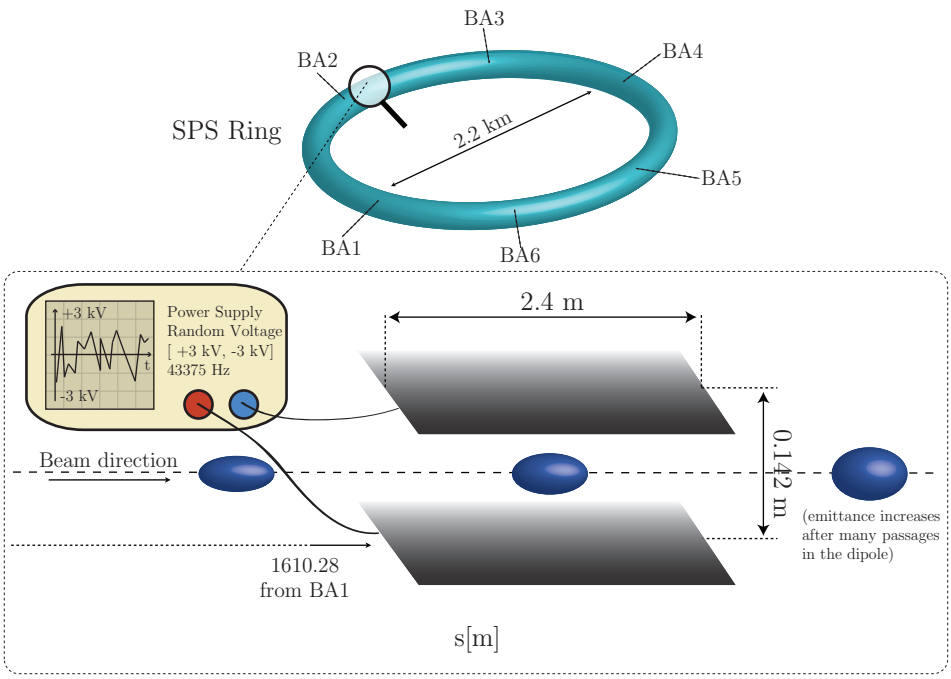

Figure 4.8: SPS dumping system.

The idea is to use an electric dipole to induce a transverse noise on the beam. SPS is already equipped with a feedback device [50] that consists in a dipole connected to a power supply that can provide a voltage between -4.5 V and 4.5 V and an amplifier that can increase the voltage up to ± 3.5 kV.

The kick that a particle receives when goes trough the dipole is:

$$k = \frac{l \Delta V}{\gamma E_0 d} \tag{4.4}$$

where l is the length of the plates, d is the distance between the plates, ΔV is the voltage between the plates, γ is the relativistic factor and E_0 is the proton rest energy. The kick will be applied on the horizontal plane.

The emittance growth per turn due to the kick k is given by [51]:

$$\Delta\epsilon = \frac{1}{2}\beta k^2 \tag{4.5}$$

with β the betatron function at the plates. If the kicks are uncorrelated and uniformly distributed in an interval centered in zero, the emittance growth per second is:

$$\langle\Delta\epsilon\rangle = \frac{1}{2}\beta\langle k^2\rangle\nu_{rev} \tag{4.6}$$

where $\nu_{rev} = 43375$ Hz is the revolution frequency of the SPS. Fixing the maximum voltage to the dipole, $\langle k^2\rangle$ can be estimated as the variance of the uniform distribution in the interval $[-k_{max}, k_{max}]$ substituting the Eq. 4.4:

$$\langle k^2\rangle = \left(\frac{l}{\gamma E_0 d}\right)^2 \int_{-\Delta V_{max}}^{\Delta V_{max}} P(U)U^2 dU \tag{4.7}$$

where U is a variable for the integration that represents ΔV and $P(U)$ is the distribution of probability given by:

$$P(U) = \frac{1}{2U},\ U \in [-\Delta V_{max}, \Delta V_{max}] \tag{4.8}$$

$$P(U) = 0,\ U \in (-\infty, -\Delta V_{max}) \cup (\Delta V_{max}, +\infty) \tag{4.9}$$

and

$$\langle k^2\rangle = \frac{1}{3}\left(\frac{l\Delta V_{max}}{\gamma E_0 d}\right)^2 \tag{4.10}$$

and the emittance growth per second becomes:

$$\langle\Delta\epsilon\rangle = \frac{1}{6}\beta\left(\frac{l\Delta V_{max}}{\gamma E_0 d}\right)^2 \nu_{rev} \tag{4.11}$$

it is also interesting to consider the normalized emittance, that is the emittance times the relativistic γ factor (the relativistic β can be considered 1):

$$\langle\Delta\epsilon_n\rangle = \frac{1}{6}\frac{\beta}{\gamma}\left(\frac{l\Delta V_{max}}{E_0 d}\right)^2 \nu_{rev} \tag{4.12}$$

to estimate the maximum voltage to apply to the dipole, a first step is to calculate what is the voltage to double the initial emittance in a second. The values used

for this task are: an initial normalized emittance of 1.5 μrad $\cdot$ m, and this is $\langle \Delta\epsilon_n \rangle$ per second if the goal is to double the emittance. A β function at the dipole of 81.8 m, a γ factor, at 120 GeV, of 127, a dipole length l of 2.4 m, a dipole plates distance d of 0.142 m and a rest energy of the proton E_0 of $\sim$ 1 GeV. With these parameters the maximum voltage required to double the emittance in one second is $\sim$ 1 kV.

To have a rough estimation of the flux of particle it is possible to solve the mono-dimensional case:

$$N \int_{6\sigma_0}^{+\infty} \frac{1}{\sqrt{2\pi}\sigma_0} e^{-\frac{x^2}{2\sigma_0^2}} dx \tag{4.13}$$

here N is the total number of particles per bunch ($\sim 10^{11}$) and σ_0 is the r.m.s. of the bunch along the x direction at the beginning. After one second of increasing in emittance the new distribution of particles will be:

$$N \int_{6\sigma_0}^{+\infty} \sqrt{\frac{\epsilon_0}{\epsilon_1}} \frac{1}{\sqrt{2\pi}\sigma_1} e^{-\frac{x^2}{2\sigma_0^2}\frac{\epsilon_0}{\epsilon_1}} dx \tag{4.14}$$

with ϵ_0 and ϵ_1 respectively the emittance before the dumping and the emittance after one second of dumping. With 1 kV of maximum voltage in the random power generator the ratio $\frac{\epsilon_0}{\epsilon_1}$ is $\frac{1}{2}$, and, with this ratio, the flux of particles is $\sim 10^6$ per second. With an $\epsilon_1 = 1.1\epsilon_0$ the ratio of particles becomes $\sim$ 400 per second that is more reasonable for the resolution in time of the Roman Pot. The corresponding voltage is $\sim$ 330 V.

This is, of course, a very preliminary estimation because it is in the mono dimensional approximation, but also because it is impossible to predict the real behavior of the machine when the emittance starts to increase: for example the non linear effects of the machine (sextupolar components of the magnets) can start to have a significant role in the dynamic of the beam producing instabilities that dramatically increases the flux of particles in an unpredictable way. The strategy to follow during the experiment is to start with few tens of volts in the electric dumper and to increase up to see a constant flux of particles in the Roman Pots. The result should be compatible with the value of some hundreds of volts.

Crystal

The silicon crystal used as primary collimator will be 0.5 mm thick, oriented along the (111) planes; the bend angle will be $\alpha = 150$ μrad and a length along the beam $L = 1$ mm. This gives a bend radius $R = 6.67$ m and, consequently, a critical radius for 120 GeV protons of $R_c = 21.46$ cm. In these conditions, the

particles deflected in the second collimator of tungsten (TAL) should have large impact parameters, of about 6-8 mm.

The crystal bend radius, which produces the maximum extraction efficiency for 120 GeV protons, is about 1-2 m, i.e. about 5-10 times R_c. The selected crystal parameters, α and L are a sound compromise between the optimal values for SPS and those eventually required for LHC in the framework of a future LHC collimation system with crystals. A crystal with the presented parameters can be achieved with both anticlastic and quasi-mosaic bending techniques, that are the main techniques used to create the bended crystal used in the past experiments.

Roman Pot

The model of the Roman Pot used in the simulation is schematized in Fig. 4.9.

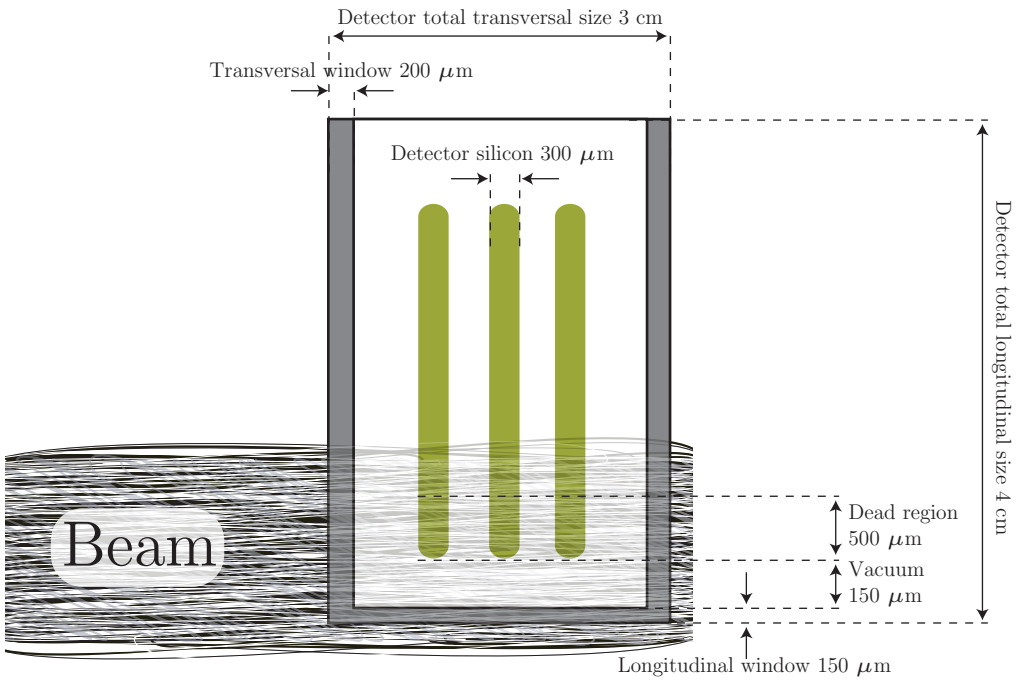

Figure 4.9: Roman Pot layout.

A particle that crosses the Roman Pot can see three different area: the longitudinal window made of aluminum with an interaction length of $L_b = 3$ cm(Al); the clearance slot, made of steel with an interaction length of $L_s = 400$ μm(Fe); the third area is the detector made of iron and silicon with an interaction length of $L_d = 400$ μm(Fe) + 900 μm(Si) for the first Roman Pot and $L_d = 400$ μm(Fe) +

1500 μm(Si) for the second Roman Pot that will be with 5 strips of silicon instead the three strips of the first Roman Pot. The vacuum in the box is around 10^{-6} tor, that is negligible from the point of view of the scattering.

The simulation of the experiment is designed considering the nuclear interaction and the ionization energy losses that a proton can experience crossing the Roman Pot, consequently modifying the trajectory, the angle and the energy of the proton.

From the point of view of the detection it is important to consider that the first 500 μm of the silicon strip is insensitive to the particles, this means that the first 800 μm of the detector are not used for detection.

4.4 Crystal characterization in the SPS: simulation results

The main results of the SPS simulation with crystal and Roman Pots, are performed at 120 GeV. This energy will be the first energy tested in the CRYSTAL experiment and is a good starting point to understand if the simulator works well because the rigidity of the protons should not be big (at least smaller than 270 GeV) and the signal on the Roman Pots should be clear and easy to see. The

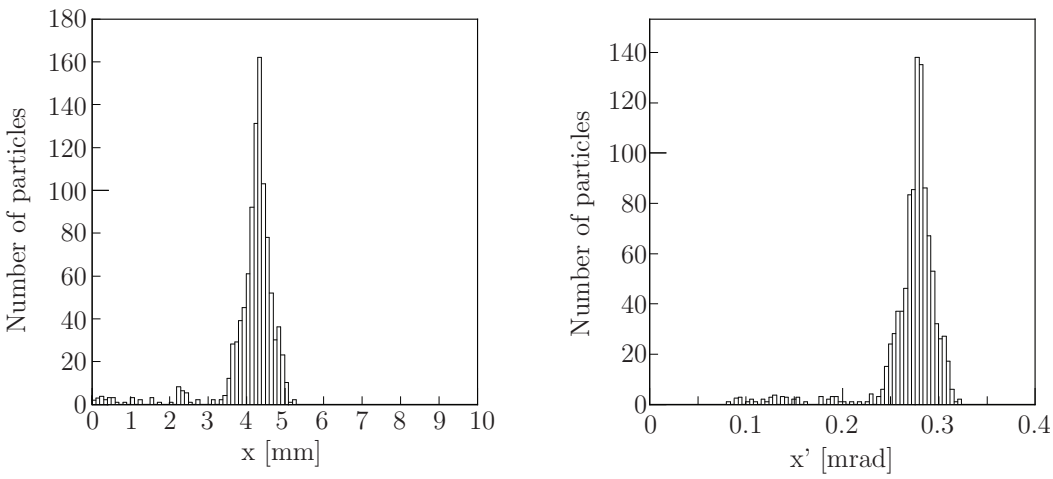

Figure 4.10: Impact parameters x and x' on the Roman Pot 1 when $\theta_o = 0$ μrad. Single turn simulation.

first simulated layout is the situation with the crystal aligned to the angle of particles, that is when the crossing angle between the planes of the crystal and the maximum of the angle distribution in the region of the crystal is zero (θ_o). Under this condition the crystal is mainly working in channeling and the peak on the Roman Pot is evident. The result is shown in Fig. 4.10; the $x = 0$ of the plot

is scaled of the 6 σ in the point of Roman Pot 1 plus an additional offset of 1 mm as explained in the previous section. The plot of Fig. 4.10 is the output of the simulation after few turns, when the effect of the random scattering inside the Roman Pot is negligible.

The effect of the random scattering in the Roman Pots is evident in multi turns as shown in Fig. 4.11

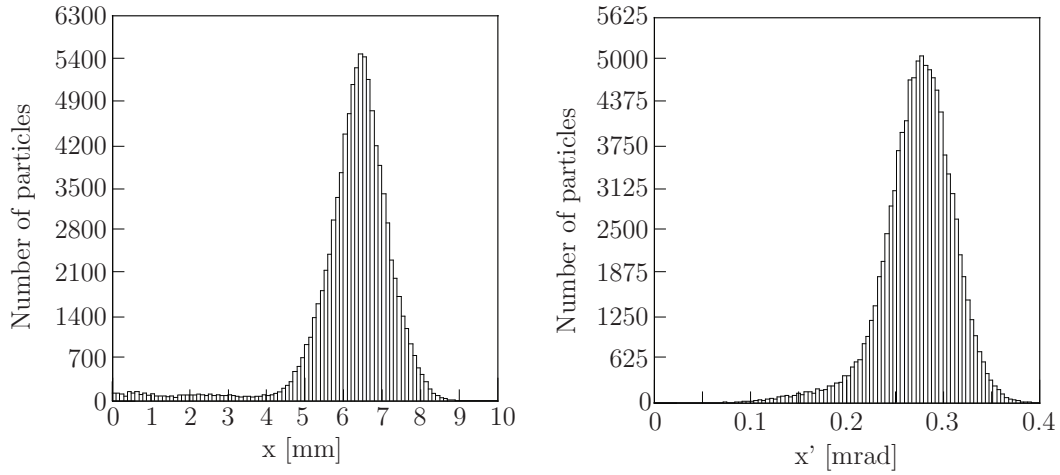

Figure 4.11: Impact parameters x and x' on the Tungsten Absorber (TAL) when $\theta_o = 0$ μrad. Multi turn simulation.

Here the multiple scattering creates a bigger spread in the impact parameter and in the angle, and the resulting distribution is due by the effect of the Roman Pot. These two preliminary plots are already interesting for the goal of this simulation, that is to see if the simulator, composed by MadX plus the CRYM routine plus the simulation of Roman Pot multiple scattering, can predict the behavior of particles in a real machine.

In order to stress the simulator and to verify the other properties of the crystal, the multi turn simulation was performed with the crystal rotated of different angles. The first rotation is $\theta_o = 20$ μrad and the result is shown in Fig. 4.12. Another interesting case is when $\theta_o = -200$ μrad: in this condition the distributions are broanded and the Volume Reflection maximum is smoothed down. This configuration is shown in Fig. 4.13. The last situation is when $\theta_o = 75$ μrad that is when the crystal is working as an amorphous layer and the protons hit the crystal mainly for diffusion and multiple scattering. This result is in Fig. 4.14.

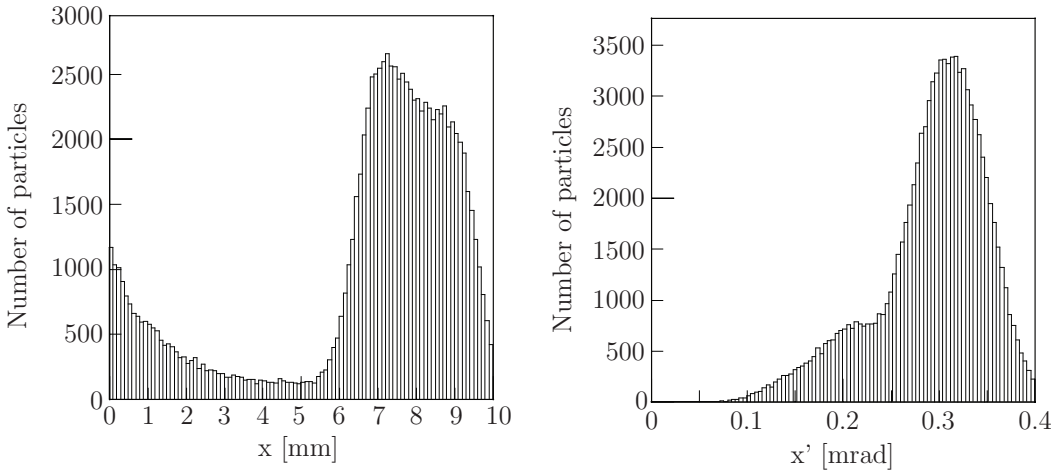

Figure 4.12: Impact parameters x and x' on the Tungsten Absorber (TAL) when $\theta_o = 20$ μrad. Multi turn simulation.

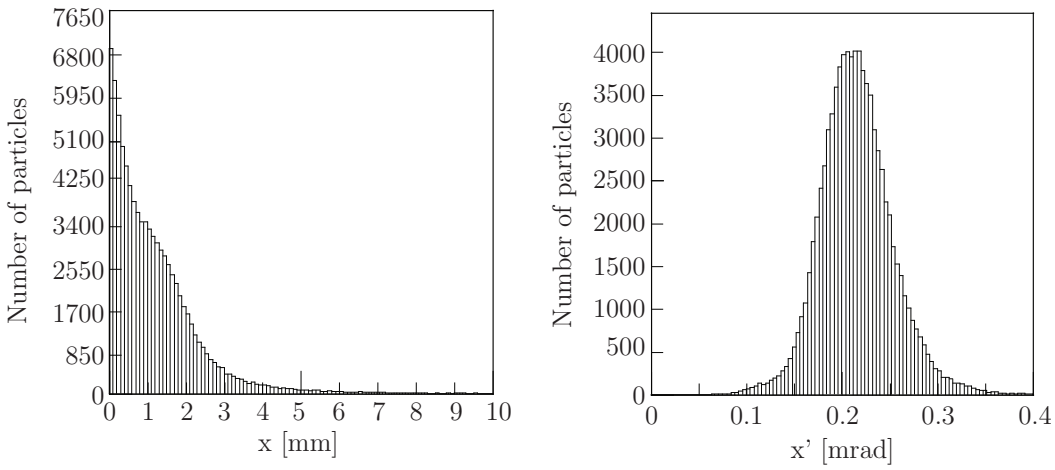

Figure 4.13: Impact parameters x and x' on the Tungsten Absorber (TAL) when $\theta_o = -200$ μrad. Multi turn simulation.

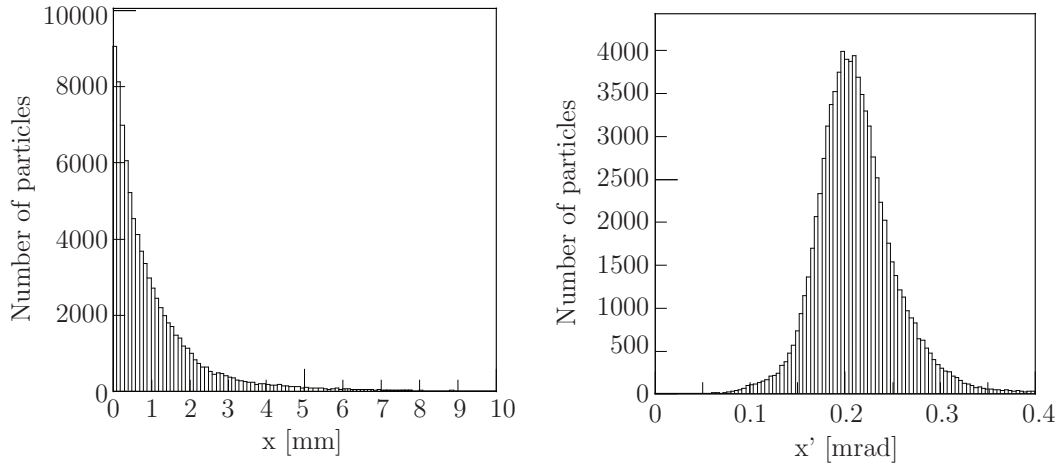

Figure 4.14: Impact parameters x and x' on the Tungsten Absorber (TAL) when $\theta_o = 75$ μrad. Multi turn simulation.

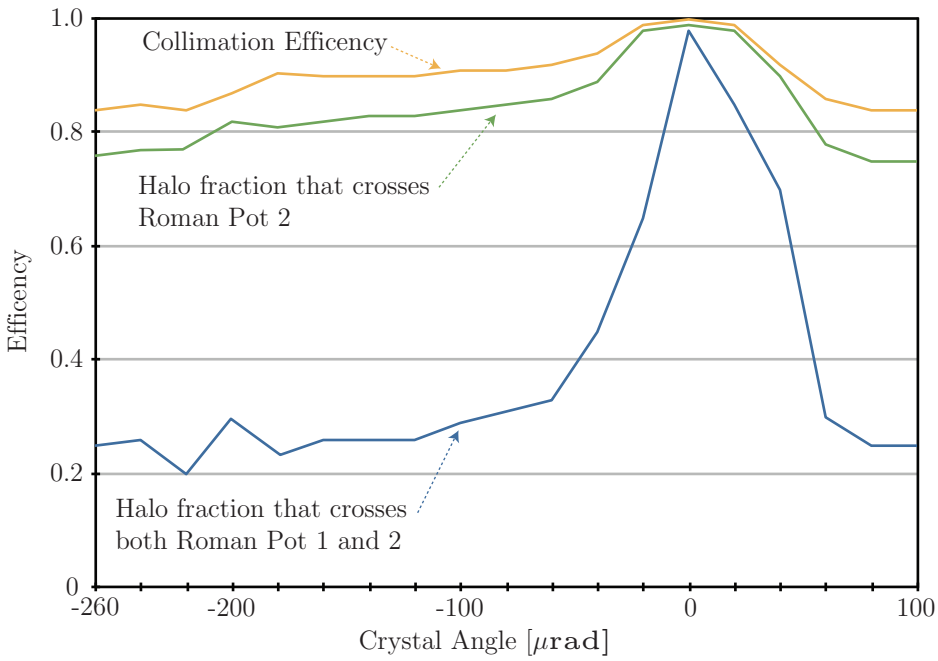

Figure 4.15: Crystal simulation collimation efficiency.

The collimation efficiency as a function of the crystal orientation is reported in Fig. 4.15. In this figure it is also plotted the halo fraction which crosses the sensitive area of the Roman Pot 2 and the fraction of the halo that crosses the active areas of the Roman Pot 1 and the Roman Pot 2.

The first parameter, the one trough Roman Pot 2, is the probability to measure the impact parameter at the TAL; the other parameter, the one trough Roman Pot 1 and Roman Pot 2, is the probability to detect the angle of the incoming particle because if a particle crosses both detectors it is possible to determine two points and consequently the direction of the trajectory. When θ_o is close to zero, i.e. the crystal is in channeling, the particles are deflected with an angle big enough to warrant a probability to intercept both Roman Pots close to 1. For other crystal orientations, that is when crystal crossings will occur, the probability to detect angles decreases sharply.

This simulation can be used to choose the best alignment of the crystal with the beam trajectory, moreover can predict the signal that will be detected by the Roman Pots at different angles. The experience of this simulation, in conjunction with the experimental results of CRYSTAL, will be an optimum starting point to develop a more reliable simulation for the TOTEM experiment. Moreover it will refine the prediction of a gain in acceptance when the crystal is applied on the beam line.

Chapter 5

Conclusions

The upgrade of LHC is an hot topic now that the machine started its operations. This thesis shows different strategies for the upgrade of the two main experiments ATLAS and CMS and for the upgrade of the TOTEM acceptance. The idea developed for TOTEM is also used to simulate the UA9 experiment that will be performed in 2009 in SPS.

The results obtained can be summarized as:

- the reduction of l^*, the distance between the last quadrupolar magnet and the Interaction Point, is a way to squeeze the beam increasing the luminosity. The preliminary study of a triplet at 13 m from IP shows that to reduce the β^* from 0.55 m to 0.25 m, keeping the maximum β function (and consequently the aperture) constant, it is required a quadrupole with an high field based on Nb_3Sn technology.

- A possible way to solve the previous issue is to introduce two quadrupoles, Q0A and Q0B, with a gradient compatible with NbTi technology, at 13 m from IP in order to reduce the β^*. This new optics can keep under control the *beta* function inside the triplet limiting the problems of aperture and chromaticity of a low β^* optics. With the Q0 option it is possible to push the β^* to 0.25 m with a triplet close to the nominal one, or to 0.15 m with a triplet like the one considered in the Phase-I upgrade of LHC.
  Looking only at the β^*, the value of the luminosity increases linearly with the reduction of the β^*. Unfortunately to keep constant the separation of the squeezed beams it is necessary to increase the crossing angle with a reduction of the luminosity. With a compensation of the long-range beam-beam effect, or with a zero crossing angle scheme (such as D0 or Crab-Cavities), the gain in luminosity due to $\beta^* = 0.25$ m is a factor 2. Anyway the Q0 solution is in the framework of a Phase-II luminosity upgrade, that is the upgrade of a

factor 10 in integrated luminosity: a factor 2 can come from the Q0 option and another factor 5 is provided from an increase of the beam current, or a reduction of emittance or a reduction of the crossing angle.
To integrate the new quadrupoles into the experiments ATLAS or CMS there are several issues to consider and in particular the misalignment problems and the energy deposition. From the point of view of the misalignments the tolerances required are the same of the nominal triplet, so in principle this is not a challenging problem, but the structure that has to fix the triplet should be created inside the experiments that are not made to sustain the weight of a magnet with a precision of tens of microns.
The other issue, the energy deposition, is strongly dependent on the final luminosity of the interaction region. In case of 10^{35} $cm^{-2}s^{-1}$ the magnets require a shielding system to prevent the increase of heat load on the superconducting coils. Moreover the temperature margin of NbTi technology can be not enough and the Nb_3Sn should be used.

- The other upgrade considered in this thesis regards the acceptance of the TOTEM experiment. It will look for the elastic and diffractive cross section of protons with a momentum of 7 TeV. The device that catches the protons, the Roman Pot, is placed at a transversal distance of 10 σ from the center of the beam. A proton that loses in a collision less than 70 GeV will be, at the Roman Pot, with an amplitude smaller than 10 σ, and the device will not detect this proton.
  The proposal is to put a crystal, before the Roman Pot, at 6 σ from the center of the beam, in order to intercept protons with an energy loss smaller than 70 GeV and deflect them into the Roman Pot. With a multi-layer crystal, that provides a kick of 10 μrad, the simulation shows that it is possible to increase the acceptance of the Roman Pot when the energy loss is between 0 and 70 Gev.
  The acceptance will increases from 0 up to 20 % depending on the energy loss considered. The main issue of this idea is to understand how the trajectory of the proton changes when a crystal is introduced along its path. The crystal is a non-linear device that provides an angular deflection according to the potential of the crystal planes, but the kick given by the crystal can suffer of a random spread due to several phenomenon of collisions inside the material. The accuracy of the model is crucial to predict the impact parameters on the Roman Pot in order to reconstruct the orbit of the particle and the vertex of collision. The present model is an extrapolation of a model developed with experimental data with protons at 400 GeV; the extrapolation of such data to 7 TeV must be confirmed in experiments with LHC.

- In order to check the crystal model for TOTEM another simulation was developed to predict the results of an experiment, UA9, with crystals that will take place in 2009 in the SPS machine.
  This experiment will check the possibility to use crystals as primary collimators for a future application in LHC. The simulation of this experiment was performed with the same technique used for TOTEM and the predictions of impact parameters on the Roman Pots, deflection angles, efficiency of the crystal, etc. are in very good agreement with results of other simulations. The comparison with experimental data will give important informations about the goodness of the crystal model and its affordability.

These results are published in original papers presented in several international conferences and specialized workshops.

Chapter 6

Appendix: Superconductors Database

The project is hosted on the link http://sdb.web.cern.ch.

The Superconductors Database was developed as a tool to let people find informations about superconductivity in an easy and fast way. With the term "superconductivity" it is possible to identify several objects such as materials, cables, magnets etc. The aim of the project is to provide a tool to collect the wide family of objects that share superconductivity.

Project design

The task to collect in a simple way different kind of scientific fields and, at the same time, to provide a clear user interface, is not easy to achieve with a simple web+script+database interface. Something smarter should be used; the creation of an ad-hoc tool is not reasonable because the problems of stability and security that can emerge from a code not well tested. For these reasons the choice of the develop platform of the project is the open source engine MediaWiki [52].

MediaWiki interacts with the user and with the administrator via web, the back-end is any standard SQL database like MySQL or Oracle. With a web based user interface it is possible to create a collaborative database managed by everyone without knowledge of scripts or html or other low level languages. This idea is very exploited in the first well-known application of the MediaWiki engine that is Wikipedia [53].

The main page of the database is in Fig. 6.1

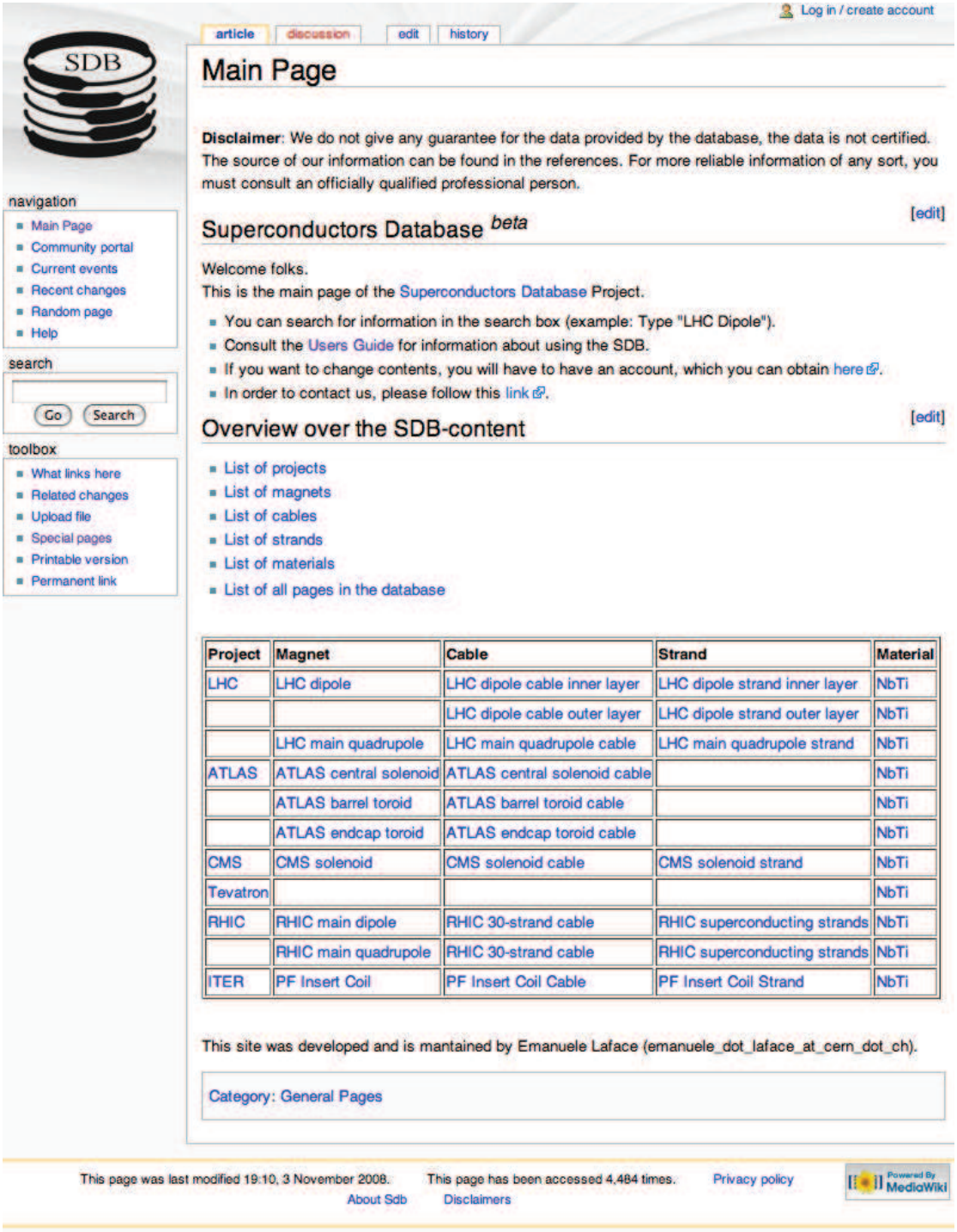

Log in / create account

article | discussion | edit | history

navigation
- Main Page
- Community portal
- Current events
- Recent changes
- Random page
- Help

search

Go Search

toolbox
- What links here
- Related changes
- Upload file
- Special pages
- Printable version
- Permanent link

Main Page

Disclaimer: We do not give any guarantee for the data provided by the database, the data is not certified. The source of our information can be found in the references. For more reliable information of any sort, you must consult an officially qualified professional person.

Superconductors Database *beta* [edit]

Welcome folks.
This is the main page of the Superconductors Database Project.

- You can search for information in the search box (example: Type "LHC Dipole").
- Consult the Users Guide for information about using the SDB.
- If you want to change contents, you will have to have an account, which you can obtain here.
- In order to contact us, please follow this link.

Overview over the SDB-content [edit]

- List of projects
- List of magnets
- List of cables
- List of strands
- List of materials
- List of all pages in the database

Project	Magnet	Cable	Strand	Material
LHC	LHC dipole	LHC dipole cable inner layer	LHC dipole strand inner layer	NbTi
		LHC dipole cable outer layer	LHC dipole strand outer layer	NbTi
	LHC main quadrupole	LHC main quadrupole cable	LHC main quadrupole strand	NbTi
ATLAS	ATLAS central solenoid	ATLAS central solenoid cable		NbTi
	ATLAS barrel toroid	ATLAS barrel toroid cable		NbTi
	ATLAS endcap toroid	ATLAS endcap toroid cable		NbTi
CMS	CMS solenoid	CMS solenoid cable	CMS solenoid strand	NbTi
Tevatron				NbTi
RHIC	RHIC main dipole	RHIC 30-strand cable	RHIC superconducting strands	NbTi
	RHIC main quadrupole	RHIC 30-strand cable	RHIC superconducting strands	NbTi
ITER	PF Insert Coil	PF Insert Coil Cable	PF Insert Coil Strand	NbTi

This site was developed and is mantained by Emanuele Laface (emanuele_dot_laface_at_cern_dot_ch).

Category: General Pages

This page was last modified 19:10, 3 November 2008. This page has been accessed 4,484 times. Privacy policy
About Sdb Disclaimers

Figure 6.1: Superconductors Database: Main page.

The data archive is based on five main categories: Projects, Magnets, Cables, Strands, Materials.

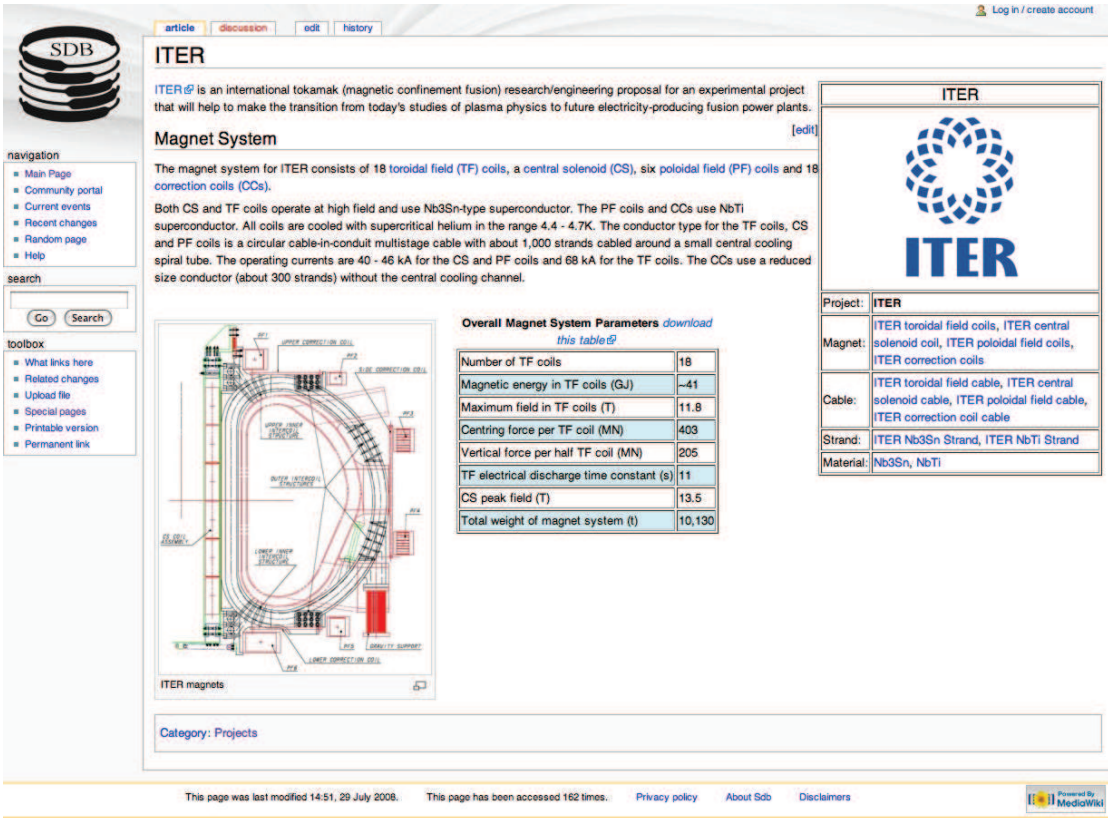

Figure 6.2: Superconductors Database: Example of a Project.

A project (Fig. 6.2) is a device or an experiment based on the characteristics of superconductivity, for example LHC is a project of an accelerator based on superconducting dipoles and quadrupoles; ITER is the project of a reactor for nuclear fusion and will be based on a toroidal superconducting magnet used to confine the fusion plasma.

Magnets (Fig. 6.3) are, in general, the first application of superconductors: there are magnets for nuclear magnetic resonance, for particles accelerators etc. Each project can contain the reference to several different magnets; for example LHC is made up of dipoles, quadrupoles, sextupoles and high order multipoles correctors, all these magnets are different from the point of view of the design, the cable used for the coils, and the technology in general. Each magnet is related to a project and to the cable used to build the coils.

Cables and strands (Fig. 6.4 and 6.5) are linked one to each other and in general are also related to a specific magnet of a project.

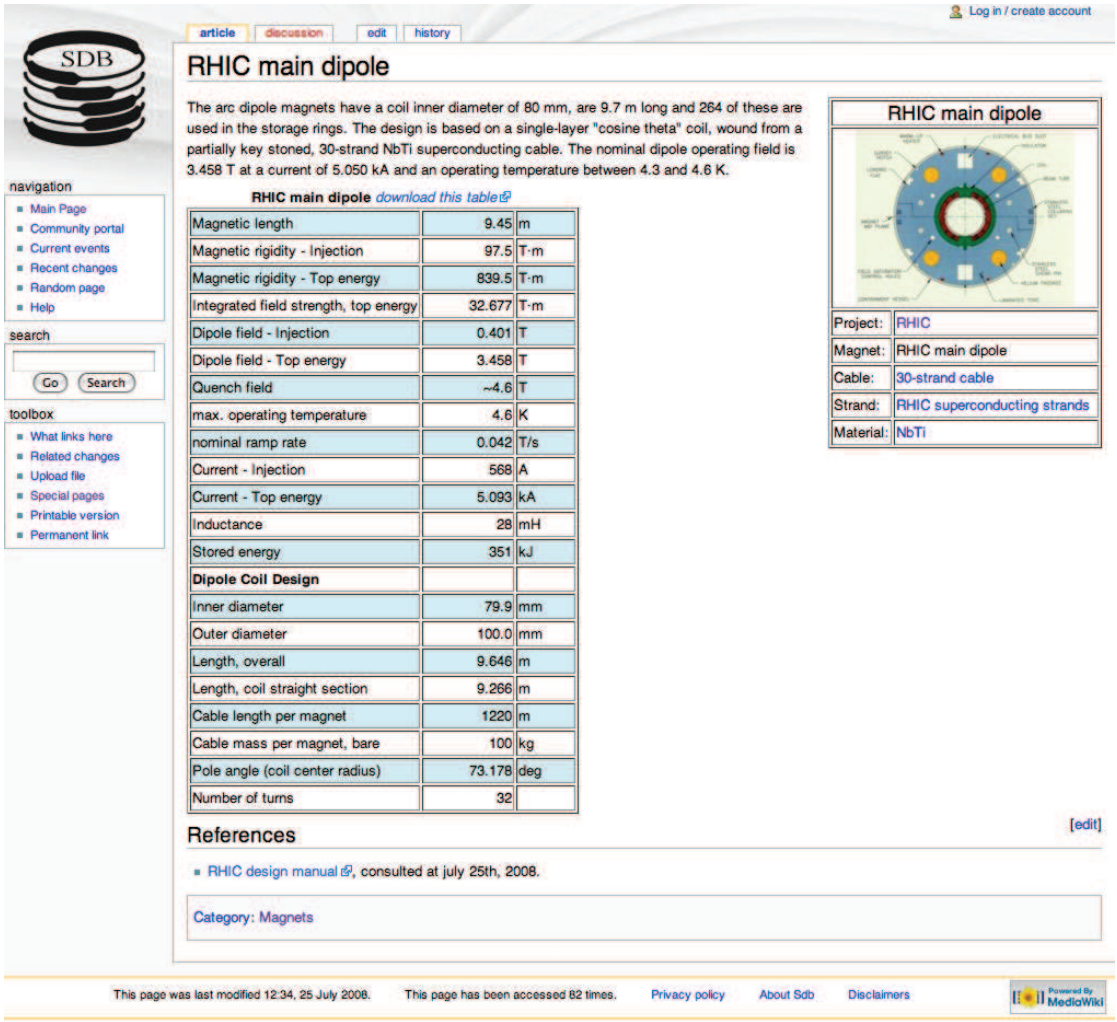

Log in / create account

article | discussion | edit | history

SDB

navigation
- Main Page
- Community portal
- Current events
- Recent changes
- Random page
- Help

search

Go Search

toolbox
- What links here
- Related changes
- Upload file
- Special pages
- Printable version
- Permanent link

RHIC main dipole

The arc dipole magnets have a coil inner diameter of 80 mm, are 9.7 m long and 264 of these are used in the storage rings. The design is based on a single-layer "cosine theta" coil, wound from a partially key stoned, 30-strand NbTi superconducting cable. The nominal dipole operating field is 3.458 T at a current of 5.050 kA and an operating temperature between 4.3 and 4.6 K.

RHIC main dipole *download this table*

Magnetic length	9.45	m
Magnetic rigidity - Injection	97.5	T·m
Magnetic rigidity - Top energy	839.5	T·m
Integrated field strength, top energy	32.677	T·m
Dipole field - Injection	0.401	T
Dipole field - Top energy	3.458	T
Quench field	~4.6	T
max. operating temperature	4.6	K
nominal ramp rate	0.042	T/s
Current - Injection	568	A
Current - Top energy	5.093	kA
Inductance	28	mH
Stored energy	351	kJ
Dipole Coil Design		
Inner diameter	79.9	mm
Outer diameter	100.0	mm
Length, overall	9.646	m
Length, coil straight section	9.266	m
Cable length per magnet	1220	m
Cable mass per magnet, bare	100	kg
Pole angle (coil center radius)	73.178	deg
Number of turns	32	

RHIC main dipole

Project:	RHIC
Magnet:	RHIC main dipole
Cable:	30-strand cable
Strand:	RHIC superconducting strands
Material:	NbTi

References

[edit]

- RHIC design manual, consulted at july 25th, 2008.

Category: Magnets

This page was last modified 12:34, 25 July 2008. This page has been accessed 82 times. Privacy policy About Sdb Disclaimers

Powered By MediaWiki

Figure 6.3: Superconductors Database: Example of a Magnet.

The collectable data for any of these objects (projects, cables and strands) is, in principle, without constraint: it is possible to insert and archive any kind of data, picture or attached document. In general it is useful to follow the main line of the user guide [54], in order to have an homogeneous presentation of data, but this is not a mandatory rule and the data can be adjusted in function of the wishes of the user.

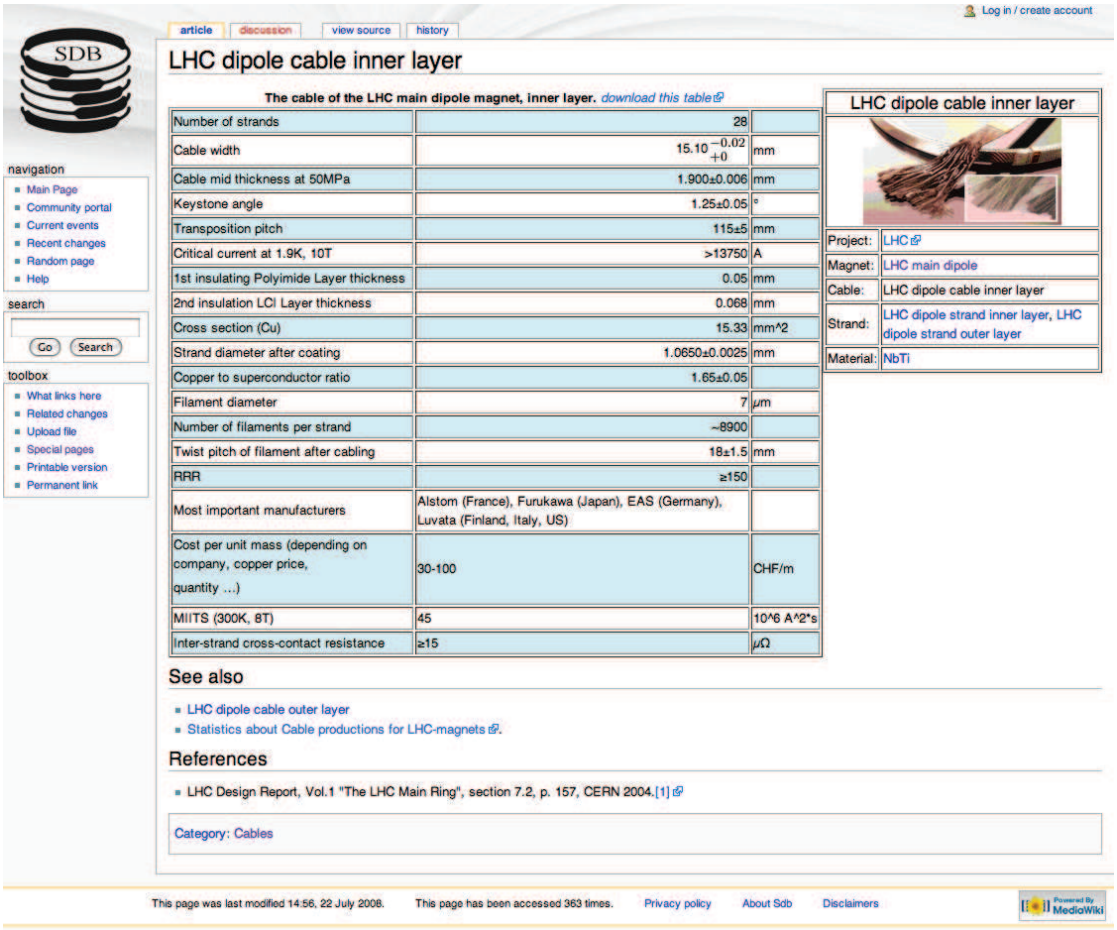

article | discussion | view source | history

Log in / create account

SDB

navigation
- Main Page
- Community portal
- Current events
- Recent changes
- Random page
- Help

search

Go Search

toolbox
- What links here
- Related changes
- Upload file
- Special pages
- Printable version
- Permanent link

LHC dipole cable inner layer

The cable of the LHC main dipole magnet, inner layer. *download this table*

Number of strands	28	
Cable width	$15.10^{-0.02}_{+0}$	mm
Cable mid thickness at 50MPa	1.900±0.006	mm
Keystone angle	1.25±0.05	°
Transposition pitch	115±5	mm
Critical current at 1.9K, 10T	>13750	A
1st insulating Polyimide Layer thickness	0.05	mm
2nd insulation LCI Layer thickness	0.068	mm
Cross section (Cu)	15.33	mm^2
Strand diameter after coating	1.0650±0.0025	mm
Copper to superconductor ratio	1.65±0.05	
Filament diameter	7	μm
Number of filaments per strand	~8900	
Twist pitch of filament after cabling	18±1.5	mm
RRR	≥150	
Most important manufacturers	Alstom (France), Furukawa (Japan), EAS (Germany), Luvata (Finland, Italy, US)	
Cost per unit mass (depending on company, copper price, quantity ...)	30-100	CHF/m
MIITS (300K, 8T)	45	10^6 A^2*s
Inter-strand cross-contact resistance	≥15	μΩ

LHC dipole cable inner layer

Project:	LHC
Magnet:	LHC main dipole
Cable:	LHC dipole cable inner layer
Strand:	LHC dipole strand inner layer, LHC dipole strand outer layer
Material:	NbTi

See also

- LHC dipole cable outer layer
- Statistics about Cable productions for LHC-magnets.

References

- LHC Design Report, Vol.1 "The LHC Main Ring", section 7.2, p. 157, CERN 2004.[1]

Category: Cables

This page was last modified 14:56, 22 July 2008. This page has been accessed 363 times. Privacy policy About Sdb Disclaimers

Figure 6.4: Superconductors Database: Example of a Cable.

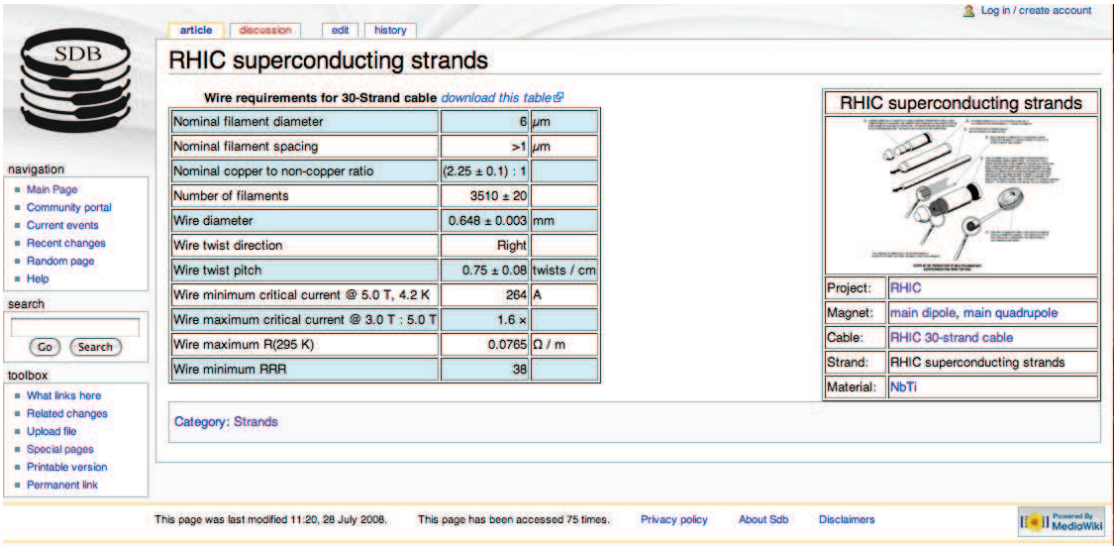

Figure 6.5: Superconductors Database: Example of a Strand.

For the materials (Fig. 6.7), the catalogue is more complicated than for projects, cables and strands, this is due to the interaction of the MediaWiki engine with an older database for materials called MATPRO [55]. This database contains informations about several materials and the data can be retrieved as tables or plots (Fig. 6.6).

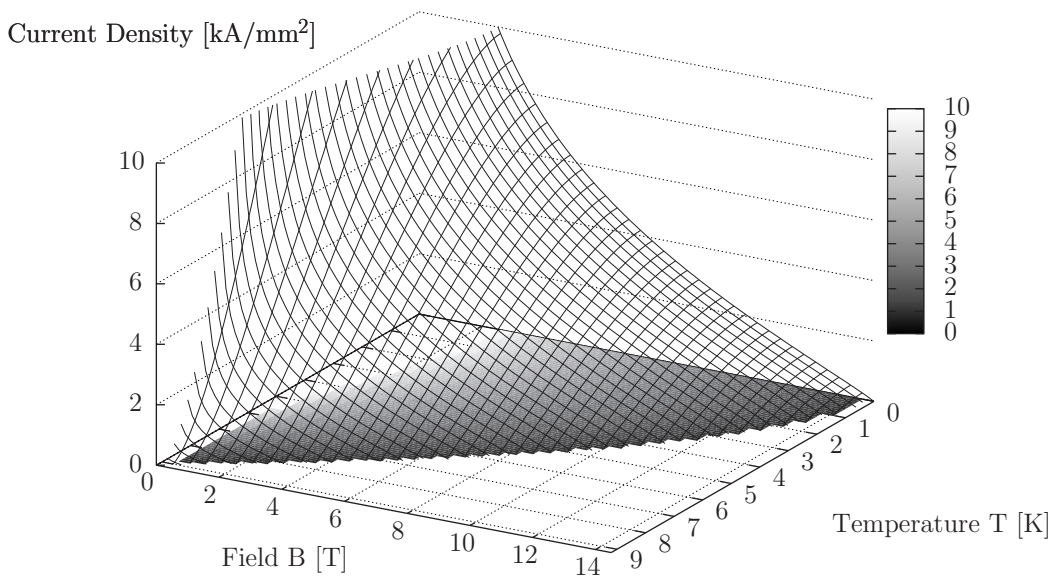

Figure 6.6: Example of MATPRO critical surface for Nb-Ti.

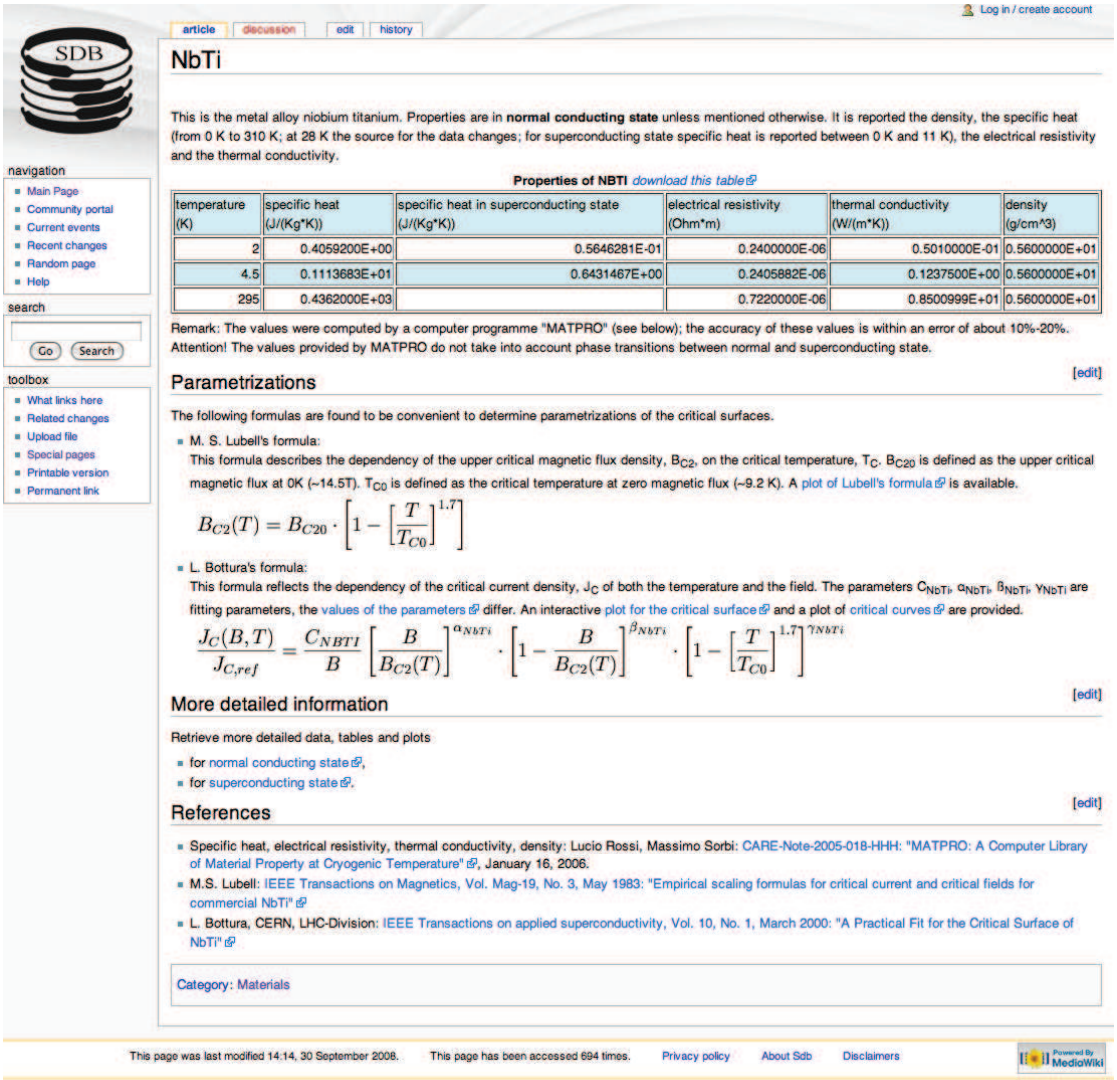

Log in / create account

article | discussion | edit | history

navigation
- Main Page
- Community portal
- Current events
- Recent changes
- Random page
- Help

search

Go Search

toolbox
- What links here
- Related changes
- Upload file
- Special pages
- Printable version
- Permanent link

NbTi

This is the metal alloy niobium titanium. Properties are in **normal conducting state** unless mentioned otherwise. It is reported the density, the specific heat (from 0 K to 310 K; at 28 K the source for the data changes; for superconducting state specific heat is reported between 0 K and 11 K), the electrical resistivity and the thermal conductivity.

Properties of NBTI *download this table*

temperature (K)	specific heat (J/(Kg*K))	specific heat in superconducting state (J/(Kg*K))	electrical resistivity (Ohm*m)	thermal conductivity (W/(m*K))	density (g/cm^3)
2	0.4059200E+00	0.5646281E-01	0.2400000E-06	0.5010000E-01	0.5600000E+01
4.5	0.1113683E+01	0.6431467E+00	0.2405882E-06	0.1237500E+00	0.5600000E+01
295	0.4362000E+03		0.7220000E-06	0.8500999E+01	0.5600000E+01

Remark: The values were computed by a computer programme "MATPRO" (see below); the accuracy of these values is within an error of about 10%-20%. Attention! The values provided by MATPRO do not take into account phase transitions between normal and superconducting state.

Parametrizations [edit]

The following formulas are found to be convenient to determine parametrizations of the critical surfaces.

- M. S. Lubell's formula:
  This formula describes the dependency of the upper critical magnetic flux density, B_{C2}, on the critical temperature, T_C. B_{C20} is defined as the upper critical magnetic flux at 0K (~14.5T). T_{C0} is defined as the critical temperature at zero magnetic flux (~9.2 K). A plot of Lubell's formula is available.

$$B_{C2}(T) = B_{C20} \cdot \left[1 - \left[\frac{T}{T_{C0}}\right]^{1.7}\right]$$

- L. Bottura's formula:
  This formula reflects the dependency of the critical current density, J_C of both the temperature and the field. The parameters C_{NbTi}, α_{NbTi}, β_{NbTi}, γ_{NbTi} are fitting parameters, the values of the parameters differ. An interactive plot for the critical surface and a plot of critical curves are provided.

$$\frac{J_C(B,T)}{J_{C,ref}} = \frac{C_{NBTI}}{B}\left[\frac{B}{B_{C2}(T)}\right]^{\alpha_{NbTi}} \cdot \left[1 - \frac{B}{B_{C2}(T)}\right]^{\beta_{NbTi}} \cdot \left[1 - \left[\frac{T}{T_{C0}}\right]^{1.7}\right]^{\gamma_{NbTi}}$$

More detailed information [edit]

Retrieve more detailed data, tables and plots

- for normal conducting state,
- for superconducting state.

References [edit]

- Specific heat, electrical resistivity, thermal conductivity, density: Lucio Rossi, Massimo Sorbi: CARE-Note-2005-018-HHH: "MATPRO: A Computer Library of Material Property at Cryogenic Temperature", January 16, 2006.
- M.S. Lubell: IEEE Transactions on Magnetics, Vol. Mag-19, No. 3, May 1983: "Empirical scaling formulas for critical current and critical fields for commercial NbTi"
- L. Bottura, CERN, LHC-Division: IEEE Transactions on applied superconductivity, Vol. 10, No. 1, March 2000: "A Practical Fit for the Critical Surface of NbTi"

Category: Materials

This page was last modified 14:14, 30 September 2008. This page has been accessed 694 times. Privacy policy About Sdb Disclaimers

Figure 6.7: Superconductors Database: Example of a Material.

MATPRO is not the only external tool used in the database: any CGI (Common Graphic Interface) written in Phyton, Perl or C can be, in principle, added on the web structure and integrated into the database increasing in this way the value of the data stored into the DB.

Project, magnets, cables, strands and materials are objects with properties very different and this is the main reason to choose the MediaWiki structure to archive these kind of data. The engine used in MediaWiki can also accept various kind of files like pictures or pdf, it is possible in this way to add the papers of references for each page presented on the site. The data on the database are provided without

warranty because it is a collaborative database and it is not possible in principle to check every single number, but set of data without references are rejected by the policy of the database.

Use and administration

The main reason to use MediaWiki, as presented in the previous section, is to have flexibility in the kind of data that can be collected in the database. There is another reason to use this tool: the administration and the use of the database is totally transparent to the user and no knowledge of SQL language is required to use the superconductors database.

By default a user can only consult the database, this policy was decided to prevent vandalism and anonymous changes in the data. This restriction is mandatory in order to reduce the load of the system administrator in term of check of reliability of data. An user that wants to edit or create a page can send a request using a simple form with a CAPTCHA (Completely Automated Public Turing test to tell Computers and Humans Apart) [56] used to prevent spammers. The user must be authorized from an administrator.

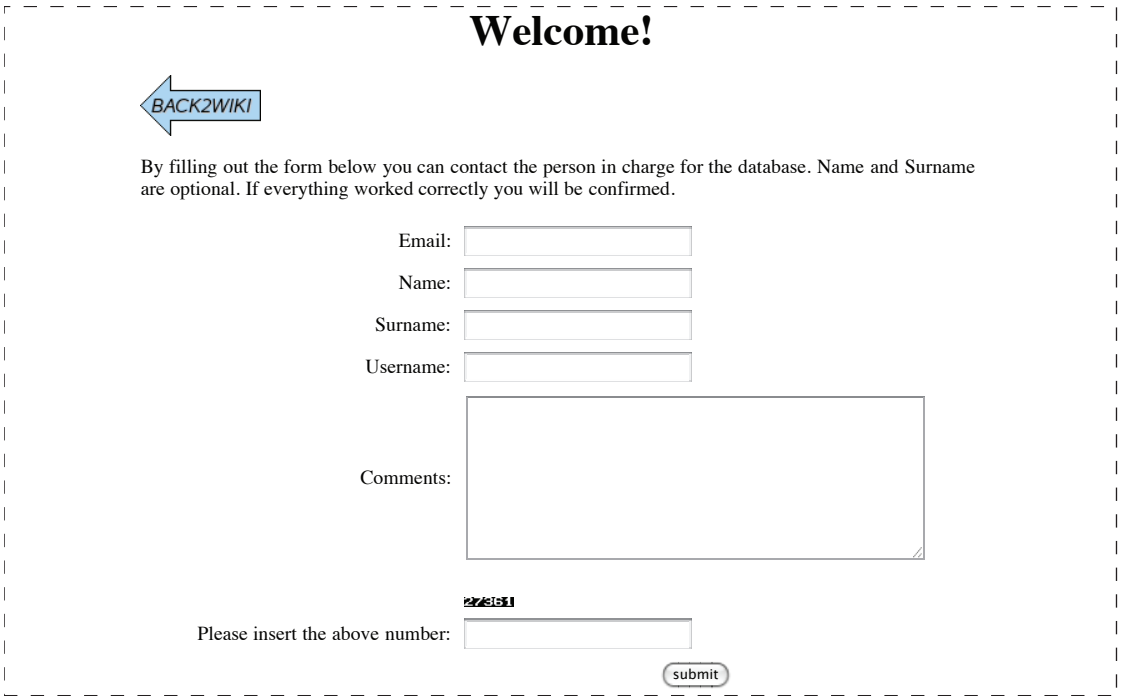

Figure 6.8: Superconductors Database: Contact Form.

A registered user can modify any content on the database and can also create

a new page. The language used to create a page is textual; an example is the page of NbTi material (Fig. 6.7) and the code that generates that page is the following:

```
[[Category:Materials]]

This is the metal alloy niobium titanium. Properties are in
'''normal conducting state''' unless mentioned otherwise.
It is reported the density, the specific heat (from 0 K to 310
K; at 28 K the source for the data changes; for superconducting
state specific heat is reported between 0 K and 11 K), the
electrical resistivity and the thermal conductivity.

{| {{datatablestyle}}
|+'''Properties of NBTI''' {{datatablelink}}
|-
| bgcolor="#CCFFFF" | temperature (K)
| bgcolor="#CCFFFF" |  specific heat (J/(Kg*K))
| bgcolor="#CCFFFF" | specific heat in superconducting state (J/(Kg*K))
| bgcolor="#CCFFFF" |  electrical resistivity (Ohm*m)
| bgcolor="#CCFFFF" |  thermal conductivity (W/(m*K))
| bgcolor="#CCFFFF" |  density (g/cm^3)
|-
| align="right" | 2
| align="right" | 0.4059200E+00
| align="right" | 0.5646281E-01
| align="right" | 0.2400000E-06
| align="right" | 0.5010000E-01
| align="right" | 0.5600000E+01
|-
| bgcolor="#CCFFFF" align="right" | 4.5
| bgcolor="#CCFFFF" align="right" | 0.1113683E+01
| bgcolor="#CCFFFF" align="right" | 0.6431467E+00
| bgcolor="#CCFFFF" align="right" | 0.2405882E-06
| bgcolor="#CCFFFF" align="right" | 0.1237500E+00
| bgcolor="#CCFFFF" align="right" | 0.5600000E+01
|-
| align="right" | 295
| align="right" | 0.4362000E+03
| align="right" |
| align="right" | 0.7220000E-06
| align="right" | 0.8500999E+01
| align="right" | 0.5600000E+01
|}

Remark: The values were computed by a computer programme "MATPRO" (see below);
the accuracy of these values is within an error of about 10%-20%. Attention!
The values provided by MATPRO do not take into account phase transitions between
normal and superconducting state.

==Parametrizations==

The following formulas are found to be convenient to determine parametrizations
of the critical surfaces.
* M. S. Lubell's formula:<br>This formula describes the dependency of the upper
critical magnetic flux density, B<sub>C2</sub>, on the critical temperature,
T<sub>C</sub>. B<sub>C20</sub> is defined as the upper critical magnetic flux
at 0K (~14.5T). T<sub>C0</sub> is defined as the critical temperature at zero
magnetic flux (~9.2 K). A [{{SERVER}}/cgi-bin/Sdb/plots/lubell plot of Lubell's
formula] is available.
:<math>{B_{C2}(T)} = B_{C20} \cdot \left[1-\left[\frac{T}{T_{C0}}\right]^
```

```
{1.7}\right]</math>

* L. Bottura's formula:<br>This formula reflects the dependency of the critical
current density, J<sub>C</sub> of both the temperature and the field. The
parameters C<sub>NbTi</sub>, ?<sub>NbTi</sub>, <sub>NbTi</sub>,
?<sub>NbTi</sub> are fitting parameters, the [{{SERVER}}/sdb/plot/parameters.html
values of the parameters] differ. An  interactive [{{SERVER}}/cgi-bin/{{SITENAME}}/
plots/bottura3 plot for the critical surface] and a plot of [{{SERVER}}/cgi-bin/
{{SITENAME}}/plots/bottura2 critical curves] are provided.
:<math>\frac {J_C(B,T)}{J_{C,ref}} = \frac {C_{NBTI}}{B} \left[\frac{B}{B_{C2}(T)}\right]^
{\alpha_{NbTi}} \cdot \left[1-\frac{B}{B_{C2}(T)}\right]^{\beta_{NbTi}}\cdot\left[1-
\left[\frac{T}{T_{C0}}\right]^{1.7}\right]^{\gamma_{NbTi}}</math>

== More detailed information ==

Retrieve more detailed data, tables and plots
* for [{{SERVER}}/cgi-bin/{{SITENAME}}/matprointerface?NBTI normal conducting state],
* for [{{SERVER}}/cgi-bin/{{SITENAME}}/matprointerface?NBTISUP superconducting state].

==References==

* Specific heat, electrical resistivity, thermal conductivity, density: Lucio Rossi,
Massimo Sorbi: [http://documents.cern.ch/archive/electronic/other/uploader/
CARE/INTNOTE/note-2005-018-HHH.pdf CARE-Note-2005-018-HHH:
"MATPRO: A Computer Library of Material Property at Cryogenic Temperature"],
January 16, 2006.
* M.S. Lubell: [http://ieeexplore.ieee.org/xpls/abs_all.jsp?arnumber=1062311
IEEE Transactions on Magnetics, Vol. Mag-19, No. 3, May 1983: "Empirical scaling
formulas for critical current and critical fields for commercial NbTi"]
* L. Bottura, CERN, LHC-Division: [http://ieeexplore.ieee.org/xpls/
abs_all.jsp?arnumber=828413 IEEE Transactions on applied superconductivity,
Vol. 10, No. 1, March 2000: "A Practical Fit for the Critical Surface of NbTi"]
```

The syntax is not complex, the only tags are for special behaviors, for example the mathematical equations are written in latex between the tags

```
<math></math>
```

the code is rendered by latex and converted in a picture automatically included in the page. In this way the user doesn't care how to insert equations or special object into the page but everything is managed by standard parsers of MediaWiki engine.

The other big advantage of this interface is that the database indexing is totally automatized: any new page or any change in a page is automatically saved into the database and the search engine can directly look for any content of the page. The user can just write the page and this page will be available for everyone through the search button on the main page.

The administration of the database is as easy as the creation of the pages: every task on the data, such as the erasing of a page or the creation of a new user, can be performed trough the interface of MediaWiki directly from web without a direct manipulation on the SQL structure. This kind of administration becomes very interesting because of the wide availability of tools for administration provided by

MediaWiki: just to show an example for each page it is available the full history of that page (Fig. 6.9):

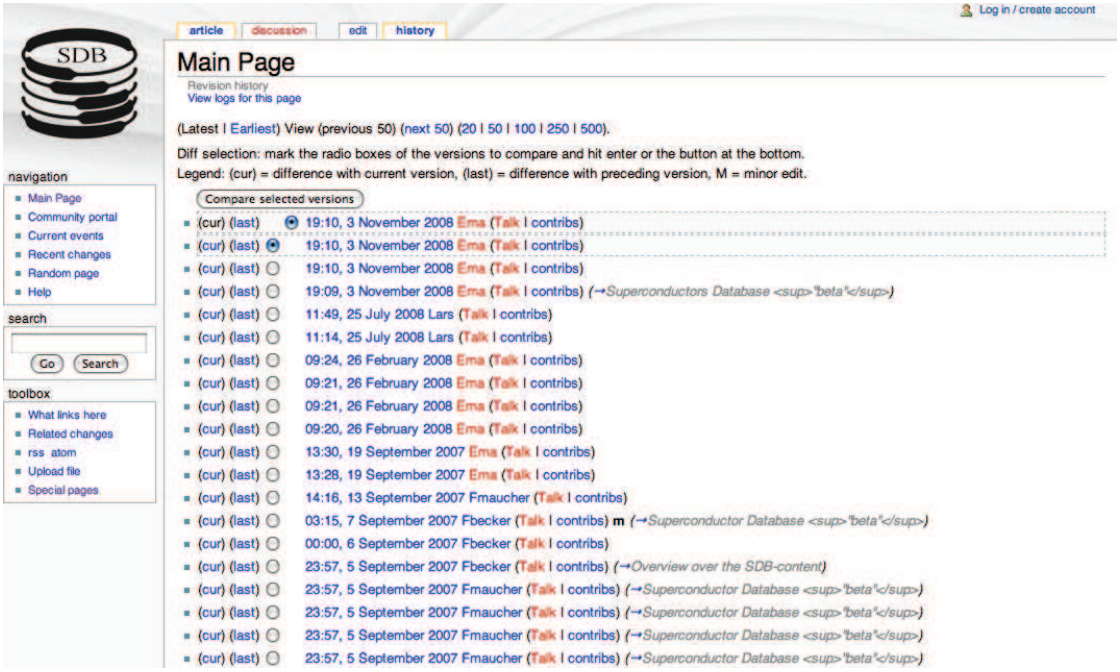

Figure 6.9: Superconductors Database: An History Page.

any release of the page is clickable and contains the version of the page in the specific time, so it is possible to move back in time and recover all the informations in case of mistake or troubles. Because of the nature of the interface, this history is also available for the users management (for example) and it is possible to see the history of the creation of the users and any information about the management of the database in general.

This way of administration permits to anyone without detailed skills of databases and computer science in general, to manage everything with the only help of the user guide provided by the site. It also exists, of course, an extraordinary administration, the backup of the hard disk, the recovery from crashes, the security prevention from hackers attacks etc, that must be performed by a specialist in information technology, but all this exceptional administration can be solved easily hosting the website on a web server managed by the IT people at CERN.

To understand if this project is useful, it is possible to consider the ranking position in the Google search engine (that is based on the method of cross reference invented by Larry Page [57]) and it is also possible to use a log analyzer for statistics in order to see how many people retrieve data from the database site.

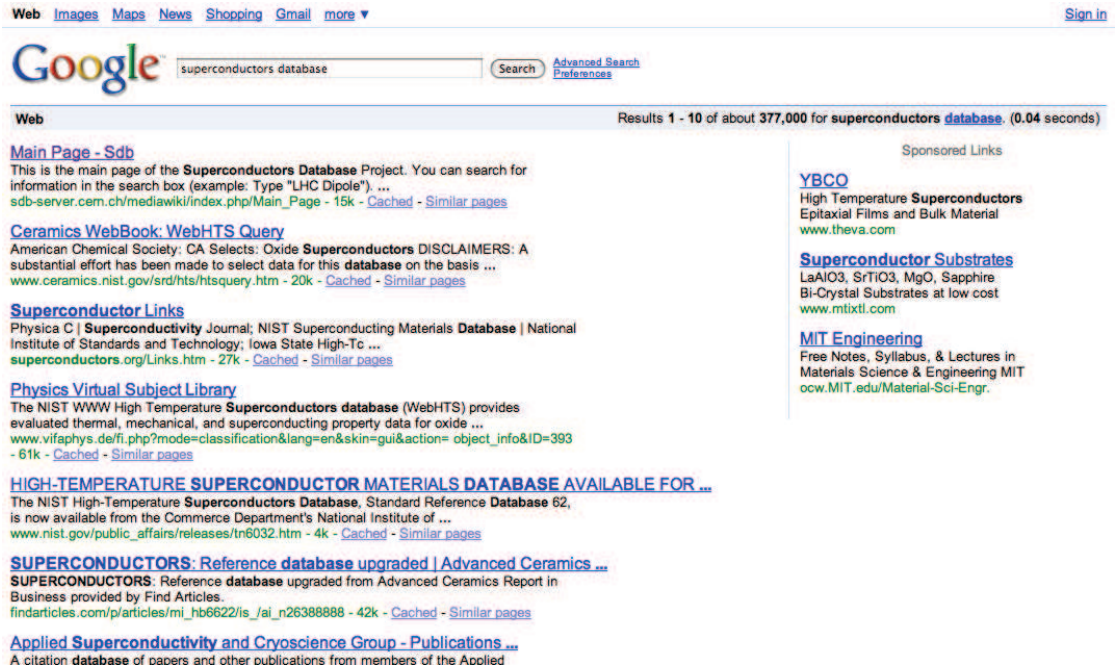

Figure 6.10: Superconductors Database: Ranking in Google.

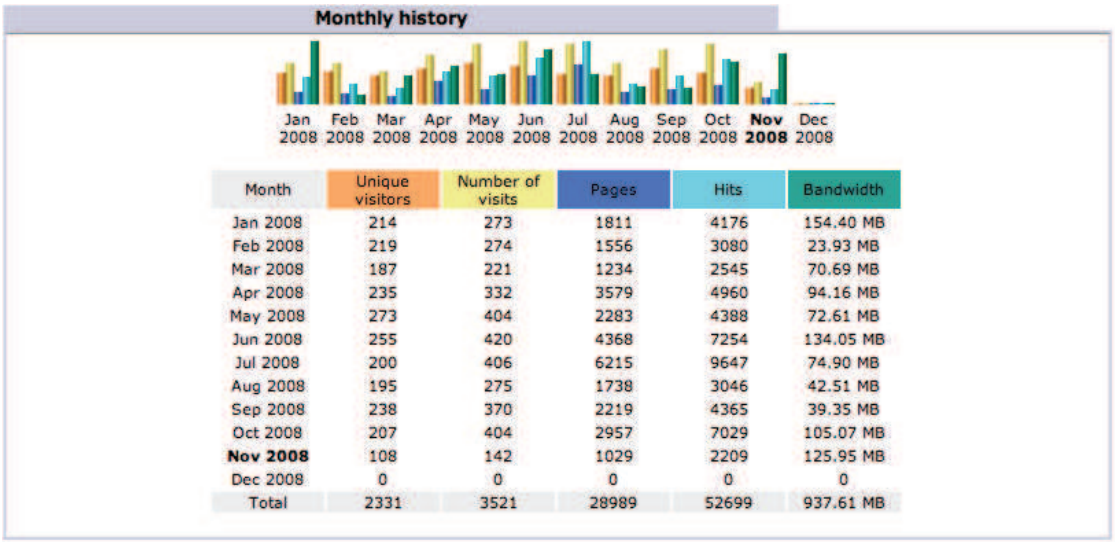

Month	Unique visitors	Number of visits	Pages	Hits	Bandwidth
Jan 2008	214	273	1811	4176	154.40 MB
Feb 2008	219	274	1556	3080	23.93 MB
Mar 2008	187	221	1234	2545	70.69 MB
Apr 2008	235	332	3579	4960	94.16 MB
May 2008	273	404	2283	4388	72.61 MB
Jun 2008	255	420	4368	7254	134.05 MB
Jul 2008	200	406	6215	9647	74.90 MB
Aug 2008	195	275	1738	3046	42.51 MB
Sep 2008	238	370	2219	4365	39.35 MB
Oct 2008	207	404	2957	7029	105.07 MB
Nov 2008	108	142	1029	2209	125.95 MB
Dec 2008	0	0	0	0	0
Total	2331	3521	28989	52699	937.61 MB

Figure 6.11: Superconductors Database: Usage statistics.

Today (November, 13th 2008) the result of Google for the query "Superconductors Database" shows as first one the SDB project (Fig. 6.10). This is due to

two main reasons: the first one is that CERN is in general well ranked in the world because of the importance of scientific work developed there; the second reason is that the Superconductors Database is linked, in the page of superconductivity, by the english version of Wikipedia that is considered the most important online encyclopedia available on internet.

The high ranking in Google generates a flux of visitors that arrives to the database page; a resume of the usage is shown in Fig. 6.11. This table was generated by the free real-time logfile analyzer to get advanced statistics AWStats ([58]) and the full statistics are available here: http://sdb-server.cern.ch/cgi-bin/awstats.pl. The number of visitors per day is ~ 10, that, for the small community of superconductivity, is an interesting number of people and it means that the project is considered useful by the community.

This tool of data archiving can be improved easily with the contribution of other people because anyone can add data and expand the project. An increase in the number of data will correspond to an increase in the usefulness of the database for anyone involved in a project related to superconductors.

Bibliography

[1] E. Laface *et al.*, "Interaction Region with Slim Quadrupoles," *Proceeding of EPAC 2006, Edinburg, Scotland*, pp. 2014–2016, Jun 2006.

[2] E. Laface *et al.*, "Q0 with l*=13 m," *Proceedings of 3rd CARE-HHH-APD Workshop, IFIC, Valencia, Spain*, Oct 2006.

[3] E. Laface *et al.*, "Q0 Status," *Proceedings of CARE-HHH-APD IR'07, INFN, Frascati, Italy*, Nov 2007.

[4] E. Laface *et al.*, "Investigations on a Q0 doublet optics for the LHC luminosity upgrade," *Proceeding of EPAC 2008, Genova, Italy*, Jun 2008.

[5] E. Laface *et al.*, "Crystals application in the TOTEM experiment to increase the acceptance of a Roman Pot," *Proceeding of EPAC 2008, Genova, Italy*, Jun 2008.

[6] E. Laface, "Superconductors Database (http://sdb.web.cern.ch)."

[7] F. Schmidt *et al.*, "MadX manual (http://mad.web.cern.ch/mad/uguide.html)."

[8] F. Schmidt *et al.*, "MAD-X PTC Integration," no. CERN-AB-2005-036, Jul 2005.

[9] G. Battistoni *et al.*, "The FLUKA code: Description and benchmarking," *AIP Conf. Proc.*, vol. 896, no. SLAC-REPRINT-2007-184, pp. 31–49, 2007.

[10] O. S. Brüning *et al.*, *LHC Design Report*. Geneva: CERN, 2004.

[11] F. Gianotti, "Collider Physics : LHC," CERN, Geneva, Tech. Rep. ATL-CONF-2000-001, Apr 2000.

[12] O. S. Brüning *et al.*, "LHC Luminosity and energy upgrade: A Feasibility Study," CERN, Geneva, Tech. Rep. CERN-LHC-Project-Report-626, Dec 2002.

[13] *Design study of the Large Hadron Collider (LHC) : a multiparticle collider in the LEP tunnel*. Geneva: CERN, 1991.

[14] "LHC MadX optics v6.5 (http://proj-lhc-optics-web.web.cern.ch/proj-lhc-optics-web/V6.5/)."

[15] J.-P. Koutchouk *et al.*, "A more robust and flexible lattice for LHC." CERN, Tech. Rep. LHC-Project-Report-107, Jun 1997.

[16] W. Scandale, "Revisiting the problem of the LHC insertion symmetry," CERN, Geneva, Tech. Rep. SL-Note-94-42-AP, Apr 1994.

[17] J.-P. Koutchouk *et al.*, "Modular optical design of the LHC experimental insertions," CERN, Tech. Rep. LHC-Project-Report-14, Jul 1996.

[18] S. Y. Lee, *Accelerator Physics; 2nd ed.* London: World Scientific, 2004.

[19] L. R. Evans and J. Gareyte, "Beam beam effects," CERN, Tech. Rep. CERN-SPS-86-8-DI-MST, Apr 1986.

[20] O. S. Brüning *et al.*, "Performance Limits and IR Design Challenges of a Possible LHC Luminosity Upgrade Based on Nb-Ti SC Magnet Technology," no. LHC-Project-Report-785, Aug 2004.

[21] O. S. Brüning, "Accumulation and Ramping in the LHC," CERN, Geneva, Tech. Rep. LHC-PROJECT-NOTE-218, Feb 2000.

[22] M. N. Dubinin *et al.*, "Search for Higgs Boson at LHC in the Reaction $pp \rightarrow \gamma\gamma + jet$ at a Low Luminosity." CERN, Geneva, Tech. Rep. hep-ph/9712335, Dec 1997.

[23] W. Scandale and F. Zimmermann, "Injector upgrade: Dicussion and synthesis," *Proceedings of 3rd CARE-HHH-APD Workshop, IFIC, Valencia, Spain*, 2006.

[24] W. Scandale and F. Zimmermann, "Tentative conclusions of LUMI'06," *Proceedings of 3rd CARE-HHH-APD Workshop, IFIC, Valencia, Spain*, pp. 189–191, 2006.

[25] J.-P. Koutchouk and G. Sterbini, "An Early Beam Separation Scheme for the LHC Luminosity Upgrade." no. CARE-Conf-2006-033-HHH, Aug 2006.

[26] R. Calaga *et al.*, "Crab Compensation for LHC Beams," CERN, Geneva, Tech. Rep. LHC-PROJECT-Report-1136, Sep 2008.

[27] U. Dorda *et al.*, "LHC beam-beam compensation using wires and electron lenses." *Proceedings of CARE-HHH-APD IR'07, INFN, Frascati, Italy*, 2007.

[28] V. Siltsev, "On possible use of electron lenses in LHC," *Proceedings of 3rd CARE-HHH-APD Workshop, IFIC, Valencia, Spain*, 2007.

[29] N. V. Mokhov *et al.*, "Protecting LHC IP1/IP5 Components Against Radiation Resulting from Colliding Beam Interactions." CERN, Geneva, Tech. Rep. LHC-Project-Report-633, Apr 2003.

[30] M. Buénerd, "The TOTEM project at LHC," Grenoble 1. Inst. Sci. Nucl., Grenoble, Tech. Rep. ISN-95-83, Sep 1995.

[31] V. Avati and K. Österberg, "Acceptance calculations methods for low-β^* optics," CERN, Geneva, Tech. Rep. TOTEM Internal Note 05-2, Feb 2006.

[32] S. Mandelstam, "Determination of the Pion-Nucleon Scattering Amplitude from Dispersion Relations and Unitarity," *Phys. Rev.*, no. 112, pp. 1344–1360, Jun 1958.

[33] E. D. Courant and H. S. Snyder, "Theory of the Alternating-Gradient Synchrotron," *Ann. Phys.*, vol. 3, pp. 1–48, 1958.

[34] K. Brown and R. V. Servranckx, "Optics modules for circular accelerator design." SLAC, Tech. Rep. SLAC-PUB-3957, May 1986.

[35] M. Venturini and W. Kozanecki, "The Hourglass effect and the measurement of the transverse size of colliding beams by luminosity scans," no. SLAC-PUB-8699, p. 7, Nov 2000.

[36] J.-P. Koutchouk *et al.*, "A Solution for Phase-one Upgrade of the LHC Low-beta Quadrupoles Based on Nb-Ti." CERN, Tech. Rep., Apr 2007.

[37] T. Sen, "Alignment tolerances of IR quadrupoles in the LHC," FERMILAB, Batavia, IL, Tech. Rep. FERMILAB-CONF-99-304, Nov 1999.

[38] S. Roesler *et al.*, "The Monte Carlo Event Generator DPMJET-III," SLAC, Stanford, CA, Tech. Rep. hep-ph/0012252., Dec 2000.

[39] E. Wildner *et al.*, "Are large-aperture NbTi magnets compatible with 1E35?" no. CARE-HHH-APD IR07, INFN, Frascati, Nov 2007.

[40] A. M. Taratin and V. S. A., ""Volume reflection" of high-energy charged particles in quasi-channeling states in bent crystals," *Phys. Lett. A*, vol. 119, pp. 425–428, Jan 1987.

[41] W. Scandale *et al.*, "High-Efficiency Volume Reflection of an Ultrarelativistic Proton Beam with a Bent Silicon Crystal," *Phys. Rev. Lett.*, vol. 98, p. 154801, 2007.

[42] W. Scandale and A. Carnera, "Double volume reflection of a proton beam by a sequence of two bent crystals," *Phys. Lett. B*, vol. 658, no. 4, pp. 109–111, 2008.

[43] R. W. Assmann *et al.*, "Equilibrium Beam Distribution and Halo in the LHC." no. LHC-Project-Report-592, p. 4, Jul 2002.

[44] R. W. Assmann *et al.*, "Requirements for the lhc collimation system." no. LHC-Project-Report-599., p. 4, Jul 2002.

[45] W. Scandale and A. M. Taratin, "Simulation of CRYSTAL, the Bent Crystal Based Collimation Experiment in the SPS." CERN, Tech. Rep. CERN-AT-2008-021, Aug 2008.

[46] W. Scandale and M. Prest, "Proposal of the Crystal Experiment," CERN, Geneva, Tech. Rep. CERN-SPSC-2008-014., Apr 2008.

[47] "SPS Optics Repository (http://project-sps-optics.web.cern.ch/project-SPS-optics/optics2008/SPS/SPSRing/2008/)."

[48] P. Strolin, *Resonant extraction from the CERN intersecting storage rings.* CERN, 1969, no. CERN/SPS/69-9.

[49] W. Herr, "Diffusion of particles induced by transverse noise and its application to crystal extraction experiments." CERN, Geneva, Tech. Rep. CERN-SL-92-53-AP, Nov 1992.

[50] L. Vos, "Transverse feedback system in the CERN SPS." no. CERN-SL-91-40-BI, Oct 1991.

[51] H. G. Hereward, "How good is the r.m.s. as a measure of beam size?" CERN, Tech. Rep. CERN/MPS/DL 69-15, 1969.

[52] "Mediawiki foundation http://www.mediawiki.org/wiki/MediaWiki."

[53] "Wikipedia the free encyclopedia http://www.wikipedia.org."

[54] "Superconductors database: The complete user guide http://sdb-server.cern.ch/mediawiki/index.php/Users_Guide."

[55] L. Rossi and M. Sorbi, "MATPRO: a computer library of material property at cryogenic temperature," CERN, Tech. Rep. CARE-NOTE-2005-018-HHH, 2006.

[56] L. Grossman, "Computer Literacy Tests: Are You Human?" *TIME*, Jun 2008.

[57] L. Page, "Scoring documents in a linked database," United States Patent and Trademark Office, Tech. Rep., Sep 2007.

[58] "Awstats http://awstats.sourceforge.net/."